# Quality of Service Improvements in Weather Impacted Satellite Communication Networks

by

**Kamal Harb**
M.A.Sc. in Electrical Engineering
B.Sc. in Electrical Engineering

A thesis submitted to the Faculty of Graduate Studies and Research

in partial fulfillment of the requirements for the degree of

**Doctor of Philosophy in Electrical and Computer Engineering**

Ottawa-Carleton Institute for Electrical and Computer Engineering (OCIECE)
Department of Systems and Computer Engineering

Carleton University

Ottawa, Ontario, Canada, K1S 5B6

September 2010

*Your file Votre référence*
*ISBN:* 978-0-494-70522-3
*Our file Notre référence*
*ISBN:* 978-0-494-70522-3

# Abstract

Making accurate prediction of channel attenuations can be of immense value in improving the quality of signals in high frequency satellite communication channels. Such prediction of weather related attenuation factors for the impending weather conditions is an objective of this thesis. The thesis also describes an intelligent weather aware control system (IWACS) that uses both International Telecommunication Union-Radiocommunications (ITU − R) and the predictions made from Markov model to maintain the quality of service (QoS) in channels that are impacted by rain, gaseous, cloud, fog, and scintillation attenuations. Based on that, a three dimensional relationship is proposed using our adaptive scheme to estimate atmospheric attenuations with both propagation angle and predicted rainfall rate ($RR_{pr}$) at a given location and operational frequency. This novel method of predicting weather characteristics supplies valuable data for mitigation planning and subsequently for developing an enhanced back propagation-learning algorithm to iteratively tune the IWACS based on the decision support system (DSS) technique with the returned signal to noise ratio (SNR) values for activating the weighted modulation/codepoint to its optimal values for different cases. The tuning in this case is done by adaptively selecting appropriate channel frequency, modulation, coding, propagation angle, transmission power level, and data transmission rate to improve channel robustness. The ultimate outcome is maximization of the capacity of the network under different weather conditions. Simulation results are presented to show the effectiveness of the proposed scheme.

**Dedicated to my late father Menwal,**

**mother Sania,**

**brothers Walid, Mike, Jamal,**

**sisters Samar, Sahar, Suzan, Jihan,**

**wife Sabah, son Walid,**

**uncles Hani, Adel, Daoud, Yehya,**

**and the extended family for their**

**endless love and unlimited support.**

# Acknowledgements

I would like to express my utmost gratitude and deepest appreciation for the following people whose continuous support and efforts made this work possible.

First, my supervisor, Dr. Richard Yu, for his visionary leadership, innovation, his views on the conduct of my research, and passion for science that have continuously been a catalyst of motivation and totality.

Second, the author is thankful to Dr. Pramod Dhakal for his untiring help in refining the research work and in improving the presentation of this thesis. Dr. Dhakal's role in granting me the opportunity to work with him at EION Inc. in ISS project, which built the foundation of this research work, is also duly acknowledged. His technical insights, dedication to advancement of individuals who work with him, qualities in technical expression and writing, and constructive criticism in all aspects of research have made significant influence in the success of this work.

Third, I would like to thank Professors Michel Nakhla, Mohamed El-Tanany, Halim Yanikomeroglu, Robert Holton, Ioannis Lambadaris, Ashraf Matrawy, Hussein Al Zubaidy, and Ilia Polushin of Carleton, Kalai Kalaichelvan, Rama Munikoti, Wahab Almuhtadi, and Anand Srinivasan of Eion, Abdul Lakhani and Andre Bigras of Telesat, Rami Abielmona and Mofid Harb of Larus, office administrators especially Danny Lemay, Jerry Buburuz, Jennifer Poll, Coleen Kornelsen, Anna Lee, and Blazenka Power, my friends Shafiqul Islam, Aziz El-Solh, and Jason Rhinelander, my cousin Ayoub and Nadia Saad for their endless support.

Fourth, I thank my brother Mike and extended family for their unremitting encouragement, and sacrifices throughout the years that continue to be of paramount significance to my work.

Finally, my beloved wife Sabah for her delightful aura, infinite patience, and understanding at stressful times, completion of this work would have been difficult without her great support.

# Contents

List of Tables . . . . . viii

List of Figures . . . . . ix

List of Abbreviations . . . . . xii

List of Symbols . . . . . xiv

**1 Introduction** **1**

1.1 Research Overview . . . . . 3

1.2 Thesis Contributions . . . . . 6

1.2.1 Published, Accepted, and Submitted Papers . . . . . 7

1.3 Thesis Organization . . . . . 9

**2 Background and Literature Review** **10**

2.1 Introduction . . . . . 10

2.2 Satellite Communications Background . . . . . 11

2.3 Electromagnetic Waves and Their Relationships with The Medium . . . . . 13

2.4 Impacts of Atmospheric Attenuations on Satellite Communications . . . . . 14

2.4.1 Rain Attenuation . . . . . 16

2.4.2 Gaseous Attenuation . . . . . 17

2.4.3 Cloud and Fog Attenuations . . . . . 19

2.4.4 Scintillation Attenuation . . . . . 20
2.4.5 Free Space Attenuation . . . . . 22
2.5 QoS and SLA . . . . . 24
2.6 Summary . . . . . 24

**3 Estimating the Effect of Rainfall Rate on Satellite Communication Links 26**
3.1 Introduction . . . . . 26
3.2 Rainfall Rate Calculation . . . . . 27
3.3 Definition of Bi-Linear Interpolation . . . . . 29
3.4 Rain Attenuation Development . . . . . 31
3.4.1 ITU – R Original Method . . . . . 32
3.4.2 ITU – R Approximation Method . . . . . 38
3.4.3 Iterative Approximation Method . . . . . 39
3.4.4 Algorithm for Iterative Approximation Method . . . . . 46
3.5 Summary . . . . . 49

**4 Prediction of Rainfall Rate Using Markov Theory 50**
4.1 Introduction . . . . . 50
4.2 Rainfall Rate Prediction . . . . . 51
4.2.1 Classification of Rain . . . . . 51
4.2.2 Markov Model Implementation . . . . . 53
4.2.3 Predicted Rainfall Rate . . . . . 57
4.2.4 The Values of Weights and Transition Probabilities . . . . . 62
4.3 Summary . . . . . 63

**5 Calculation of Atmospheric Attenuation 65**
5.1 Introduction . . . . . 65

5.2 Migrating ITU − R Model from the Design Domain to the Operational Domain . 66
5.3 Fusing ITU − R Method with Markov Model . . . . . 67
5.4 Calculating Atmospheric Attenuation Using Historical and Predicted Data . . . . . 68
5.4.1 Calculating Rain Attenuation . . . . . 68
5.4.2 Calculating Gaseous Attenuation . . . . . 74
5.4.3 Calculating Clouds and Fog Attenuations . . . . . 80
5.4.4 Calculating Scintillation Attenuation . . . . . 85
5.5 Summary . . . . . 90

**6 Signal Attenuation Prediction and Intelligent Weather Aware Control System 92**
6.1 Introduction . . . . . 92
6.2 Calculating Total Attenuation from Historical Data and
Predicted Data . . . . . 93
6.2.1 Calculating Atmospheric Attenuations Using Historical Data . . . . . 93
6.2.2 Calculating Atmospheric Attenuation Using Predicted Data . . . . . 94
6.2.3 Free Space Calculation . . . . . 95
6.2.4 Calculating Total Attenuation . . . . . 96
6.3 Intelligent Weather Aware Control System . . . . . 97
6.3.1 Decision Support System . . . . . 101
6.4 Relating Total Attenuation with Signal to Noise Ratio . . . . . 103
6.5 Signal to Noise Ratio Adjustment . . . . . 108
6.6 Simulation Results and Discussions . . . . . 109
6.7 Summary . . . . . 119

**7 Conclusions and Future Works 120**
7.1 Conclusions . . . . . 120
7.2 Future Works . . . . . 122

**References** 124

**Appendix** 131

**Appendix A – Rainfall Rate Calculation and Bi-Linear Interpolation Code** 132

**Appendix B – Rain Attenuation Calculation Code Using Historical Data** 143

**Appendix C – Total Attenuation Calculation Code Using Historical Data** 155

**Appendix D – Total Attenuation Calculation Code Using Predicted Data** 161

**Appendix E – Signal to Noise Ratio Calculation Code** 166

# List of Tables


2.1 VSAT Frequency Spectrum Allocation. . . . . 15

2.2 Gas Molecules Percentage in The Atmosphere. . . . . 18

3.1 Data Format. . . . . 28

3.2 Bi-Linear Interpolation. . . . . 31

3.3 Variables as Defined by ITU − R. . . . . 33

3.4 Rain Attenuation Comparison Between ITU − R Original and Approximation Methods at Different Frequencies for $F_s = 30$ and $\theta = 40$. . . . . 41

3.5 Rain Attenuation Comparison Among ITU − R Original Method, ITU − R Approximation Method, and Iterative Approximation Method (IAM) at Different Frequencies. . . . . 47

4.1 Comparison of Accurate and Predicted Rainfall Rate Data at Different Time. . . . . 61

6.1 Noise Temperature in Antenna. . . . . 105

6.2 Forward Link Modes and Performance at Vancouver Station for Propagation Angle $= 30\ Degrees$ and Frequency of Operation $= 20\ GHz$. . . . . 112

6.3 Forward Link Modes and Performance at South West of King City Station for Propagation Angle $= 45\ Degrees$ and Frequency $= 20\ GHz$. . . . . 113

# List of Figures


1.1 A satellite broadcast system in the presence of horrendous weather conditions. . . . 2

2.1 Scintillation attenuation effect on signal propagation along the path. . . . . 21

2.2 Free space effect on signal propagation. . . . . 23

3.1 Grid point location. . . . . 30

3.2 Earth space path. . . . . 34

3.3 ITU – R Original and Approximation Methods for small rainfall rate. . . . . 40

3.4 ITU – R Original, ITU – R Approximation, and IAMs comparison for relatively high rainfall rate and low sample frequency ($F_s$). . . . . 43

3.5 ITU – R Original, ITU – R Approximation, and IAMs comparison for relatively high rainfall rate and medium sample frequency ($F_s$). . . . . 44

3.6 ITU – R Original, ITU – R Approximation, and IAMs comparison for relatively high rainfall rate and large sample frequency ($F_s$). . . . . 45

4.1 Presentation of the five rainfall rate classes. . . . . 52

4.2 Presentation of the three different weights. . . . . 54

4.3 First Order Markov Chain model with transition probabilities for switching between states. . . . . 55

4.4 Comparison of random data and predicted rainfall rate values. . . . . 59

4.5 Comparison of actual and predicted rainfall rate values at South West of King City. 60

5.1 Rain attenuation – function of rainfall rate and propagation angle at Hazelton Station, Canada. . . . . 71
5.2 Rain attenuation – function of rainfall rate and frequency at Atlin Station, Canada. 72
5.3 Predicted rain attenuation – function of predicted rainfall rate and propagation angle at South West of King City Station, Canada. . . . . 74
5.4 Gaseous attenuation – function of rainfall rate and propagation angle at Hazelton Station, Canada. . . . . 78
5.5 Gaseous attenuation – function of rainfall rate and frequency at Atlin Station, Canada. . . . . 79
5.6 Predicted gaseous attenuation – function of predicted rainfall rate and propagation angle at South West of King City Station, Canada. . . . . 80
5.7 Clouds and fog attenuations – function of rainfall rate and propagation angle at Hazelton Station, Canada. . . . . 83
5.8 Cloud and fog attenuations – function of rainfall rate and frequency at Atlin Station, Canada. . . . . 84
5.9 Predicted cloud and fog attenuations – function of predicted rainfall rate and propagation angle at South West of King City Station, Canada. . . . . 85
5.10 Scintillation attenuation – function of rainfall rate and propagation angle at Hazelton Station, Canada. . . . . 88
5.11 Scintillation attenuation – function of rainfall rate and frequency at Atlin Station, Canada. . . . . 89
5.12 Predicted scintillation attenuation – function of predicted rainfall rate and propagation angle at South West of King City Station, Canada. . . . . 90

6.1 Atmospheric attenuations – function of rainfall rate and propagation angle at Hazelton Station, Canada. . . . . 95

6.2 Predicted atmospheric attenuation – function of predicted rainfall rate and propagation angle at South West of King City Station, Canada. . . . . 96
6.3 Predicted total attenuation – function of predicted rainfall rate and propagation angle at South West of King City Station, Canada. . . . . 97
6.4 Intelligent weather aware control system for satellite networks. . . . . 99
6.5 Network optimization decision support system . . . . . 102
6.6 Output SNR at Vancouver Station, Canada. . . . . 106
6.7 Output SNR at South West of King City Station, Canada. . . . . 107
6.8 Output Adjusted SNR at Vancouver Station, Canada. . . . . 109
6.9 Output SNR at Vancouver Station, Canada. . . . . 110
6.10 Output SNR at Vancouver Station, Canada. . . . . 111
6.11 Adjusted output SNR at South West of King City Station, Canada. . . . . 113
6.12 Output SNR at South West of King City Station, Canada. . . . . 114
6.13 Output SNR at South West of King City Station, Canada. . . . . 115

# List of Abbreviations

| | |
|---|---|
| ACTS | Advanced Communications Technology Satellite |
| Ar | Argon |
| BER | Bit Error Rate |
| $CH_4$ | Methane |
| $CO_2$ | Carbon Dioxide |
| CPU | Central Processing Unit |
| DSCP | Defense Satellite Communications Program |
| DSS | Decision Support System |
| ECM | Electronic Countermeasures |
| FCM | Fade Countermeasure |
| He | Helium |
| $H_2O$ | Water Vapour |
| IAM | Iterative Approximation Method |
| IDSCP | Initial Defense Satellite Communications Program |
| IS | Intelligent System |
| ISS | Intelligent Satellite Service |
| ITU-R | International Telecommunication Union-Radiocommunications |
| IWACS | Intelligent Weather Aware Control System |
| Kr | Krypton |

| | |
|---|---|
| $N_2$ | Nitrogen |
| Ne | Neon |
| NO | Nitrogen Oxide |
| $N_2O$ | Nitrous Oxide |
| $NO_2$ | Nitrogen Dioxide |
| $O_2$ | Oxygene |
| $O_3$ | Ozone |
| QoS | Quality of Service |
| RA | Rain Attenuation |
| $RR_{ep}$ | Rainfall Rate for Exceed Percentage Probability |
| $RR_{pr}$ | Predicted Rainfall Rate |
| SLA | Service Level Agreement |
| SNR | Signal to Noise Ratio |
| $SO_2$ | Sulphur Dioxide |
| TVRO | Television Receive Only |
| T1VSAT | T1 Very Small Aperture Terminals |
| US | United States |
| USSR | Union of Soviet Socialist Republics |
| VSAT | Very Small Aperture Terminal |

# List of Symbols

| Symbol | Definition |
|---|---|
| $A_0$ | Free space attenuation |
| $A_{Cloud\&Fog}$ | Cloud and fog attenuations |
| $A_{Gas}$ | Gaseous attenuation |
| $A_{Rain}$ | Rain attenuation |
| $A_{Scintillation}$ | Scintillation attenuation |
| $A_t$ | Total attenuation |
| $A_W$ | Atmospheric attenuations |
| $B_r$ | Equivalent bandwidth |
| $d$ | Distance between transmitter and receiver |
| $D$ | Geometrical diameter of the earth-station antenna |
| $D_{eff}$ | Effective antenna diameter |
| $\varepsilon_0$, $\varepsilon_1$, $\varepsilon_2$ | Complex dielectric permittivities of water |
| $E_{ep}$ | Earth-space path |
| $ep$ | Exceed percentage probability |
| $E_s$ | Symbol energy |
| $\eta$ | Antenna efficiency |
| $f$ | Frequency |
| $f_l$ | Lowest frequency of interest |

| | |
|---|---|
| $f_h$ | Highest frequency of interest |
| $F_s$ | Sample frequency |
| $F_{ep}$ | Frozen precipitation |
| $f_p$ | Principal relaxation frequency |
| $f_{sc}$ | Secondary relaxation frequency |
| $\gamma_0$ | Dry air attenuation |
| $\gamma_v$ | Water vapour attenuation |
| $G_r$ | Received antenna gain |
| $G_t$ | Transmitted antenna gain |
| $h_0$ | Mean $0°C$ isotherm height above mean sea level |
| $h_L$ | Height of the turbulent layer |
| $h_R$ | Mean rain height above mean sea level |
| $h_v$ | Equivalent height for water vapour |
| $h_S$ | Height above mean sea level of earth station |
| $K$ | Boltzman constant |
| $K_H, \alpha_H$ | Constant coefficients of horizontal polarization |
| $K_t$ | Specific attenuation coefficient |
| $K_\tau, \alpha_\tau$ | Frequency-dependent coefficients |
| $K_V, \alpha_V$ | Constant coefficients of vertical polarization |
| $L_E$ | Effective path length |
| $L_G$ | Horizontal projection |

| | |
|---|---|
| $L_{ep}$ | Liquid precipitation |
| $L_R$ | Actual slant-path length |
| $L_S$ | Slant-path length below rain height |
| $L_{Scintillation}$ | Effective path length for scintillation |
| $L_w$ | Total columnar content of liquid water |
| $L_v$ | Statistics of the total columnar content |
| $\lambda$ | Wavelength |
| $M$ | Integration of liquid water density |
| $M_C$ | Average annual convective rainfall amount |
| $M_S$ | Average annual stratiform rainfall amount |
| $N$ | Noise power |
| $N_0$ | Thermal noise power spectral density |
| $N_r$ | Noise figure of low-noise amplifier |
| $N_{wet}$ | Radio refractivity |
| $p$ | Probability |
| $P_0$ | Transition probability matrix of the zero-order Markov Chain |
| $P_1$ | Transition probability matrix of the first-order Markov Chain |
| $P_2$ | Transition probability matrix of the second-order Markov Chain |
| $ph$ | Pressure |
| $P_{ep}$ | Percentage probability of rainfall |
| $P_r$ | Received power |

| | |
|---|---|
| $P_R$ | Probability of rainy periods |
| $pr$ | Exceed percentage probability according to predicted rainfall rate |
| $P_t$ | Transmitted power |
| $P(x)$ | Zero-order Markov Chains |
| $P(x, y)$ | First-order Markov Chains |
| $P(z\|xy)$ | Second-order Markov Chains |
| $R_e$ | Effective radius of earth |
| $R_h$ | Rain height |
| $\rho$ | Latitude of the earth station |
| $\rho_w$ | Water vapour density |
| $r_p$ | Horizontal reduction factor |
| $r_{ph}$ | Pressure factor |
| $R_s$ | Transmission rate |
| $\sigma_{ref}$ | Standard deviation of the signal amplitude |
| $T$ | Effective noise temperature |
| $\theta$ | Propagation angle |
| $\tau$ | Polarization tilt angle relative to the horizontal |
| $T_a$ | Antenna noise temperature |
| $t_k$ | Temperature in $Kelvin$ |
| $T_r$ | Noise temperature of the receiver |
| $T_s$ | Symbol duration |

| | |
|---|---|
| $v_p$ | Vertical adjustment factor |
| $W(0)$ | Present weight |
| $W(1)$ | Previous one hour weight |
| $W(2)$ | Previous two hours weight |
| $X$ | Longitude |
| $Y$ | Latitude |

# Chapter 1

# Introduction

Recently, satellite based communications networks at Ku and Ka bands have been rapidly expanding. These high frequency operations have enabled a wide variety of available and potential applications and services including communications, navigation, tele-medicine, remote sensing, distributed sensors networks, and wireless access to the Internet. However, at high frequencies, weather can cause significant variations in signal level, phase, polarization tilt angle relative to the horizontal, and angle of arrival. These effects are broadly known as signal attenuations which varies with parameters such as location, frequency of operation, transmission power, propagation angle, modulation, coding, and transmission rate. The impact eventually translates into degeneration of Quality of Service (QoS) in networks, which is explained later in this thesis. Thus, due to new bandwidth and frequency requirements, the problems of attenuations due to various atmospheric factors have come to receive increased level of prominence. The problem becomes particularly pronounced at frequencies above 10 $GHz$ [1–5].

Signal propagation for satellite networks has a long path from the source to the destination. Therefore, it is immensely susceptible to attenuations mainly caused by weather factors for different satellite functions and service providers as shown in Figure 1.1 [1, 2, 6–8]. The major atmospheric and weather related factors in signal attenuation are rain fade, gaseous absorption, cloud

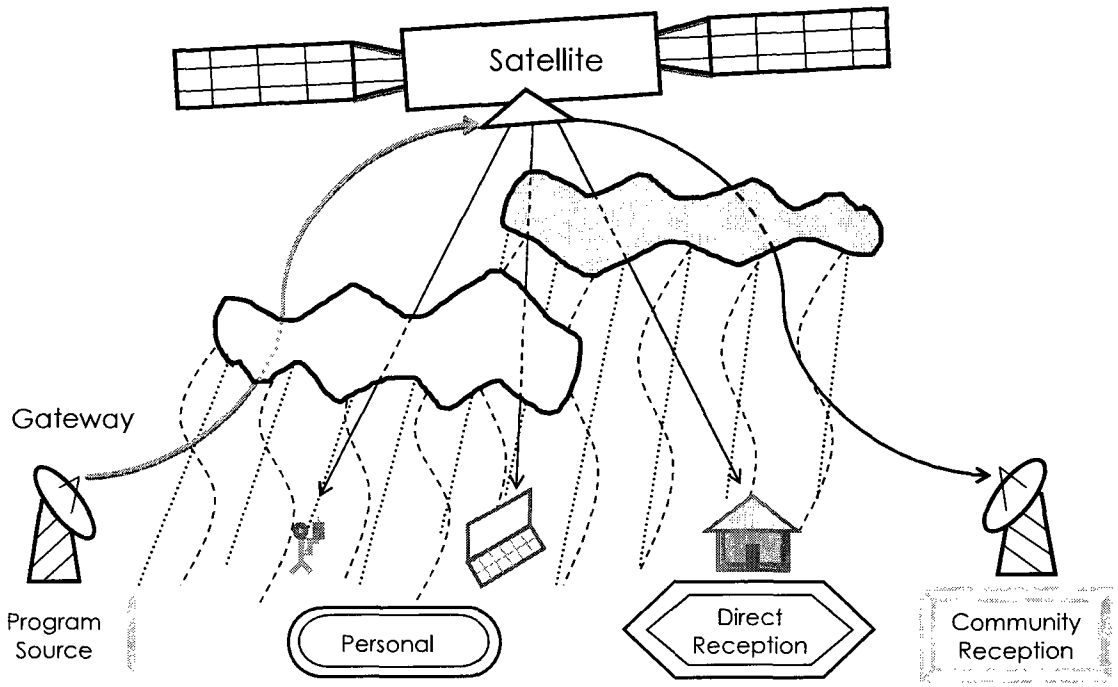


**Figure 1.1:** A satellite broadcast system in the presence of horrendous weather conditions.

and fog attenuations, and tropospheric scintillation. Among them, the rain attenuation (RA), also known as rain fade, is the dominant cause of signal impairment, especially at frequencies higher than 10 $GHz$ and in a variety of applications including Very Small Aperture Terminal (VSAT) and Television Receive Only (TVRO) [7–12].

Control systems attempt to minimize the effect of attenuation by adjusting the transmission parameters and signal characteristics. In doing that, the existing systems relay the knowledge of atmospheric attenuation, to activate appropriate transmission control. The consequence is that the optimality and effectiveness of the control of transmission parameters is dependent on the accuracy of the detailed knowledge of occurrence probabilities for different impairments. Knowing the

expected impairments due to different attenuation factors, more specifically the non-uniformity of weather factors, would help us utilize the appropriate control for mitigating impairments. This is achieved by actuating the right combination of characterizations like up-link power control, adaptive coding, antenna beam shaping, and site diversity [13, 14], and, therefore, improve QoS provisioning.

## 1.1 Research Overview

Weather impacts in satellite communications are widely discussed in literature. Empirical methods could be found for estimating signal attenuation based on weather condition. Of all, the methodology developed by International Telecommunication Union-Radiocommunications ($\mathrm{ITU-R}$) is widely used in the industry [15–18].

Other prior works could also be found in related areas. For example, in [14], authors present prediction models and analytical techniques for a range of operational parameters involving low margin, low propagation angle, inclined geosynchronous, and low earth orbit systems. The paper estimated rain and scintillation attenuations while assuming gaseous attenuation as constant. Authors of [19] present a statistical analysis of rain fade data on satellite to ground propagation path. Authors of [20] presented a method for rain attenuation prediction which yielded good results during low rain and low propagation angle. Cumulative distribution of rainfall rate and the risk of exceeding rain fade margin in monthly and yearly basis has been estimated in [21]. An empirical model is proposed in [22] based on statistical measurements at $\mathrm{Ku}$ and $\mathrm{Ka}$ bands for fade duration as a function of attenuation and frequency. The work cited in [23] uses modeling of channels to obtain signal attenuation due to clouds and precipitation. It presents an empirical model for fade duration prediction as a function of rain attenuation and frequency without considering other weather factors. Authors of [24] predicted rainfall rate ($\mathrm{RR_{pr}}$) by using weather radar reflection data instead of ground based measurement. The work presented in [25] discusses a method, called two level Markov model, to predict multi-path fading of signals. While [26], cites difficulty

in approximating the losses due to limited availability of experimental data on clouds, [27] cites problem in developing accurate models due to ambiguity of cloud water content and cloud's extent limit. These techniques have helped to mature the control systems in satellite communication. Lately, emerging frequency requirements have brought the problems of atmospheric attenuations to prominence.

Empirical approaches that deal only with combined effects are in prevalence due to absence of detailed knowledge of occurrence probabilities for different impairments. Nevertheless, the knowledge of expected total impairment is used to select appropriate methods for mitigating impairments. Some of these methods include up-link power control, adaptive coding, antenna beam shaping, and site diversity [13, 28].

ITU − R maintains a large database for probability of precipitation and other parameters. It provides mathematical equations and analytical approaches to estimate rainfall rate and different atmospheric attenuations around the world from this data. However, ITU − R techniques were developed in view of finding the average conditions and the boundary conditions, which are more useful for the design of control system and less for the day-to-day operation of those systems. Moreover, ITU − R techniques were developed at a time when the high frequency operations above Ku − band, where losses become really significant, were not expected. Consequently, there was a great room to, first, improve the ITU − R techniques to keep them accurate at higher frequency operations, and, second, to decouple them from the fifteen years average data provided by ITU − R [10, 15, 16, 29]. However, if we are able to make them work with predicted weather data, those techniques could help satellite service providers achieve better operation, as much as they helped in the system design in the past [7, 9, 30, 31].

Thus, signal fading caused by different weather conditions limits the QoS of satellite links and system availability. In order to prevent the loss of signal due to attenuation, satellite service providers transmit signals down with extra power in areas with extreme weather conditions. This extra power is called rain fade margin. For example, users can still be watching television during

rain from home satellite dishes, when the loss of signal strength due to rain is less than the rain fade margin. Users will lose picture when signal loss exceeds the rain fade margin; this occurs when there is enough water in the atmosphere to completely block the signal, or more likely, when the signal loss caused by the combination of water in the atmosphere and water on the dish exceeds a threshold.

Moreover, transmission power cannot be increased beyond a specified level due to safety regulations [32, 33]. Therefore, the fade countermeasure (FCM) system must also employ various other ways to increase system's throughput and availability.

Signal to noise ratio (SNR) achieved at the receiver's end, which is a measure of signal strength for satellite signal relative to attenuations and background noise, plays an important role for the returned feedback to the transmitter for the selected parameters.

Properly predicting atmospheric attenuations can support mitigation planning by adaptively selecting appropriate power level, coding, and modulation to maintain Service Level Agreement (SLA). For this to happen, there are different tradeoff parameters that should be dealt with in order to get appropriate results. Thus, efficient weather prediction is an important factor in order to improve QoS in satellite networks. Some of the main factors that can be controlled for better performance under different weather conditions include: Changing data rate, type of modulation, coding, frequency, signal power, and frame size [3, 34].

Despite many notable work done regarding weather characteristics in satellite networks, the need for techniques that would estimate attenuation and apply effective control of high frequencies, high rainfall rate, and severe weather conditions, has been tremendous since most of the existing works consider low rainfall rate. Similarly, provisioning of the propagation of signal characteristics in weather impacted satellite networks for reliable satellite communications merits further investigations especially in developing computationally efficient prediction control methods. This need for computationally efficient models for accounting challenging propagation environments and predicting parameters for satellite networks have already been well documented [13, 14, 19–23, 28].

Our preliminary research in this problem [3] demonstrated that a better control of satellite signal parameters and improved system performance could be achieved by taking into account the major weather related contributors of signal attenuation separately. Our methodology of predicting rainfall rate and then using that estimated attenuation due to rain, gas, cloud, fog, and scintillation yielded greater accuracy in estimating weather related attenuation. This work estimated constituent weather related attenuations for reasonable rainfall conditions and for different propagation angles and frequencies of operation at a given location. However, in doing so, this work had to rely on historical data collected by ITU – R that provided an average rainfall in a yearly basis for specific locations throughout the world, based on fifteen years of historical data. During the research, it was realized that the tuning of channel parameters achieved through that methodology could have been further enhanced if real-time measurements were used to gain a closer forecast of weather conditions. The work reported in this thesis was inspired by that premise. And, as research thrust has been put to improving QoS on satellites based networks with the use of intelligent prediction methods on signal quality in presence of weather related attenuation. The work presented in this thesis should be of significant interest to the research community.

Moreover, the proposed method yields flexible system based on optimized algorithms that lends control based on weather prediction that made with actual data. Consequently, it should allow the control systems to better react with impending weather entities before problems actually manifest. Therefore, it is believed that this work should mount to a noticeable contribution to improve the control of satellite networks.

## 1.2 Thesis Contributions

The contributions towards improving the operation of satellite communication systems, made by the work reported in this thesis, include the following:

1. A new rain attenuation calculation method, named Iterative Approximation Method (IAM),

which brings marked improvements over ITU – R methods currently in use; it also extends the accuracy of calculations of rain attenuation over a wide range of signal frequency, propagation angle, and rainfall rate not achieved by the existing techniques.

2. Extensions of ITU – R method for calculating rain, gas, cloud, fog, and scintillation attenuations so as to factor rainfall rate, frequency, and propagation angle in calculation.

3. Introduction of a three dimensional relationship model for estimating atmospheric attenuations in relation to rainfall rate, frequency, and propagation angle; the method thus results in faster decision making and improved responsiveness.

4. A new approach for predicting rainfall rate based on actual weather data and Markov theory.

5. A methodology for estimating attenuations due to rain, gas, cloud, fog, and scintillation based on rainfall rate prediction made in contribution 4.

6. An improved estimation of attenuation and control of transmission parameters compared to improvements made in contribution 1 and contribution 2.

7. An enhanced intelligent weather aware control system (IWACS) based on the decision support system (DSS) technique for achieving improved channel performance that takes into account the models of predictions described above.

### 1.2.1 Published, Accepted, and Submitted Papers

Based on this work, several papers have been published, accepted, and submitted. They are:

- K. Harb, A. Srinivasan, C. Huang, and B. Cheng, "QoS in Weather Impacted Satellite Networks," *Proc. of Pacific Rim Conference on Communications, Computers and Signal Processing*, pp. 178-181, Aug. 2007.

- K. Harb, A. Srinivasan, C. Huang, and B. Cheng, "Prediction Method to Maintain QoS in Weather Impacted Wireless and Satellite Networks," *Proc. of Systems, Man and Cybernetics (SMC)'07*, pp. 4008-4013, Oct. 2007.

- K. Harb, A. Srinivasan, C. Huang, and B. Cheng, "Intelligent Weather Aware Scheme for Satellite Systems," *Proc. of IEEE International Conference on Communications (ICC)'08*, pp. 1930-1936, May 2008.

- K. Harb, A. Srinivasan, C. Huang, and B. Cheng, "Intelligent Weather Systems with Fuzzy Logic Controller for Satellite Networks," *Proc. of IEEE Wireless Communications and Networking Conference (WCNC)'08*, pp. 3069-3074, March 2008.

- K. Harb, F. R. Yu, P. Dakhal, and A. Srinivasan, "A Decision Support Scheme to Maintain QoS in Weather Impacted Satellite Networks," *Proc. of Atmospheric and Space Environments Conference (AIAA)'10*, Canada, Aug. 2010.

- K. Harb, F. R. Yu, P. Dakhal, and A. Srinivasan, "An Intelligent QoS Control System for Satellite Networks Based on Markovian Weather," *Proc. of IEEE Vehicular Technology Conference (VTC)'10*, Sept. 2010.

- K. Harb, F. R. Yu, P. Dakhal, and A. Srinivasan, "Performance Improvement in Satellite Networks Based on Markovian Weather Prediction," to be presented at *IEEE Globecom'10*, Miami, FL, USA, Dec. 2010.

- K. Harb and F. R. Yu, "Signal Adaptation via Intelligent Controller Systems in Weather Impacted Satellite Networks," submitted to *ACM/Springer Telecommunication Systems*, 2010.

- K. Harb, F. R. Yu, P. Dakhal, and A. Srinivasan, "Intelligent Decision Controller for Provisioning Satellite Networks Based on Atmospheric Attenuations at High Frequencies," submitted to *ACM/Springer Wireless Networks*, 2010.

- K. Harb, F. R. Yu, P. Dakhal, and A. Srinivasan, "Performance Improvement in Satellite Communication Networks Based on Markovian Weather Prediction," submitted to *International Journal of Satellite Communications and Networking*, 2010.

## 1.3 Thesis Organization

The rest of this thesis is organized as follows. In Chapter 2, background and literature review are presented. Estimating the effect of rainfall rate on satellite communication links is then described in Chapter 3. Chapter 4 describes prediction of rainfall rate based on Markov modeling of weather characteristics. Chapter 5 describes the calculation of atmospheric attenuation such as rain, gaseous, cloud, fog, and scintillation attenuations. Signal attenuation prediction and the relationship with intelligent weather aware control systems for impacted atmospheric conditions is presented in Chapter 6. Finally, the conclusion of this thesis is presented in Chapter 7.

# Chapter 2

# Background and Literature Review

## 2.1 Introduction

Satellite communications were first used for military communications applications. These services, later on, were open to public for different usages such as long distance telephone network and television. Starting in 1990's, another task was added to satellite communication technology, which was the connection to the Internet via broadband data connections. Thus, the satellite communication experience has demonstrated that satellite systems can satisfy many military and civilian requirements. Satellite communications are reliable, survivable, secure, and cost effective. They can be easily identified as the ideal, if not often the only, solution to problems of communicating with highly mobile forces. This chapter will provide a brief overview on satellite communication and the impacts of atmospheric attenuations such as rain, gas, cloud, fog, and scintillation attenuations on satellite communications.

## 2.2 Satellite Communications Background

The orbiting of an artificial satellite, Sputnik, launched by the Union of Soviet Socialist Republics (USSR) in 1957, signaled the beginning of satellite communication era. The United States (US), who was in a technological race with USSR, made an all-out effort to catch up and launched its own satellite in 1958. It was the first earth satellite of the US as part of the program for the International Geophysical Year. The first regular satellite communications service was used by the US Navy in 1960. The moon was used to bounce teletypewriter signals between Hawaii and Washington, D.C., USA, during the early 1960s, thus passing messages between ships at sea and shore stations. This method of communications proved reliable when other methods failed [35, 36].

Foreseeing many profound applications, various branches of military were given resources to support their communication research and development needs. Considering the primitive state of satellite communication, large-scale improvements were sought to satisfy future needs of the Department of Defense. These needs included greater capacity for long-haul communications to previously inaccessible areas. Therefore, communications via satellites were considered a natural outgrowth for modern technology and for the continuing demand of greater capacity and higher quality in communications [5, 18, 37].

The Defense Satellite Communications Program (DSCP) of USA was initiated in 1962 [1]. In Phase I, the program was the stepping stone to Initial Defense Satellite Communications Program (IDSCP) where high quality voice transmissions were conducted between a satellite and two earth stations [38]. Experience with satellite communications has demonstrated that satellite systems can satisfy many military requirements. They are reliable, survivable, secure, and a cost effective method of telecommunications.

In the 1970s, the high frequency spectrum was overcrowded and free frequencies were at a premium. High frequency jamming and Electronic Countermeasures (ECM) techniques became highly sophisticated during that period. As a result, the need for new and advanced long-range

transmission methods became apparent.

Phase II of DSCP changed from an all-analog communications system to an all-digital communications system. The performance capability provided by Phase II DSCP was limited by equipment availability. Phase II satellites provided a great increase in effective radiated power and RF bandwidths. These satellites used wide coverage and narrow beam antennas [35, 38].

In 1972, Canada launched its first domestic communication satellite by TELESAT, Anik A1, to serve the vast Canadian continental area. It acts as space repeaters capable of receiving transmissions from earth stations and retransmitting them to other earth stations in Canada. The antenna coverage of the satellite provides the capability of serving virtually all of Canada. TELESAT Canada is a Canadian satellite communications company founded on May 2, 1969. The company is headquartered in Ottawa, Ontario as well as having offices in the United States and Brazil. It has launched several satellites and became one of the leaders in the satellite communication domain [39].

There are currently six companies providing fixed satellite service to the U.S.: GE Americom, Alascom, AT&T, COMSAT, GTE, and Hughes Communications. They operate thirty six satellites with a net worth over four billion dollars. The ground stations which communicate with these satellites are innumerable and may have a similar net worth. Canada has joined United States (1974) after launching the first domestic satellite service, followed by Indonesia (1976), Japan (1978), India (1982), Australia (1985), Brazil (1985), Mexico (1985), and many others [40]. INTELSAT has had competition in the international market from Pan American Satellite since 1986. Each year 10 to 20 communications satellites are launched in space.

The following section present electromagnetic waves and their relationship with satellite communication media.

## 2.3 Electromagnetic Waves and Their Relationships with The Medium

The careers of satellite communication signals are especially created electromagnetic waves consisting of electric and magnetic field components. In most practical cases these waves self-propagate in a vacuum or in any other medium [41]. The components oscillate in phase perpendicular to each other and perpendicular to the direction of energy propagation. Electromagnetic waves are classified into several types according to their frequency, examples being radio waves, microwaves, tera-hertz radiation, infrared radiation, visible light, ultraviolet radiation, X – rays, and Gamma – rays.

Radio waves can be made to carry information by varying a combination of amplitude, frequency, and phase of the wave within a frequency band.

When electromagnetic radiation impinges upon a conductor, it couples to the conductor, travels along it, and induces an electric current on the surface of that conductor by exciting the electrons of the conducting material. This effect (called skin effect) is used in antennas. Electromagnetic radiation may also cause certain molecules to absorb energy and thus to heat up; this is exploited in microwave ovens.

Electromagnetic radiation carries energy and momentum that may be imparted to matter with which it interacts. Of all the characteristics, we are interested in the following for improving the QoS in satellite networks:

1. Frequency: Sending more information requires the usage of high frequency operation, and sending signal over a long distance requires low frequency operation.

2. Path length: Signal attenuations varied widely with distance between transmitter and receiver. The greater the distance, the higher the signal losses. However, the locations of stations are often dictated by needs and, therefore, there is less flexibility in altering the path

length.

3. Propagation angle: As propagation angle increases from around 5 $degrees$ up to 90 $degrees$, the path length becomes shorter and attenuations decrease. However, propagation below 5 $degrees$ suffer largely from fog and cloud as the path length reaches its maximum. Usually, this propagation is used in the case of reflection from the first sky layers.

4. Transmit power: This factor has some limitations according to safety and health requirements. However, to offset signal attenuation power could be increased up to its maximum allowable level.

Satellite signals pan through rain, snow, and other condition on the way. But in general, weather conditions have little to no effect on RF signal of a 2.4 $GHz$ system. For 2.4 $GHz$ systems, you may find attenuation up to 0.08 $dB/mile$ (0.05 $dB/km$) in a heavy rain condition (4 $inches/hr$). A thick fog may result in as much as 0.03 $dB/mile$ (0.02 $dB/km$) attenuation. However the loss become significant at Ku and Ka bands [3, 8, 42].

In fact, terrestrial microwave transmissions are more susceptible to the effects of rain attenuation because their signal paths are entirely in the troposphere and the signal may pass through an entire rain cell. Table 2.1 shows the relationships of frequency bands with rainfall rate and their coverage area [43]. It could be noted that for C – band signals to be affected by rain, it would require a rain storm approaching hurricane conditions. On the contrary, Ku and Ka bands are highly susceptible to rain. These results and their effects are discussed later on in this thesis.

## 2.4 Impacts of Atmospheric Attenuations on Satellite Communications

Atmospheric attenuations refer to the weakening of data signals as they travel through a respective media. As the signal travels through the media, it encounters various forms of resistances to

**Table 2.1:** VSAT Frequency Spectrum Allocation.

| **Band** | **Frequency** $GHz$ | **Area Foot-print** | **Power Delivered** | **Rainfall effect** |
|---|---|---|---|---|
| C | $3-7$ | Large | Low | Minimum |
| Ku | $10-18$ | Medium | Medium | Moderate |
| Ka | $18-31$ | Small | High | Severe |

signal propagation. Thus signals encounter loss as they pass through the atmospheric layers under different weather conditions [12]. The extent signal interaction with the media depends on the inherent characteristics of the signal, such as the carrier frequency.

Transmissions at $\mathrm{C}-$ band, which has longer wavelength than transmissions at $\mathrm{Ku}-$ band, were less susceptible to different weather attenuations. For example, $\mathrm{L}-$ band radars, that are used for clear air turbulence studies, operate on a wavelength and frequency of around ($\lambda = 20$ cm) and 1.5 $GHz$, respectively. $\mathrm{S}-$ band radars operate on a wavelength of ($\lambda = 15$ cm $\sim 7.5$ cm) and a frequency of (f $= 2 \sim 4$ GHz). $\mathrm{C}-$ band frequency has a wavelength of approximately ($\lambda = 7$ cm), $\mathrm{X}-$ band radars operate on a wavelength of ($\lambda = 3$ cm) and a frequency of (f $= 10$ GHz) and $\mathrm{Ku}-$ band frequency (f $= 12.6 \sim 18.6$ GHz) has a wavelength of approximately ($\lambda = 2.380$ cm $\sim 1.612$ cm). Any raindrop in the path of either signal, which approaches half the wavelength in diameter, will cause attenuation [43–45].

Rain attenuation's impairment for satellite signals becomes particularly severe as the frequency increases. In $\mathrm{C}-$ band, it is not as critical as that in higher bands as shown in Table 2.1. However, the diameter of a raindrop is definitely detrimental for $\mathrm{Ku/Ka}-$ band signal's passage. It is to be noted, $\mathrm{Ku}-$ band attenuation in rain is approximately nine times that of $\mathrm{C}-$ band [44–47]. In general, weather conditions have little to no effect on the RF signal of a 2.4 $GHz$ system.

These attenuations become particularly severe at frequencies higher than 10 $GHz$, especially for small aperture antenna such as VSAT and TVRO [1,9,30,43,48]. Weather attenuation – which is considered the dominant cause for signal impairment – is a function of frequency, propagation angle, rain intensity, raindrop size distribution, and raindrop temperature [20, 23]. Fades of larger

than 20 $dB$ were observed at least 0.1 % of the time in subtropical rain zones and 0.01 % of the time in a dry rain zone [22]. Also, the effect of clouds is around 2 $dB$ for all rain zones. Accurately computing the effect of different weather attenuations on satellite networks [12–14, 49], remains one of the main motivations of this thesis.

ITU − R manages a detailed coordination and recording procedures for using weather data for space systems and earth stations. ITU − R processes and publishes data as well as carrying out the examination of frequency assignment notices submitted by governments for inclusion in the formal coordination procedures or recording in the Master International Frequency Register. ITU − R - also provides several years of data for average rainfall rate at a given location on earth, other propagation variable such as height above mean sea level, and signal parameters. All these parameters are used to compute different weather attenuations such as rain, gaseous, cloud and fog, and scintillation attenuations [7, 15, 29, 50] for specific coordinates throughout the world.

### 2.4.1 Rain Attenuation

Rain attenuation (RA) is one of the most common and often most misunderstood and complicated phenomena that affects satellite signals. Rain attenuation is all about signal absorption and the scattering of incoming signal. By far, the greatest single event reduction in signal power is caused by rain, not so much water vapor. We first explain rain attenuation extensively and then propose solutions to control the effect of RA on satellite signal propagation.

Rain attenuation is a function of frequency ($f$), probability ($p$), propagation angle ($\theta$), polarization tilt angle relative to the horizontal ($\tau$), raindrop temperature ($t_K$), and other factors such as rain intensity and raindrop size distribution. Therefore, it is the dominant propagation impairment when facing high frequency. Also, rain fade seems to correlate very closely with the volume of raindrops along the propagation path [11, 22]. This is opposed by the common misconception that the degree of attenuation is proportional to the quantity or the individual size of raindrops falling near the receiving site [23].

Thus, determining the specific factors that lead to attenuation is crucial to properly predicting signal propagation problems along the satellite path. Models developed from this data can be used to chart the effects of rain fade on a regional or individual site basis. From this information, antenna size needed, power level, and other factors such as modulation, coding, transfer data rate, etc. can be determined in order to counteract the effects of different weather attenuations.

According to an experiment conducted at different U.S. sites over several years period, rain attenuation is the dominant cause for signal impairment at Ka – band frequencies. Rain attenuation is a function of frequency, propagation angle, rain intensity, raindrop size distribution, and raindrop temperature [8, 20–23].

This research is conducted using the Advanced Communications Technology Satellite (ACTS) system. It enables service providers to tailor a satellite system to provide quality system availability at relatively low cost. Continuing research is being performed on rain fade compensation to allow for an inexpensive Ka – band system implementation [28, 38]. The ACTS adaptive rain fade compensation protocol was developed to ensure a T1VSAT bit error rate (BER) of less than $5.10\,e-7$ for 99.5 % of total operational time of T1VSAT [51, 52]. The compensation protocol is adaptive, has decision-making capabilities, and is implemented to maintain T1VSAT performance during periods of week signal due to fade or other factors.

### 2.4.2 Gaseous Attenuation

As signals pass through the troposphere, they undergo interactions with gas molecules that are present in the atmosphere. The composition of the gas molecules presented in the atmosphere at sea level are shown in Table 2.2 [53]. In the table, the "Others" column includes Neon ($Ne$), Helium ($He$), Krypton ($Kr$), and other compounds. Such as water vapor ($H_2O$), which is a major concentration from 0 to 2 % of the others. Trace quantities of Methane ($CH_4$), Sulphur Dioxide ($SO_2$), Ozone ($O_3$), Nitrogen Oxide ($NO$), and Nitrogen Dioxide ($NO_2$) are also present in atmosphere. Each of these gas molecules interact with the propagated signal. The interactions

**Table 2.2:** Gas Molecules Percentage in The Atmosphere.

| **Gas Molecules** | **Nitrogen** $N_2$ | **Oxygen** $O_2$ | **Argon** $Ar$ | **Carbon** $CO_2$ | **Others** |
|---|---|---|---|---|---|
| Percentage | 78 | 21 | 0.9 | 0.0999 | 0.0001 |

may or may not cause loss of energy and hence attenuation. Losses are especially high near the resonances of molecules. For example, when an asymmetric molecule like that of $H_2O$ is placed in an electric field, it will try to align itself to a minimum potential with respect to the electric field. This process causes loss of signal propagation. The complex permittivity of the gas shows a resonance – the imaginary part is the absorption. The problem further complicates with temperature variation as it changes resonance frequency. The signal absorption depends on (1) the resonant frequency, (2) the concentration of gas in the atmosphere, and (3) the length of the path.

The atmospheric pressure also plays an important role in gaseous attenuation. The resonance modes of the molecules are discrete, but as the molecules are constantly in collision with each other and moving at random, the resonance lines become broadened. Notice that, below 10 $GHz$, gaseous attenuation can be ignored for most purposes [29,53].

For gaseous absorption up to almost 300 $GHz$, the important resonances are those from atmospheric oxygen and water vapour levels. The quantities and effects of resonant gases ($CO$, $NO$, $NO_2$, $N_2O$, $SO_2$, and $O_3$) are negligible compared to water vapour at typical microwave link frequencies.

Oxygen has strong bands of resonances around $57 - 60$ $GHz$ and 119 $GHz$. At sea level, the losses can mount up to 15 $dB/km$ at between 57 $GHz$ and 63 $GHz$. Water vapour has strong resonances at 22 $GHz$, 183 $GHz$, and 324 $GHz$ [3, 34, 50]. The attenuation changes with the amount of water vapour in the atmosphere. Typical analysis and results for gaseous attenuations will be discussed in the following chapters.

### 2.4.3 Cloud and Fog Attenuations

The air contains water in all temperatures. Near the surface of earth when air temperature is usually higher, the air holds much more water vapor than that of the cold air. This water at gaseous state remains invisible. However, as the warm air rises, it expands and cools. Cool air cannot hold as much water vapor as warm air. Thus, some of the vapor condenses into tiny pieces of dusts that are floating in the air and form tiny droplets around each dust particle. When very large numbers of these droplets approach together they turn out to be a visible cloud. A cloud is a large collection of very tiny water droplets or ice crystals, usually a mixture of both. The droplets are so small and light that they can float in the air.

Clouds are white because they reflect the light, including the entire visible spectrum. If the clouds get thick enough or high enough, all the light above will not make it through, hence the gray or dark look. Also, if there are lots of other clouds around, their shadow can add to the gray or multi-colored gray appearance. Clouds move with the wind. High cirrus clouds are pushed along by the jet stream, sometimes traveling at more than 150 $km/hr$.

Fog is a cloud that touches the surface of the earth. A cloud that is not a fog on lower ground may be a fog where it contacts higher grounds such as hilltops or mountain ridges [10, 42, 54–56]. Fog begins to form when water vapor condenses into tiny liquid water droplets in the air. Conversely, water vapor is formed by the evaporation of liquid water or by the sublimation of ice.

There are many different types of fog, but fog is mostly formed when southerly winds bring warm, moist air into a region, possibly ending a cold outbreak. As the warm, moist air flows over much colder soil or snow, dense fog often forms. Warm, moist air is cooled from below as it flows over a colder surface. If the air is near saturation, moisture will condense out of the cooled air and form fog. With light winds, fog near the ground can become thick and reduce visibility to zero. Fog is thus defined as cloud which reduces visibility to less than 1 $km$. Moreover, The phenomenon which is known as flash fog can be formed suddenly, and can be dissipated just as rapidly depending on what side of the dewpoint the temperature is at.

### 2.4.4 Scintillation Attenuation

Scintillation is produced by turbulent air with variations in the refractive index and signal amplitude. This term is indicative of fast fluctuations in signal's amplitude. This attenuation is caused by the changes that happens by the variation of the refractive index of the atmosphere where signal propagates over the sky. The refractive index of air depends on temperature, giving rise to refraction effects when the temperature gradient is large. It can also be caused by rainstorms, irregularities in temperature, humidity, and pressure. An example of such effects is the mirage.

This turbulence causes attenuation for communicating signals, and the attenuation significantly relies on several factors such as antenna diameter, operating frequency, rainfall rate, and propagation angle.

The losses caused by atmospheric scintillation and multi-path propagation are indistinguishable as shown in Figure 2.1. However, in satellite communications at carrier frequencies above $10\ GHz$, scintillation may play a significant role in determining the power margin, especially for low availability systems with low propagation angle and low gain antennas when compared to other attenuations such as cloud and fog. Therefore, accurate estimates of signal degradation due to these effects must be included in the design of low margin satellite communication systems, otherwise, signal cannot be received properly at the other communication sides. The assessment of the linkage between rain and scintillation attenuations during rain are then necessary to better use a given system's capacity. Notice that, increase of attenuation even by a small amount may destroy the overall of satellite communication networks [39].

The scintillation attenuation increases up to $2\ dB$ for different propagation angles and rainfall rate values for an applied frequency of above $\mathrm{Ku}-$ band. Unfortunately, there is no model available for this attenuation fading below the propagation angle of $0.5$ degree [28, 57].

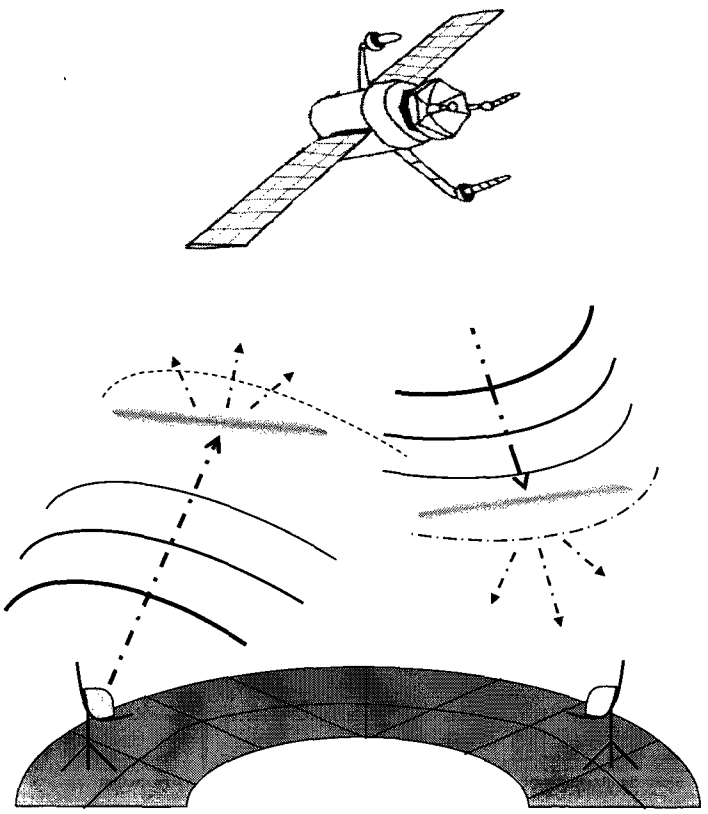

**Figure 2.1:** Scintillation attenuation effect on signal propagation along the path.

### 2.4.5 Free Space Attenuation

Free space attenuation is the loss in signal strength of an electromagnetic wave that would result from a line-of-sight path through free space as shown in Figure 2.2, with no obstacles nearby to cause reflection or diffraction. Path loss is a major component in the analysis and design of the link budget of a telecommunication system [38, 41].

Signal attenuation due to free space is primarily caused by beam divergence, as signal scattering over larger areas at increased paths from the ground station. Also, free space loss is a function of frequency of operation, propagation angle, and mainly distance between transmitter and receiver terminals as shown in Figure 2.2. The free-space path loss is proportional to the square of the distance between the transmitter and receiver, and also proportional to the square of the frequency of the radio signal. The formula of this attenuation will be explained in Chapter 5.

The most important four features of free space are [41]:

1. Uniformity everywhere: This means spatially homogeneous everywhere in the universe.

2. Free of electrical charge: Electrical charge comes in two types – positive and negative. In free space, there is no charge and so the current density flowing out of a region must result in a decrease of charge within the region.

3. Free of electric currents: An electric current is defined as a directed flow of electrons flows from a negative terminal to a positive terminal. The direction of the current flow in a material is determined by the polarity of the applied voltage. Electrons having negative charges move through a conductor in response to an electric field.

4. Infinite extent in all directions: In a free space environment, signal is able to propagate in all direction and penetrate space layers without any limitation. Signal thus fades in strength naturally as it travels from the source to the destination.

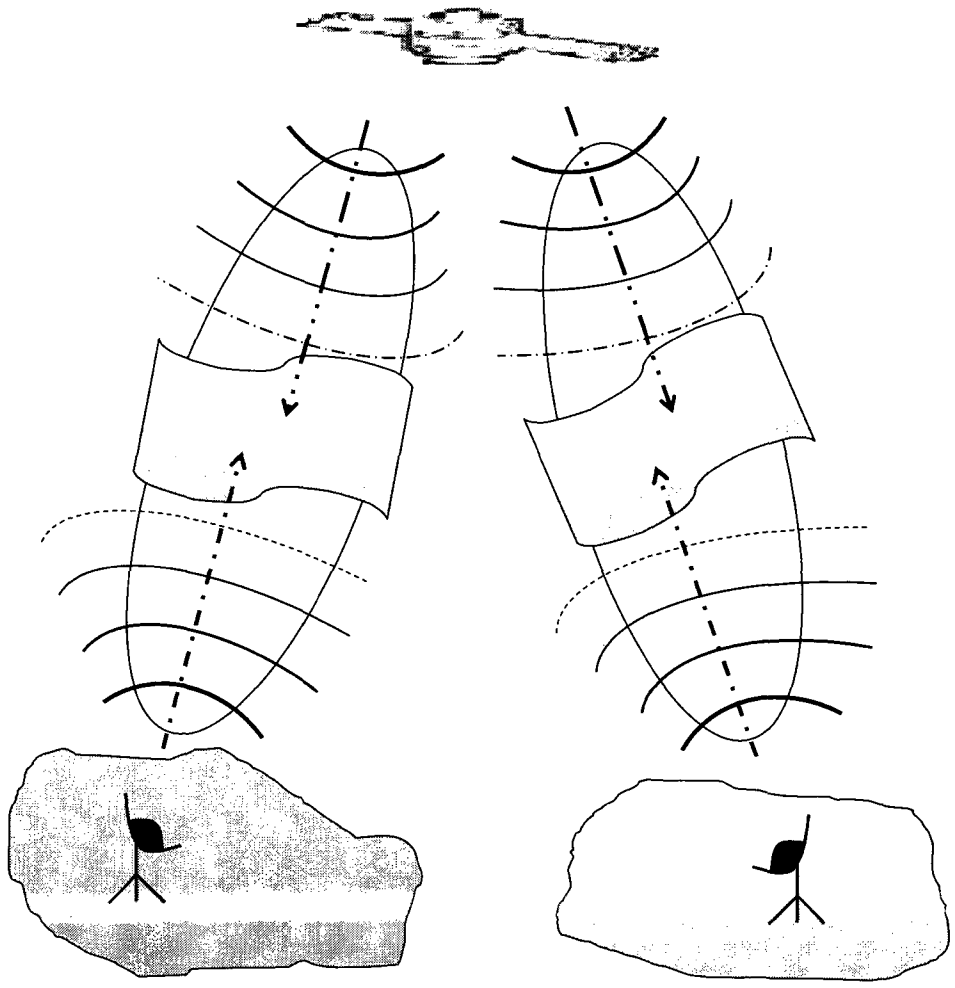

**Figure 2.2:** Free space effect on signal propagation.

## 2.5 QoS and SLA

QoS is an important requirement for satellite network users. As signal propagating between hubs and satellites, will be affected by different weather attenuations as it has to pass through several atmospheric layers. For this reason, service providers want to ensure that the signal quality received by their costumers has enough throughput to satisfy their needs. Often time the service providers and customers agree in a minimum level of throughput and availability and sign agreements called Service Level Agreements (SLA), which the providers is obliged to meet at all times.

In this thesis, we present a method to maintain QoS and SLAs by adaptively adjusting signal power, channel rate, location, propagation angle, frequency, modulation, coding, and queuing schemes to adapt with different weather conditions by the use of estimated and predicted weather knowledge.

Our main concern is based on the allocation of the maximum allowable end-to-end service quality by improving SNR. Therefore, the amount of transmission rate used for the satellite network controller is adjusted based on accurately reported statistical weather data and forecasts of service performance based on those data. Also, we will monitor the SNR at receiving end of the channel and adjust the value adjusting transmission characteristics with the use of IWACS, explained later on this thesis.

## 2.6 Summary

The satellite communication services have grown rapidly in recent times and this growth has been a global phenomenon due to economy that is requiring increased communications services. Such services are increasingly relying on higher carrying frequencies to pack greater volume of information. These higher frequencies that are carrying signals are more prone to weather losses as they pass through the earth's atmosphere. In some heavy rain conditions, it is possible for virtually all satellite signal to be absorbed by rain and other atmospheric factors such as gaseous, fog, and

cloud. These various kinds of attenuations, that can impair satellite signals, are described in depth in the following chapters.

# Chapter 3

# Estimating the Effect of Rainfall Rate on Satellite Communication Links

## 3.1 Introduction

Weather conditions have little effect on satellite signals operating at low operational frequencies. However, at higher transmission frequencies, satellite networks are greatly affected by atmospheric attenuations. This chapter introduces the existing $\mathrm{ITU}-\mathrm{R}$ methods and the Iterative Approximation Method (IAM) for calculating rainfall rate and rain attenuation [2, 9, 15, 58] combined with bi-linear interpolation and frequency extrapolation. In addition, since rain attenuation is considered a dominant impairment for wireless signal, an enhanced method for accurately determining rain attenuation is introduced as function of frequency based on processing results from a weather database.

## 3.2 Rainfall Rate Calculation

Rainfall rate is one of the factors in determining rain fade. Rain fade seems to correlate very closely both with the size of raindrops along the path of propagation and the depth of rain affected zone the signal passes through [15].

Data files are collected from ITU − R Recommendation P. 837 − 4. They represent a weather characteristic model to derive rainfall rate $RR_{ep}(Lat,\ Long)$ for exceed percentage probability $ep$, the probability of rainy periods $P_R(Lat,\ Long)$, the average annual convective rainfall amount $M_C(Lat,\ Long)$, and the average annual stratiform rainfall amount $M_S(Lat,\ Long)$ at different $X$ ($Long$ degree) and $Y$ ($Lat$ degree) locations [15, 16]. $Lat$ is considered the latitude, and $Long$ is considered the longitude. The $\mathrm{RR_{ep}}$ is computed based on historical rainfall data for the exceed percentage probability ($ep$), which can be considered an alternative to real-time data.

Other parameters are then derived from this data through the following procedure.

1. Extract variables $P_R, M_C$, and $M_S$ for the four points closest in $Lat$ and $Long$ to the geographical coordinates ($X$ and $Y$) of the desired location. Latitude grid ranges from $(90°N)$ to $(-90°S)$, and longitude grid ranges from 0 to 360° both for 1.5° steps as shown in Table 3.1. Thus:

    a. If the location falls on the grid, these values will be taken as is from the given ITU − R tabulated data.

    b. If it does not fall on the grid, a bi-linear interpolation will be performed for the four closest grid points as shown in Figure 3.1.

2. Derive percentage probability of rainfall in an average year, $P_{ep}$, based on calculated data collected from previous steps [15], where:

$$P_{ep}(Lat, Long) = P_R(Lat, long) \cdot \left(1 - e^{-0.0117(M_S(Lat,Long)/P_R(Lat,Long))}\right) . \quad (3.1)$$

**Table 3.1:** Data Format.

| $X/Y$ | **0** | **1.5** | ... ... ... | **385.5** | **360** |
|---|---|---|---|---|---|
| **90** | (0, 90) | (1.5, 90) | ... ... ... | (385.5, 90) | (360, 90) |
| **88.5** | (0, 88.5) | (1.5, 88.5) | ... ... ... | (385.5, 88.5) | (360, 88.5) |
| . | . | . | | . | . |
| . | . | . | ... ... ... | . | . |
| . | . | . | | . | . |
| **1.5** | (0, 1.5) | (1.5, 1.5) | ... ... ... | (385.5, 1.5) | (360, 1.5) |
| **0** | (0, 0) | (1.5, 0) | ... ... ... | (385.5, 0) | (360, 0) |
| **-1.5** | (0, -1.5) | (1.5, -1.5) | ... ... ... | (385.5, -1.5) | (360, -1.5) |
| . | . | . | | . | . |
| . | . | . | ... ... ... | . | . |
| . | . | . | | . | . |
| **-88.5** | (0, -88.5) | (1.5, -88.5) | ... ... ... | (385.5, -88.5) | (360, -88.5) |
| **-90** | (0, -90) | (1.5, -90) | ... ... ... | (385.5, -90) | (360, -90) |

a. If $P_R$ is equal to zero, the result of this operation will be undetermined, and, consequently, intensity rainfall rate will also be equal to zero [9]. In this case the procedure shall be stopped.

b. If $P_R$ is not equal to zero, rainfall rate ($\mathrm{RR_{ep}}$), should be derived from the exceeded percentage probability of interest ($ep$) [1], where $ep$ should be less than or equal to $P_{ep}$, otherwise $P_{ep}$ – and thus rainfall rate – will be equal to zero and the following steps will not be required [15].

Thus, rainfall rate ($\mathrm{RR_{ep}}$) will be:

$$RR_{ep}(Lat, Long) = \frac{-B + \sqrt{B^2 - 4 \cdot A_b \cdot C}}{2 \cdot A_b} \quad mm/hr, \tag{3.2}$$

where:

$$A_b = a \cdot b, \tag{3.3}$$

[1] Although the exceed percentage probability is represented in ITU – R as $p$, the symbol $ep$ has been used in this thesis because it was discovered the many readers confuse $p$ as a symbol for probability.

$$B = a + c \cdot \ln\left(ep/P_{ep}\left(Lat,\ Long\right)\right), \tag{3.4}$$

$$C = \ln\left(ep/P_{ep}\left(Lat,\ Long\right)\right), \tag{3.5}$$

$$a = 1.11, \tag{3.6}$$

$$b = \frac{\left(M_C(Lat, Long) + M_S(Lat, Long)\right)}{22932 \cdot P_{ep}}, \tag{3.7}$$

and

$$c = 31.5 \cdot b\,. \tag{3.8}$$

## 3.3 Definition of Bi-Linear Interpolation

Bilinear interpolation is an extension of linear interpolation for interpolation of variables whose values depend on two other linearly related variables. The key idea is to perform a linear interpolation in two different directions. Figure 3.1 shows the four diamond dots that represent the given data points around the interpolated location. It also shows the circle dot that is surrounded by the point diamond dots. The circle dot is the point at which the interpolation should be done using the bi-linear interpolation [58, 59]. The value of the unknown function ($G$) that is located at the longitude ($X$) and the latitude ($Y$) can be computed as:

$$\begin{aligned} K_{11} &= K(X_1,\ Y_1), \\ K_{12} &= K(X_1,\ Y_2), \\ K_{21} &= K(X_2,\ Y_1), \\ K_{22} &= K(X_2,\ Y_2). \end{aligned} \tag{3.9}$$

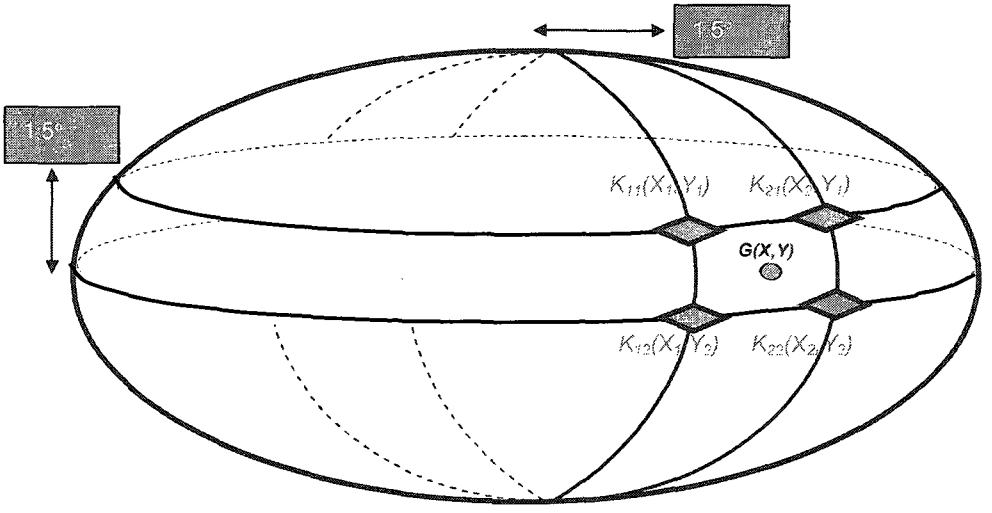


**Figure 3.1:** Grid point location.

First, the linear interpolation is done in the $X$ direction. This yields:

$$T_1 \approx \frac{X_2 - X}{X_2 - X_1} K_{11} + \frac{X - X_1}{X_2 - X_1} K_{21} \tag{3.10}$$

and

$$T_2 \approx \frac{X_2 - X}{X_2 - X_1} K_{12} + \frac{X - X_1}{X_2 - X_1} K_{22} \,. \tag{3.11}$$

Then, the interpolation is done in the $Y$ direction. This yields:

$$G(X,\, Y) \approx \frac{Y_2 - Y}{Y_2 - Y_1}\, T_1 \,+\, \frac{Y - Y_1}{Y_2 - Y_1}\, T_2 \,. \tag{3.12}$$

**Table 3.2:** Bi-Linear Interpolation.

| **Bi-Linear** | $(X, Y)$ | $(X_1, Y_1)$ | $(X_1, Y_2)$ | $(X_2, Y_1)$ | $(X_2, Y_2)$ |
|---|---|---|---|---|---|
| $X, Y$ | (296.27, 68.5) | (295.5, 67.5) | (295.5, 69) | (297, 67.5) | (297, 69) |
| $M_C$ | 2.73 | 3.15 | 3.1 | 1.32 | 2.54 |
| $M_S$ | 96.884 | 89.79 | 87.28 | 114.85 | 112.48 |

The result of these interpolations give us the desired estimation for $G(X,\ Y)$ as:

$$G(X,Y) \approx \frac{K_{11}}{(X_2-X_1)(Y_2-Y_1)}(X_2 - X)(Y_2 - Y) + \frac{K_{21}}{(X_2-X_1)(Y_2-Y_1)}(X - X_1)(Y_2 - Y) + \cdots$$
$$\cdots + \frac{K_{12}}{(X_2-X_1)(Y_2-Y_1)}(X_2 - X)(Y - Y_1) + \frac{K_{22}}{(X_2-X_1)(Y_2-Y_1)}(X - X_1)(Y - Y_1)\,. \tag{3.13}$$

Thus, this formula provides interpolated values for all necessary propagation parameters at a given location on earth that does not fall on a grid point given in Table 3.1. Table 3.2 shows an example for interpolating two weather parameters at a given longitude ($X$) and latitude ($Y$). The first parameter is the average annual convective rainfall amount ($M_C$) and the second parameter is the average annual stratiform rainfall amount ($M_S$). These parameters are used to estimate different weather attenuations using bi-linear interpolation to obtain their approximated values. Also, bi-linear method is used to interpolate other parameters such as mean rain height above sea level, liquid precipitation, and other ITU $-$ R parameters that are used to estimate different attenuations that are presented in this thesis.

## 3.4 Rain Attenuation Development

This section, at first, provides ITU $-$ R recommended procedure for estimating long-term statistics of slant-path rain attenuation and then the improved method that has been proposed [29]. The ITU $-$ R original method developed in 1986 has been presented as ITU $-$ R Original Method. Then to improve the computational efficiency of the calculation, ITU $-$ R developed the approximation method, hereon identified as ITU $-$ R Approximation Method, which is an extension to the ITU $-$ R

Original Method. The significant contribution made by the ITU – R Approximation Method was that the rain attenuation calculations were made much faster without significant loss of accuracy of results. This, however, was the case when rainfall rate values were low. Therefore, improving the accuracy of rain attenuation estimation at high rainfall rate for the entire frequency range in use by the satellite systems remained as a challenge. It turns out that, the IAM gives remarkably good results for rain attenuation up to the highest rainfall rate values at frequencies as high as Ka – band while remaining computationally more efficient than the ITU – R Approximation Method.

In all three methods, the value of rain attenuation is dependent on a number of propagation parameters including propagation angle, frequency, atmospheric attenuation, and location. The propagation angle, which has been depicted in Figure 3.2 as ($\theta$), is dependent on the locations of the ground stations and the satellite. Other factors affected by location of the communicating points include: Mean rain height above mean sea level ($h_R$), liquid precipitation ($L_{ep}$), frozen precipitation ($F_{ep}$), height above mean sea level of earth station ($h_S$), earth-space path ($E_{ep}$), horizontal projection ($L_G$), slant-path length below rain height ($L_S$), and rain height ($R_h$). These parameters and others as defined by ITU – R is shown in Table 3.3. Frequency is the only location for independent variable that affect rain attenuation. In the following subsection, we describe ITU – R Original Method, ITU – R Approximation Method, and Iterative Approximation Method (IAM).

### 3.4.1 ITU – R Original Method

The ITU – R Original Method provides an estimate of long-term rain attenuation based on statistical data collected on parameters like annual rainfall and probability of precipitation. The results obtained by this method are close to the measured values but allowance should be given for the variability in rainfall rate statistics.

The original algorithm for estimating the rain attenuation is as follows:

1. For areas around the world where no specific information is available: The mean $0°C$

**Table 3.3:** Variables as Defined by ITU – R.

| Name of Variable | Unit | Description |
|---|---|---|
| $F_{ep}$ | $Km$ | Frozen precipitation |
| $h_0$ | $Km$ | Mean $0°C$ isotherm height above mean sea level |
| $h_R$ | $Km$ | Mean rain height above mean sea level |
| $h_S$ | $Km$ | Height above mean sea level of earth station |
| $h_v$ | $Km$ | Equivalent height for water vapour |
| $K_H$ | | Constant coefficients of horizontal polarization |
| $K_V$ | | Constant coefficients of vertical polarization |
| $\alpha_H$ | | Constant coefficients of horizontal polarization |
| $\alpha_V$ | | Constant coefficients of vertical polarization |
| $K_t$ | $Kelvin$ | Specific attenuation coefficient |
| $K_\tau$ | | Frequency-dependent coefficients |
| $\alpha_\tau$ | | Frequency-dependent coefficients |
| $L_{ep}$ | $Km$ | Liquid precipitation |
| $L_v$ | $kg/m^2$ | Statistics of the total columnar content |
| $L_w$ | $kg/m^2$ | Total columnar content of liquid water |
| $M$ | $kg/m^3$ | Integration of liquid water density |
| $M_C$ | | Average annual convective rainfall amount |
| $M_S$ | | Average annual stratiform rainfall amount |
| $N_{wet}$ | | Radio refractivity |
| $ph$ | $hpa$ | Pressure |
| $P_R$ | | Probability of rainy periods |
| $R_h$ | $Km$ | Rain height |
| $\rho$ | $degree$ | Latitude of the earth station |
| $t_k$ | $Kelvin$ | Temperature |

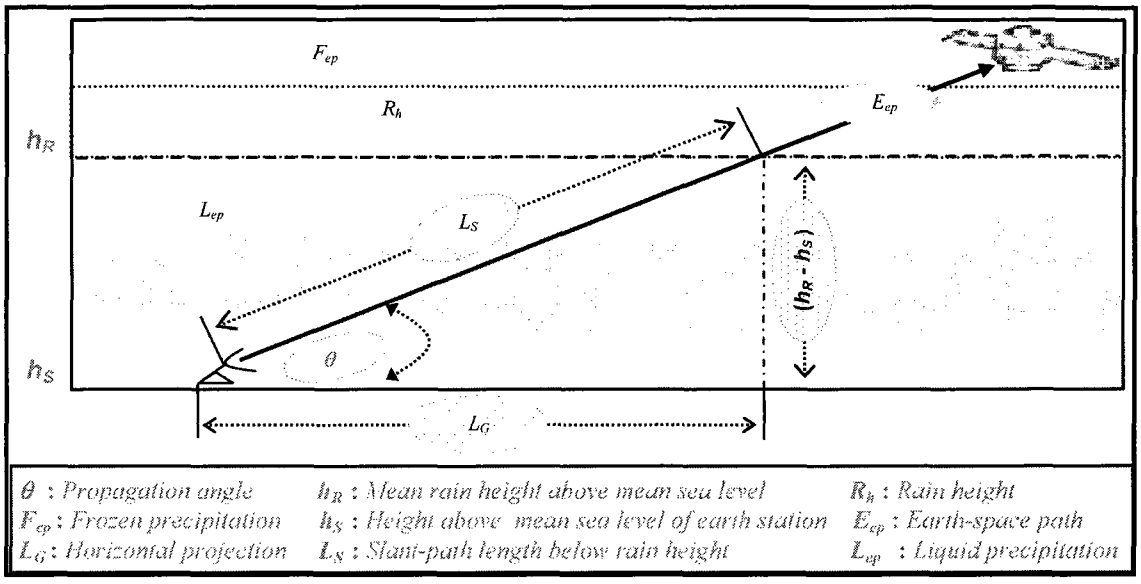


**Figure 3.2:** Earth space path.

isotherm height above mean sea level $h_0$ in $(km)$ can be obtained from data file HEIGHT0 .txt (this file may be downloaded from the ITU – R Bureau - BR). Note that this file contains data with resolution of $1.5$ $degrees$ in both latitude and longitude [30]. The same applies for the grid point data described in the previous section.

2. Obtain mean rain height above mean sea level, $h_R$, from $0°C$ isotherm $h_0$, given in [30], as:

$$h_R = h_0 + 0.36 \quad km. \tag{3.14}$$

3. Compute slant-path length, $L_S$, below rain height [9,15,16,30] using the following formulas:

   (a) $\theta \leq 5$ $degrees$:

$$L_S = \frac{2(h_R - h_S)}{\left(\sin^2\theta + \frac{2(h_R - h_S)}{R_e}\right)^{1/2} + \sin\theta} \quad km. \tag{3.15}$$

   Note: $R_e$ represents the effective radius of Earth, $(8,500\ km)$

(b) $\theta > 5$ *degrees*:

$$L_S = \frac{(h_R - h_S)}{\sin\theta} \quad km. \tag{3.16}$$

Here, if $(h_R - h_S) \leq 0$, then predicted rain attenuation (RA) for any time percentage is equal to zero. Therefore, reset RA value to zero and skip the rest of the steps.

4. Calculate horizontal projection, $L_G$, of slant-path length from:

$$L_G = L_S \cdot \cos\theta \quad km. \tag{3.17}$$

5. Find $\mathrm{RR_{ep}}$ for $ep = 0.01$ % of an average year. If $\mathrm{RR_{0.01}}$ is equal to zero, then predicted RA is equal to zero for a given time percentage and skip steps 6 to 11.

6. Compute specific attenuation, $\gamma_R$, using frequency-dependent coefficients as given in [15] for $k$, $a$, and $\mathrm{RR_{ep}}$, calculated in Section (4.1) for $ep = 0.01$ %, determined from (3.2), by using:

$$\gamma_R = K_\tau \cdot (RR_{0.01})^{\alpha_\tau} \quad dB/km. \tag{3.18}$$

For linear and circular polarization and for all path geometries, coefficients in (3.18) can be computed as:

$$K_\tau = \left[K_H + K_V + (K_H - K_V)\cos^2\theta\cos 2\tau\right]/2 \tag{3.19}$$

and

$$\alpha_\tau = \left[K_H\alpha_H + K_V\alpha_V + (K_H\alpha_H - K_V\alpha_V)\cos^2\theta\cos 2\tau\right]/2k, \tag{3.20}$$

where $K_V, \alpha_V$ and $K_H, \alpha_H$, are constant coefficients of vertical and horizontal polarizations. Also, the determined path propagation angle ($\theta$) and the polarization tilt angle ($\tau$) relative to horizontal polarization is equal to 45 *degrees* for circular polarization.

7. Calculate horizontal reduction factor, $r_{ep}$, for $ep = 0.01$ % of time:

$$r_{0.01} = \frac{1}{1 + 0.78\sqrt{\frac{L_G \cdot \gamma_R}{f}} - 0.38\left(1 - e^{-2L_G}\right)}. \tag{3.21}$$

8. Calculate vertical adjustment factor, $v_{0.01}$, for 0.01 % of time:

$$\sigma = \tan^{-1}\left(\frac{h_R - h_S}{L_G \cdot r_{0.01}}\right) \quad degrees. \tag{3.22}$$

The actual slant-path length $L_R$ will be:

$$L_R = \begin{cases} \frac{L_R \cdot r_{0.001}}{\cos\theta} \quad km & for\ \sigma > \theta \\ \\ \frac{(h_R - h_S)}{\sin\theta} \quad km & for\ \sigma \leq \theta \end{cases} \tag{3.23}$$

and the variable $\chi$ is equal to:

$$\chi = \begin{cases} 36 - |\rho| \quad \text{degree} & for\ |\rho| < 36° \\ \\ 0 \quad \text{degree} & otherwise \end{cases} \tag{3.24}$$

where $\rho$ is the latitude of the earth station.

The vertical adjustment factor is [29]:

$$v_{0.01} = \frac{1}{1 + \sqrt{\sin\theta}\left(31\left(1 - e^{-\left(\theta/(1+\chi)\right)}\right)\frac{\sqrt{L_R \cdot \gamma_R}}{f^2} - 0.45\right)}. \tag{3.25}$$

9. Obtain the effective path length as:

$$L_E = L_R \cdot v_{0.01} \ km. \tag{3.26}$$

10. Estimate RA for exceeded $ep = 0.01\ \%$ of an average year as follows:

$$A_{Rain(0.01)} = \gamma_R \cdot L_E \ dB. \tag{3.27}$$

11. For other exceeding percentages of an average year ranging from $0.001\ \%$ to $50\ \%$, estimations of RA can be computed from the following equation as:

$$\begin{aligned} A_{Rain(ep)} = A_{Rain(0.01)} \cdot \ \cdots \\ \cdots \cdot \left(\tfrac{ep}{0.01}\right)^{-\left(0.655+0.033\ln(ep)-0.045\ln\left(A_{Rain(0.01)}\right)-\beta(1-ep)\sin\theta\right)} \ dB, \end{aligned} \tag{3.28}$$

where

$$\beta = \begin{cases} 0 & if\ (ep \geq 1\%\ or\ |\rho| \geq 36^\circ) \\ -0.005(|\rho| - 36) & if\ \{ep \leq 1\% and\ |\rho| < 36^\circ and \theta \geq 25^\circ\} \\ -0.005(|\rho| - 36) + 1.8 - 4.25\sin\theta & otherwise \end{cases} \tag{3.29}$$

The above equation for rain attenuation (RA) was tested by ITU − R and found to be the most precise overall of all tested models [2, 9, 17, 60]. This method provides a reasonable solution for calculating RA, represented as ($A_{rain}$). In order to estimate RA at a given location, this calculation has to go through (3.18) to (3.28) for every frequency sample; a process that requires a large computational load.

### 3.4.2 ITU – R Approximation Method

In this method, calculating rain attenuation for a geographic location of our concern for a given practical rainfall rate and useful frequencies of up to 55 $GHz$ are based on a fixed frequency-sample ($F_s$). A special logic for extrapolation is then applied to calculate rain attenuation for the rest of the frequencies. However, such a calculation is made possible through a series of background calculations of other necessary parameters.

By using the ITU – R Approximation Method as described below, the rain attenuation (RA), can be computed for the entire range of useful frequencies, using (3.30) - (3.33), based on a fixed sample frequency ($F_s$) [9,29]. Thus, RA value at a specific location as a function of frequency is calculated by using the following formulas:

$$A_{Rain}(f_i) = A_{Rain}(F_s) \cdot \left(\varphi(f_i)/\varphi(F_s)\right)^{(1-H(\varphi(F_s),\varphi(f_i),A_{Rain}(F_s)))} \; dB, \tag{3.30}$$

where

$$\varphi(f_i) = \frac{f_i^2}{1+10^{-4}f_i^2}, \tag{3.31}$$

$$A_{Rain}(F_s) = \gamma_R(F_s) \cdot L_E(F_s) \; dB, \tag{3.32}$$

$$\begin{aligned} H(\varphi(F_s),\varphi(f_i),A_{Rain}(F_s)) &= 1.12\cdot 10^{-3} \cdot \cdots \\ &\cdots \cdot \left(\varphi(f_i)/\varphi(F_s)\right)^{0.5} \cdot (\varphi(F_s)A_{Rain}(F_s))^{0.55}, \end{aligned} \tag{3.33}$$

where $A_{Rain}$ is a value of rain attenuation, $f_i$, that represents the frequency ranging from 7 to 55 $GHz$, and $F_s$ is the sample frequency [29].

Therefore, if reliable attenuation data – measured at one sample frequency ($F_s$) – is available (preferably a higher frequency sample since it offers an overall better results), these empirical formulas will then generate RA as a function of the chosen frequency [9, 16, 29]. The values of RA thus obtained can be applied for frequency scaling on the communication channel where

frequencies may range from 7 to 55 $GHz$.

In this method, the value of rain attenuation at the sample frequency ($F_s$) is extrapolated to estimate the other rain attenuation at a given channel frequency. The extrapolation requires precipitation probability, propagation angle, location of the ground station, and the rain attenuation value at the sample frequency ($F_s$). The computational efficiency of this method is much superior to ITU – R Original Method. At high rainfall rate values and high frequencies, however, the errors in rain attenuation calculations accumulate such that the anomaly becomes significant. Therefore, in the next section, we will present a new method to overcome the problem of accurately approximating rain attenuation when operating at high frequencies under high rainfall rate situations.

ITU – R Approximation Method, However, is accurate only when rainfall rate is reasonably small ($RR_{0.01} = 5.968\ mm/hr$) [9,30], as shown in Figure 3.3. Also, Table 3.4 shows the results and the relative percentage error [2] in ITU – R Approximation Method with respect to ITU – R Original Method.

At high rainfall rate the deviation will be substantial, which will be demonstrated in the next section. Thus, by using high frequency sample ($F_s$) in order to match the ITU – R Original Method will not guarantee delivering enhanced solutions for all models.

### 3.4.3 Iterative Approximation Method

In this section, we describe a novel method that has been named Iterative Approximation Method (IAM) for estimating rain attenuation and compares its computational efficiency and accuracy with the previously described methods [9,30]. This IAM is not, however, related to or a derivation work of some other research works where they also chose to name their methods "Iterative Approximation Method" [61,62]. This is a unique work that deals with iterative approximation of attenuation. This method was developed through empirical studies of past data of communication systems as

[2] Error in Approximation Method with respect to ITU – R Original Method as:
$Relative\ Percentage\ Error = [(Original - Approximation)\ /\ Original] * 100\ \%$.

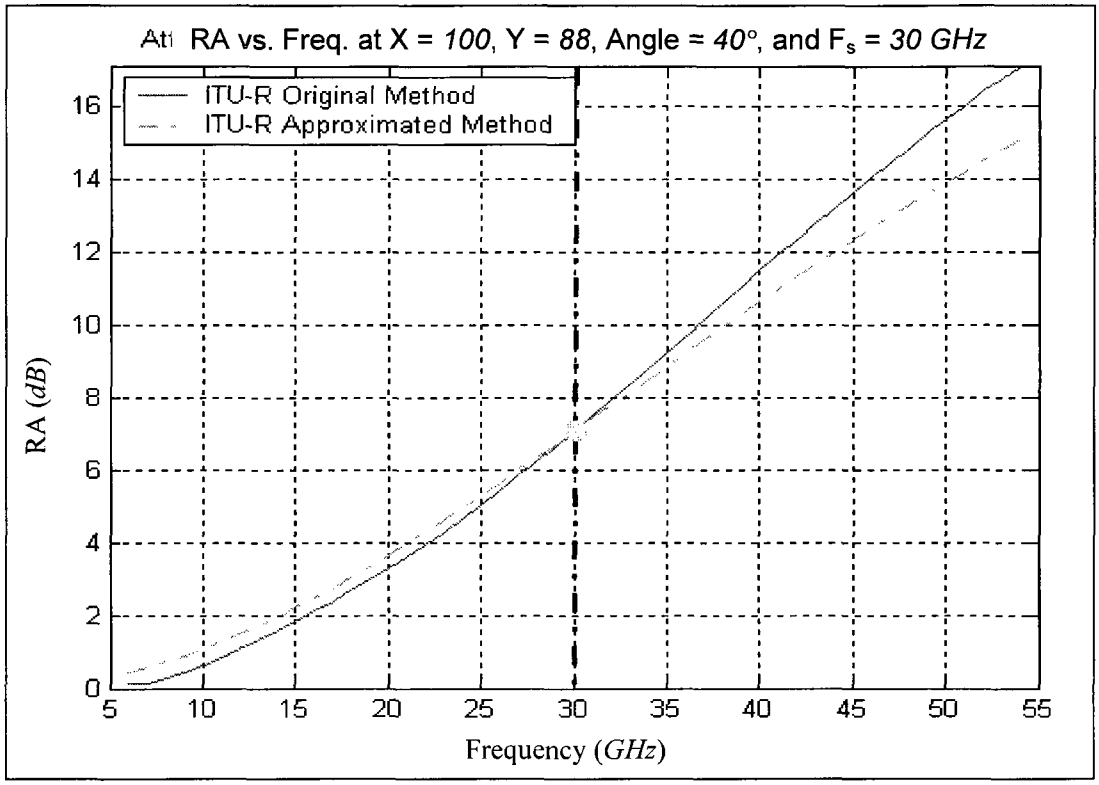


**Figure 3.3:** ITU – R Original and Approximation Methods for small rainfall rate.

**Table 3.4:** Rain Attenuation Comparison Between ITU – R Original and Approximation Methods at Different Frequencies for $F_s = 30$ and $\theta = 40$.

| **Frequency [GHz]** | **ITU – R Original Method [dB]** | **ITU – R Approximation Method [dB]** | **Relative % Error of Approximation Method w.r.t. Original** |
|---|---|---|---|
| 9 | 0.34468 | 0.71549 | 107.58 |
| 10 | 0.50705 | 0.88253 | 74.052 |
| 12 | 0.91177 | 1.2646 | 38.698 |
| 14 | 1.3783 | 1.7066 | 23.817 |
| 16 | 3.0011 | 3.3359 | 17.247 |
| 18 | 2.4166 | 2.7483 | 13.723 |
| 19 | 2.7025 | 3.0372 | 12.386 |
| 20 | 3.0011 | 3.3359 | 11.158 |
| 21 | 3.3133 | 3.6438 | 9.9754 |
| 22 | 3.6384 | 3.9599 | 8.8375 |
| 23 | 3.9784 | 4.2836 | 7.6698 |
| 25 | 4.6985 | 4.9505 | 5.3649 |
| 27 | 5.4675 | 5.6387 | 3.1316 |
| 28 | 5.8683 | 5.989 | 2.056 |
| 29 | 6.2791 | 6.3425 | 1.0106 |
| 30 | 6.6986 | 6.6986 | 0.0 |
| 31 | 7.1256 | 7.0567 | 0.96764 |
| 32 | 7.5591 | 7.4161 | 1.891 |
| 35 | 8.8815 | 8.4971 | 4.328 |
| 38 | 10.221 | 9.5715 | 6.3567 |
| 40 | 11.112 | 10.278 | 7.5017 |
| 44 | 12.852 | 11.656 | 9.31 |
| 46 | 13.696 | 12.322 | 10.034 |
| 50 | 15.313 | 13.601 | 11.184 |
| 54 | 16.82 | 14.8 | 12.013 |
| 54 | 17.178 | 15.086 | 12.18 |

opposed to that applied in [61,62].

Thus, our propose IAM is used to overcome the problem of inaccuracies in rain attenuation estimations found in ITU − R Approximation Method while remaining computationally efficient.

The ITU − R Approximation Method calculated the value of rain attenuation at a specific frequency ($F_s$) by following the empirical formulas (3.30)-(3.33), where the results lost accuracy in case of high rainfall rate and high frequency. The new method computes the rain attenuation by using equations (3.34)-(3.37) and produces rain attenuation estimates that closely matches with the results obtained from the computationally cumbersome ITU − R Original Method even at high rainfall rate and higher frequencies of 7 to 55 $GHz$. The key differentiator here is that the sample frequency ($f_n$) is not static as in the case of ITU − R Approximation Method described in the previous section. Here ($f_n$) represents the selected frequency to start the computation of rain attenuation.

$$A_{Rain}(f_{n+1}) = A_{Rain}(f_n) \cdot \left(\varphi(f_{n+1})/\varphi(f_n)\right)^{(1-H(\varphi(f_n),\varphi(f_{n+1}),A_{Rain}(f_n)))} \; dB, \tag{3.34}$$

where

$$A_{Rain}(f_n) = \gamma_R(f_n) \cdot L_E(f_n) \; dB, \tag{3.35}$$

$$H(\varphi(f_n),\varphi(f_{n+1}),A_{Rain}(f_n)) = 1.12 \cdot 10^{-3} \cdot \cdots \cdots \cdot \left(\varphi(f_{n+1})/\varphi(f_n)\right)^{0.5} \cdot (\varphi(f_n)A_{Rain}(f_n))^{0.55}, \tag{3.36}$$

$$\varphi(f_n) = \frac{f_n^2}{1+10^{-4}f_n^2}, \tag{3.37}$$

and

$$7\,GHz \leq f \leq 55\,GHz,$$

and $A_{Rain}(f_n)$ and $A_{Rain}(f_{n+1})$ are the equiprobable values of excess RA at frequencies ($f_n$) and ($f_{n+1}$) with rainfall rate respectively.

The IAM is based on getting attenuation results of next frequencies out of preceding ones [9, 30]. Thus, once RA is computed at a given location on earth at a known frequency $(f_n)$ ranging from 7 to 55 $GHz$, we can then compute RA for upper frequency $(f_{n+1})$ based on prior frequency $(f_n)$ and the process could be repeated for incrementally higher frequencies until reaching the desired frequency.

Table 3.5 shows a comparison between the results obtained from the ITU – R Original Method,

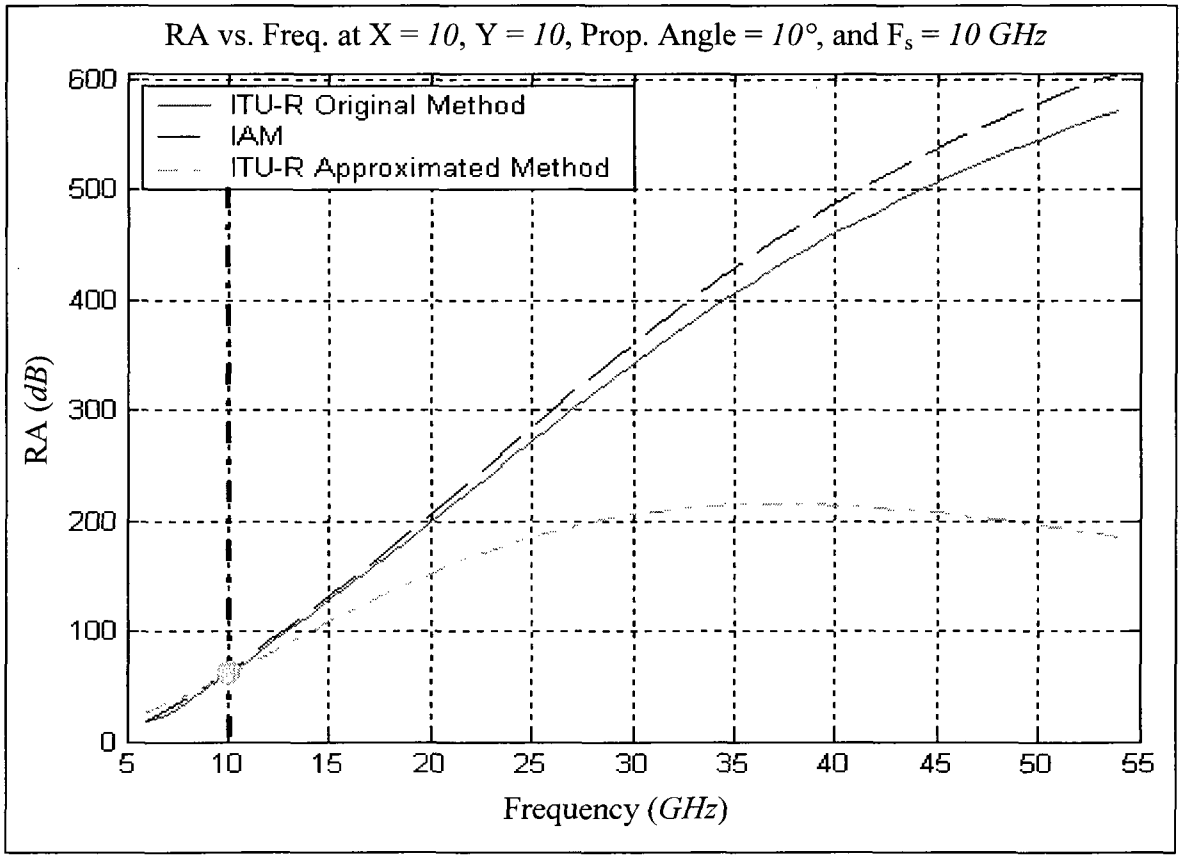


**Figure 3.4:** ITU – R Original, ITU – R Approximation, and IAMs comparison for relatively high rainfall rate and low sample frequency $(F_s)$.

ITU – R Approximation Method, and IAM for different frequencies. This comparison could be better understood by depicting the difference graphically in Figure 3.4, Figure 3.5, and Figure 3.6. From the results, it could be noted that the IAM computes RA for a given propagation angle, rainfall rate, polarization, probability, and frequency with accuracies comparable to the ITU – R mentioned methods. Also, the ITU – R Approximation Method results for relatively hight rainfall rate does not match the ITU – R Original Method for different small, medium, and high sample

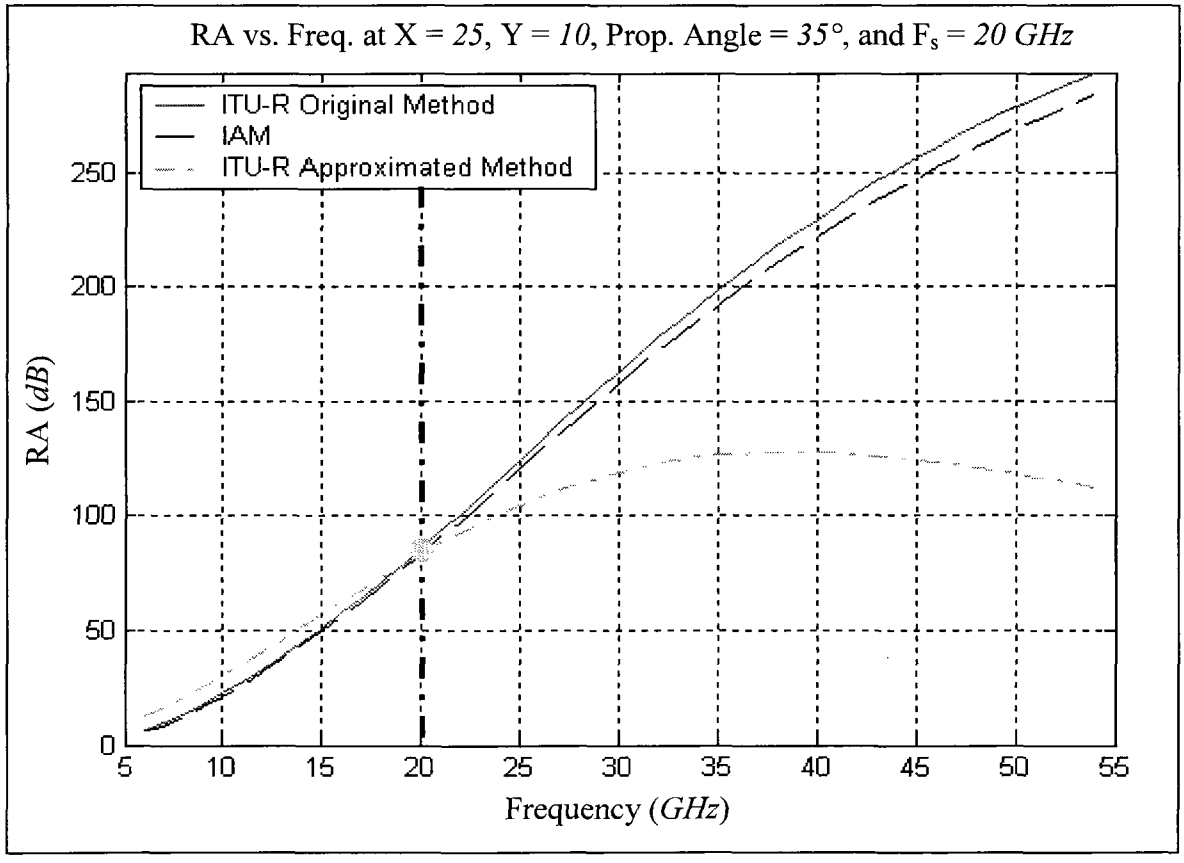


**Figure 3.5:** ITU – R Original, ITU – R Approximation, and IAMs comparison for relatively high rainfall rate and medium sample frequency ($F_s$).

frequency values as presented in Figure 3.4, Figure 3.5, and Figure 3.6. The mismatch occurred because the errors were accumulated for each new calculation since all outputs were extrapolated based on one RA value related to one frequency sample ($F_s$). ITU – R Approximation Method did not improve the accuracy of approximation even when using higher frequency sample in case of high rainfall rate.

Whereas the ITU–R Original Method is appropriate for stable weather conditions and ITU–R

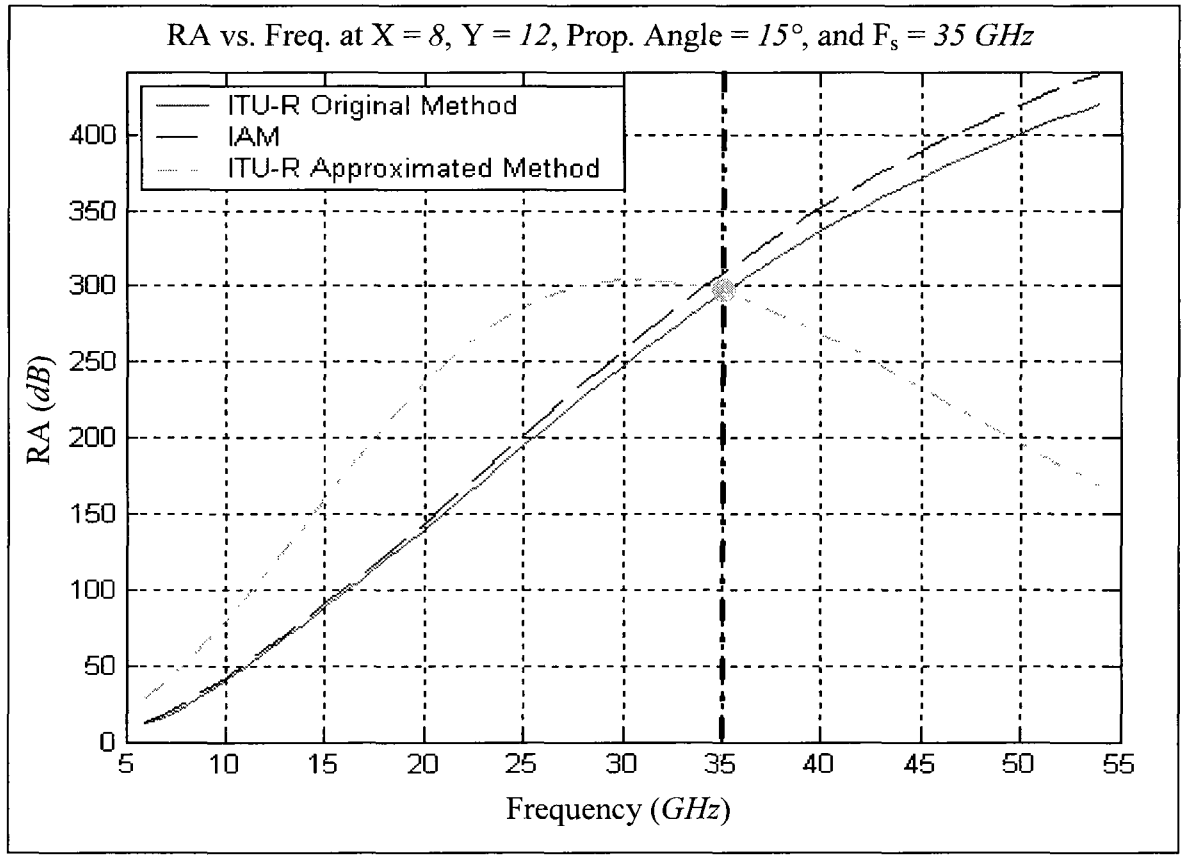


**Figure 3.6:** ITU – R Original, ITU – R Approximation, and IAMs comparison for relatively high rainfall rate and large sample frequency ($F_s$).

Approximation Method is appropriate during low rainfall rate and low frequency states, our IAM produces in highly acceptable results under different weather conditions. This is one of the major contributions of the research reported in this thesis.

Unlike ITU – R Original Method, this technique provides better CPU time efficiency as it does not require repeating the entire calculation from beginning for each frequency [29]. Because the CPU time varies with the number of simulations, the efficiency of the IAM increases dramatically over the ITU – R Original Method and comes closer to ITU – R Approximation Method. This effect is especially prominent when dealing with unstable weather conditions.

### 3.4.4 Algorithm for Iterative Approximation Method

In order to implement our IAM technique, we developed an algorithm for calculating rain attenuation (RA). In this section, the algorithm is explained. For the purpose of this work, the communication links between various stations are divided into three groups:

(a) Satellite to satellite link, where weather attenuations are absent and only free space attenuation is to be factored,

(b) Ground to satellite link or visa versa, where weather attenuation plays a major role,

(c) ground to ground link, where weather attenuation becomes ever more significant.

Since satellite to satellite link represents a special case where weather attenuation is zero, the algorithm here is explained for the general case where both atmospheric and free space attenuations play a role.

The algorithm for calculating RA on links that involve tropospheric layer in the path is stated in the following steps:

1. Select the location of transmitting and receiving terminals of the link.

**Table 3.5:** Rain Attenuation Comparison Among ITU – R Original Method, ITU – R Approximation Method, and Iterative Approximation Method (IAM) at Different Frequencies.

| **Frequency [GHz]** | **Original Method [dB]** | **Approx. Method [dB]** | **IAM [dB]** | **Relative % Error in Approximation Method** | **Relative % Error of IAM w.r.t. Original Method** |
|---|---|---|---|---|---|
| 10 | 17.72 | 25.278 | 16.554 | 42.654 | 6.5791 |
| 11 | 22.421 | 30.157 | 21.097 | 34.505 | 5.9056 |
| 12 | 27.623 | 35.276 | 26.197 | 27.706 | 5.1626 |
| 14 | 38.946 | 46.01 | 37.594 | 18.137 | 3.4699 |
| 16 | 51.164 | 57.041 | 49.784 | 11.485 | 2.6973 |
| 17 | 57.627 | 62.542 | 56.129 | 8.5277 | 2.6001 |
| 18 | 64.335 | 67.972 | 62.664 | 5.6528 | 2.5969 |
| 19 | 71.283 | 73.291 | 69.4 | 2.8168 | 2.6419 |
| 20 | 78.462 | 78.462 | 76.332 | 0 | 2.715 |
| 21 | 85.827 | 83.453 | 83.453 | 2.7662 | 2.7662 |
| 22 | 93.346 | 88.235 | 90.717 | 5.4755 | 2.8164 |
| 23 | 101.01 | 92.786 | 98.096 | 8.1451 | 2.8884 |
| 24 | 108.76 | 97.084 | 105.58 | 10.731 | 2.9175 |
| 26 | 124.42 | 104.87 | 120.67 | 15.712 | 3.0088 |
| 28 | 140.04 | 111.5 | 135.73 | 20.38 | 3.0781 |
| 29 | 147.76 | 114.38 | 143.2 | 22.59 | 3.0861 |
| 30 | 155.42 | 116.96 | 150.54 | 24.747 | 3.1388 |
| 31 | 162.97 | 119.25 | 157.82 | 26.831 | 3.1599 |
| 32 | 170.41 | 121.25 | 164.97 | 28.849 | 3.189 |
| 34 | 184.75 | 124.41 | 178.79 | 32.662 | 3.2259 |
| 36 | 198.46 | 126.52 | 191.99 | 36.247 | 3.2613 |
| 38 | 211.51 | 127.67 | 204.5 | 39.641 | 3.3168 |
| 40 | 223.82 | 127.94 | 216.33 | 42.837 | 3.3485 |
| 42 | 235.32 | 127.46 | 227.36 | 45.836 | 3.381 |
| 44 | 246.13 | 126.3 | 237.77 | 48.684 | 3.3974 |
| 48 | 265.71 | 122.4 | 256.57 | 53.933 | 3.4409 |
| 50 | 274.44 | 119.84 | 264.96 | 56.333 | 3.4534 |
| 52 | 282.61 | 116.97 | 272.84 | 58.61 | 3.4588 |
| 54 | 290.16 | 113.88 | 280.26 | 60.753 | 3.41 |
| 55 | 293.74 | 112.27 | 283.69 | 61.781 | 3.4205 |

2. Collect parameters $P_R$, $M_S$ and, $M_C$, described in Section (3.2), $h_0$, $h_S$, $K_\tau$, and $\alpha_\tau$ described in Section (3.4) according to selected location from ITU $-$ R and other fixed parameters needed to compute RA.

3. Derive the requested value of parameters $P_{ep}$, $RR_{ep}$, described in Section (3.2), $h_R$, $L_S$, $L_G$, $L_R$, $\gamma_R$, $r_{ep}$, $\sigma$, $v_{ep}$, $L_E$, and $\beta$ described in Section (3.4) from parameters collected in *step* 2.

4. Calculate RA for a given discrete frequency. The discrete frequency should fall somewhere between the lowest frequency of interest ($f_l$) and the highest frequency of interest ($f_h$) using ITU$-$R Original Method for a given rainfall rate, which can be either computed or predicted in equation (3.2). The other parameters can be computed starting from equation (3.14) and ending in equation (3.28).

5. Based on *step* 4, RA can be calculated at other frequency values belonging to the same range by using IAM technique by going through equations (3.34 - 3.37).

6. Repeat *step* 5 for other required RA by incrementing the frequency by one unit as $f_x = f_x + 1$ and going through equations (3.34 - 3.37) to cover RA's values up to the desire frequency of operation.

7. The above steps should be derived for different propagation angles, estimated or predicted rainfall rate values, and locations.

If reliable attenuation data measured at a given specific frequency is available, the previous empirical formula shown in equations (3.34 - 3.37) will provide attenuation ratio as a function of its preceding frequency.

The IAM is used to investigate rain attenuation, which depends not only on rainfall rate but also on other factors such as propagation angle, location, polarization, and frequency.

Also, the IAM works by eliminating the accumulated error compared to the case of ITU – R Approximation Method [9, 30]. Rain attenuation values that can be computed for different locations, selective propagation angle, and frequency ranging up to 55 $GHz$ with estimated rainfall rate [3,9]. We propose the IAM as one of the key research contributions made by the work reported in this thesis.

## 3.5 Summary

Rain is a dominant cause of signal attenuation. However, the extent of rain attenuation also depends on several parameters such as frequency, propagation angle, polarization tilt angle, rain intensity, raindrop size distribution, and raindrop temperature. There were two existing ways for calculating rain attenuation using ITU – R methods: The ITU – R Original Method and the ITU – R Approximating Method. We described both of these methods and their limitations in this chapter. As part of this research work, we developed a new method called IAM, which can estimate rain attenuation more accurately and efficiently than ITU – R Original Method and ITU – R Approximating Method. Moreover, the proposed method offers reduced CPU time and enhanced accuracy in estimation for higher frequencies.

IAM in this chapter does not concern whether the rainfall rate is a historical average or a real time value. Nevertheless, when it comes to real-time control the real-time value is of interest. For this matter, in the following chapter first we present prediction of rainfall rate based on actual data and then we derive rain attenuation according to predicted values.

# Chapter 4

# Prediction of Rainfall Rate Using Markov Theory

## 4.1 Introduction

This chapter describes a method for making prediction of rainfall rate. The prediction is made by using Markov theory along with ITU − R models and bi-linear interpolation. The Markovian theory was selected because it was successfully utilized in problems that has similar random characteristics like rain. Our subsequent studies proved that it can be applied to gain very effective prediction of rainfall rate [34, 63].

A Markov Chain is a discrete random process with the Markov property that goes on forever. A discrete random process means a system which is in a certain state at each "step", among predefined finite number of states. The probability by which the system enters into each of the other state in the next time period is known through statistical study of the system [64, 65]. In this chapter we use Markov theory to predict rainfall rate. The predicted rainfall rate can then be used to adjust the control parameters and, therefore, help improve the QoS in communication channels, which is the subject of discussion of subsequent chapters.

## 4.2 Rainfall Rate Prediction

In this section, we present prediction of rainfall rate using Markov theory [1] on the time series of weather data. For that reason, weather is considered a discrete random process that can assume a set of finite states. Further, it is assumed that the change from one state to another is a random discrete step with certain transition probability ($p$), whose value is derived from statistical properties of the system.

### 4.2.1 Classification of Rain

For the purpose of explaining to the reader the application of Markov modeling for predicted rainfall rate, a specific location is chosen where we divided rainfall rate ranges into five classes starting from zero $mm/hr$ up to the highest rainfall rate as follows:

**1-** Class A: from zero up to but less than 1 $mm/hr$.

**2-** Class B: from 1 up to but less than 4 $mm/hr$.

**3-** Class C: from 4 up to but less than 8 $mm/hr$.

**4-** Class D: from 8 up to but less than 14 $mm/hr$.

**5-** Class E: values greater than 14 $mm/hr$.

The discrete time interval chosen in this study has been one hour. The reason being that environment could supplied weather data in one hour intervals. However, the method can be applied for finer grain intervals given that weather data for shorter intervals are available.

The approach in grouping total rain conditions into classified blocks has been depicted in Figure 4.1. This classification in actual data provides a basis for the data required to apply Markov theory in the prediction of rainfall rate [34].

[1] It is assumed that the reader is familiar with Markov theory. References [25, 66] are recommended for those readers who are unfamiliar.

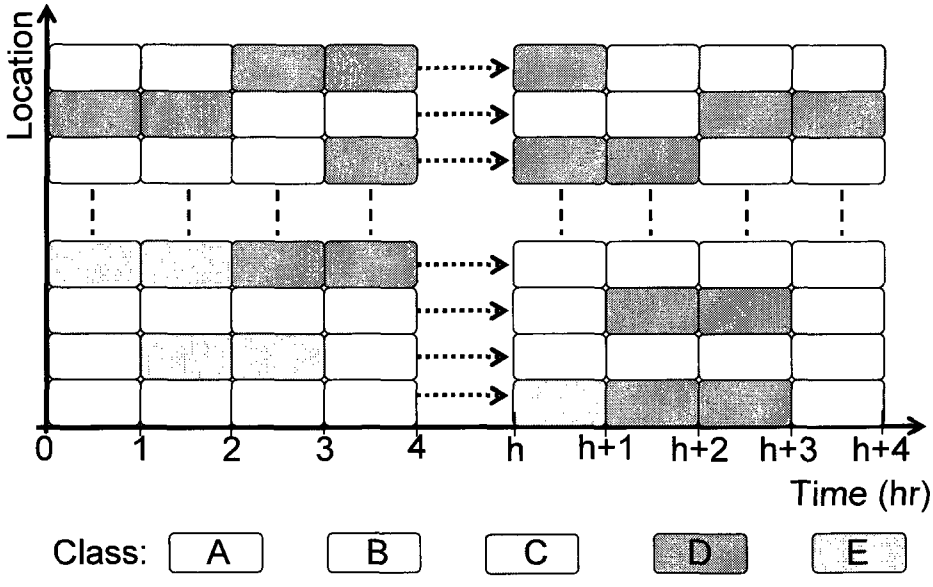


**Figure 4.1:** Presentation of the five rainfall rate classes.

To make the classification of rainfall rate to better reflect local statistical weather patterns, two parameters can be adjusted:

a- Periodicity of rainfall rate: Instead of selecting one hour interval, periodicity in minutes or hours could be used. The smaller the sampling period, the more instantaneous will be the rainfall rate values especially when dealing with rapidly changing weather conditions.

b- Number of classes: Instead of five, the number of classes could be decreased or increased to other numbers. More classes means more computational time with finer granularity of control.

### 4.2.2 Markov Model Implementation

#### I- Weight of Transition Probability Matrices

Different weights are assigned to each Markov state, zero order (present state), first order (previous state), and second order (previous to previous state), as defined in Markov Chain theory. There exist no direct formula for calculating these weights and it needs iterative search involving trial and error. The weight values need to be validates over many sets of data.

The resulting weight vector is denoted as:

$$W = \begin{bmatrix} W(0) & W(1) & W(2) \end{bmatrix}, \tag{4.1}$$

where $W(0), W(1)$, and $W(2)$ represent weight assigned to present, previous, and previous to previous intervals, respectively, as shown in Figure 4.2. Each weight in (4.1) has a different unique value and the largest value will belong to the present weight $W(0)$ and so on for the other weights. Also, these weights are positive numbers and their summation is equal to one.

This research came to conclude that there exist a set of weight that work very well for all possible sets of transition probability matrices describe below.

#### II- Transition Probability

The transition probabilities and classification of rain are directly correlated. The transition probabilities are the probabilities of moving from given state to another state.

In Markov Chain theory, the probability of a discrete event to remain in state $x$ is denoted as $P(x)$. In this representation, independent chains without any memory of past state are called zero-order Markov Chains. The transition probability matrix of zero-order Markov Chain theory ($P_0$) for the five presented classes is, thus, represented as follows:

$$P_0 = \begin{bmatrix} P_A & P_B & P_C & P_D & P_E \end{bmatrix}. \tag{4.2}$$

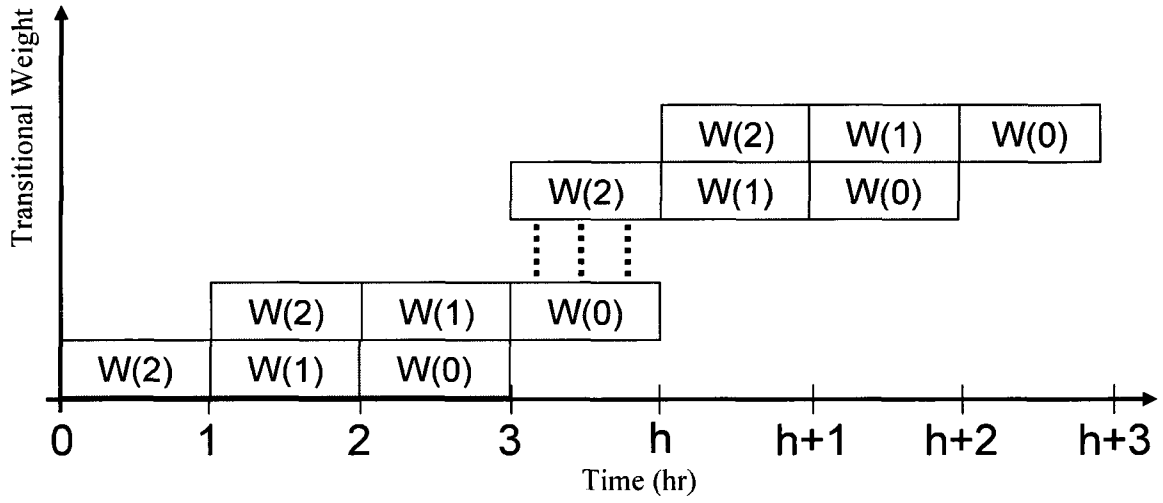


**Figure 4.2:** Presentation of the three different weights.

Then the process consisting of a finite number of states with known probabilities $P(x, y)$ of transition from state $y$ to state $x$ is considered a first order Markov Chain [64–66]. The transition probability matrix of the first-order Markov Chain for the five classes is shown below in (4.3). These transitions are depicted in a pictorial form in Figure 4.3 and can be represented by:

$$P_1 = \begin{array}{c} \\ A \\ B \\ C \\ D \\ E \end{array} \begin{array}{c} \begin{array}{ccccc} A & B & C & D & E \end{array} \\ \begin{bmatrix} P_{AA} & P_{AB} & P_{AC} & P_{AD} & P_{AE} \\ P_{BA} & P_{BB} & P_{BC} & P_{BD} & P_{BE} \\ P_{CA} & P_{CB} & P_{CC} & P_{CD} & P_{CE} \\ P_{DA} & P_{DB} & P_{DC} & P_{DD} & P_{DE} \\ P_{EA} & P_{EB} & P_{EC} & P_{ED} & P_{EE} \end{bmatrix} \end{array}. \tag{4.3}$$

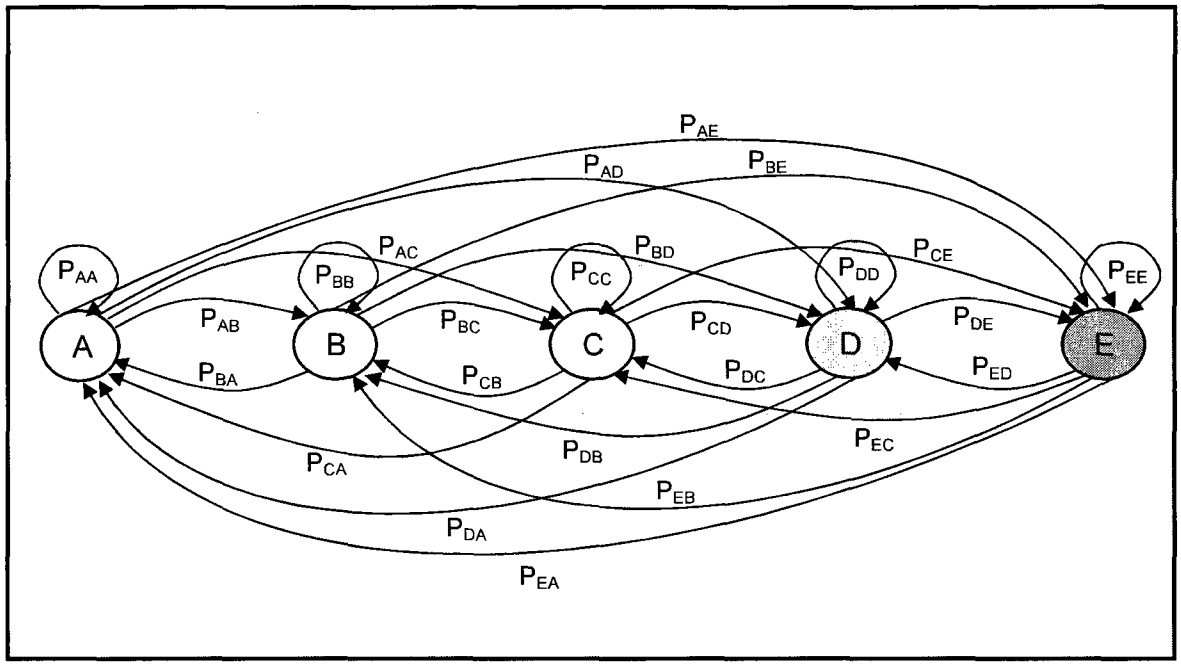


**Figure 4.3:** First Order Markov Chain model with transition probabilities for switching between states.

$$
P_2 = \begin{array}{c} \\ AA \\ AB \\ AC \\ AD \\ AE \\ BA \\ BB \\ BC \\ BD \\ BE \\ CA \\ CB \\ CC \\ CD \\ CE \\ DA \\ DB \\ DC \\ DD \\ DE \\ EA \\ EB \\ EC \\ ED \\ EE \end{array}
\begin{array}{c}
\begin{array}{ccccc} A & B & C & D & E \end{array} \\
\left[\begin{array}{ccccc}
P_{AAA} & P_{AAB} & P_{AAC} & P_{AAD} & P_{AAE} \\
P_{ABA} & P_{ABB} & P_{ABC} & P_{ABD} & P_{ABE} \\
P_{ACA} & P_{ACB} & P_{ACC} & P_{ACD} & P_{ACE} \\
P_{ADA} & P_{ADB} & P_{ADC} & P_{ADD} & P_{ADE} \\
P_{AEA} & P_{AEB} & P_{AEC} & P_{AED} & P_{AEE} \\
P_{BAA} & P_{BAB} & P_{BAC} & P_{BAD} & P_{BAE} \\
P_{BBA} & P_{BBB} & P_{BBC} & P_{BBD} & P_{BBE} \\
P_{BCA} & P_{BCB} & P_{BCC} & P_{BCD} & P_{BCE} \\
P_{BDA} & P_{BDB} & P_{BDC} & P_{BDD} & P_{BDE} \\
P_{BEA} & P_{BEB} & P_{BEC} & P_{BED} & P_{BEE} \\
P_{CAA} & P_{CAB} & P_{CAC} & P_{CAD} & P_{CAE} \\
P_{CBA} & P_{CBB} & P_{CBC} & P_{CBD} & P_{CBE} \\
P_{CCA} & P_{CCB} & P_{CCC} & P_{CCD} & P_{CCE} \\
P_{CDA} & P_{CDB} & P_{CDC} & P_{CDD} & P_{CDE} \\
P_{CEA} & P_{CEB} & P_{CEC} & P_{CED} & P_{CEE} \\
P_{DAA} & P_{DAB} & P_{DAC} & P_{DAD} & P_{DAE} \\
P_{DBA} & P_{DBB} & P_{DBC} & P_{DBD} & P_{DBE} \\
P_{DCA} & P_{DCB} & P_{DCC} & P_{DCD} & P_{DCE} \\
P_{DDA} & P_{DDB} & P_{DDC} & P_{DDD} & P_{DDE} \\
P_{DEA} & P_{DEB} & P_{DEC} & P_{DED} & P_{DEE} \\
P_{EAA} & P_{EAB} & P_{EAC} & P_{EAD} & P_{EAE} \\
P_{EBA} & P_{EBB} & P_{EBC} & P_{EBD} & P_{EBE} \\
P_{ECA} & P_{ECB} & P_{ECC} & P_{ECD} & P_{ECE} \\
P_{EDA} & P_{EDB} & P_{EDC} & P_{EDD} & P_{EDE} \\
P_{EEA} & P_{EEB} & P_{EEC} & P_{EED} & P_{EEE}
\end{array}\right]
\end{array}
. \tag{4.4}
$$

Similarly, the transition probability matrix of the second-order Markov Chain theory $P(z|xy)$ for the five classes is presented in (4.4).

The characteristics of these transition probability matrices is such that the entries for each column vectors in (4.2), (4.3), and (4.4) are positive numbers. The sum of the elements of each row in the matrices is one. The columns represent probability vectors, which are the stochastic values for transition. The transition probabilities are dependent on statistical pattern of rain at particular geography and climate.

### 4.2.3 Predicted Rainfall Rate

The value of predicted rainfall rate for the immediately following discrete time period is computed based on probability and weight combinations. These combinations present a special module of weather prediction of different weights assigned to each transition probability matrix along with Markov Chain of order $\phi$, where $\phi$ is finite and equal to 2 in our case. Thus, the prediction of the future state is dependent on the present, previous, and previous to previous states and it is independent of the other earlier states [34].

Given that the zero ($P_0$), first ($P_1$), and second order ($P_2$) transition probability matrices with the weights assigned to each matrix ($W_0$), ($W_1$), and ($W_2$), respectively. The predicted rainfall rate values can be computed as follows:

$$\begin{aligned}
PW(1) &= W(0).P_0(1) + W(1).P_1(m,1) + W(2).P_2(n,1),\\
PW(2) &= W(0).P_0(2) + W(1).P_1(m,2) + W(2).P_2(n,2),\\
PW(3) &= W(0).P_0(3) + W(1).P_1(m,3) + W(2).P_2(n,3),\\
PW(4) &= W(0).P_0(4) + W(1).P_1(m,4) + W(2).P_2(n,4),\\
PW(5) &= W(0).P_0(5) + W(1).P_1(m,5) + W(2).P_2(n,5),
\end{aligned} \tag{4.5}$$

where the numbers $(1, 2, 3, 4,$ and $5)$ represent the five classes $(A, B, C, D,$ and $E)$ shown in Figure 4.1. $P_0$ represents the row corresponding to the present state. $P_1$ represents the row corresponding to the transition from the last state to the present state. $P_2$ represents the row corresponding to the transition from the last-to-last to the last state and then to the present state. In our specific case, the $m$ can be any value ranging from 1 to 5, and $n$ can be any value ranging from 1 to 25 according to the previous and previous to previous weather state, respectively.

Also, $PW$ presented in equations (4.5) can be written in a simple mathematical form as:

$$PW(u) = W(0) \,.\, P_0(u) + W(1) \,.\, P_1(m, u) + W(2) \,.\, P_2(n, u), \tag{4.6}$$

where $u$ ranges from 1 to 5 and $PW$ represents the probability weight values of the five existing classes $(A, B, C, D,$ and $E)$, thus:

$$\begin{aligned} PW &= [PW(1) \;\; PW(2) \;\; PW(3) \;\; PW(4) \;\; PW(5)] \\ &= [PW_A \;\; PW_B \;\; PW_C \;\; PW_D \;\; PW_E]. \end{aligned} \tag{4.7}$$

Therefore, the predicted rainfall rate $(RR_{pr})$ will be belonging to the class that has the maximum probability weight of $PW$ vector collected from equation (4.7).

Figure 4.4 shows a demonstration for the effectiveness of our method for predicting rainfall rate. At the beginning, we used randomly generated values of rainfall rate to determine the weights and probability matrices elements for our model [67].

These values were then tested against rainfall rate values that were collected by Environment Canada for almost two month duration at South West of King City using weather radar near Toronto, Ontario, Canada. We applied our methodology to predict the future state out of past states. The prediction data obtained using our method and the measured rainfall data from Environment Canada are provided in Figure 4.5 and in Table 4.1. Note that only small numbers of

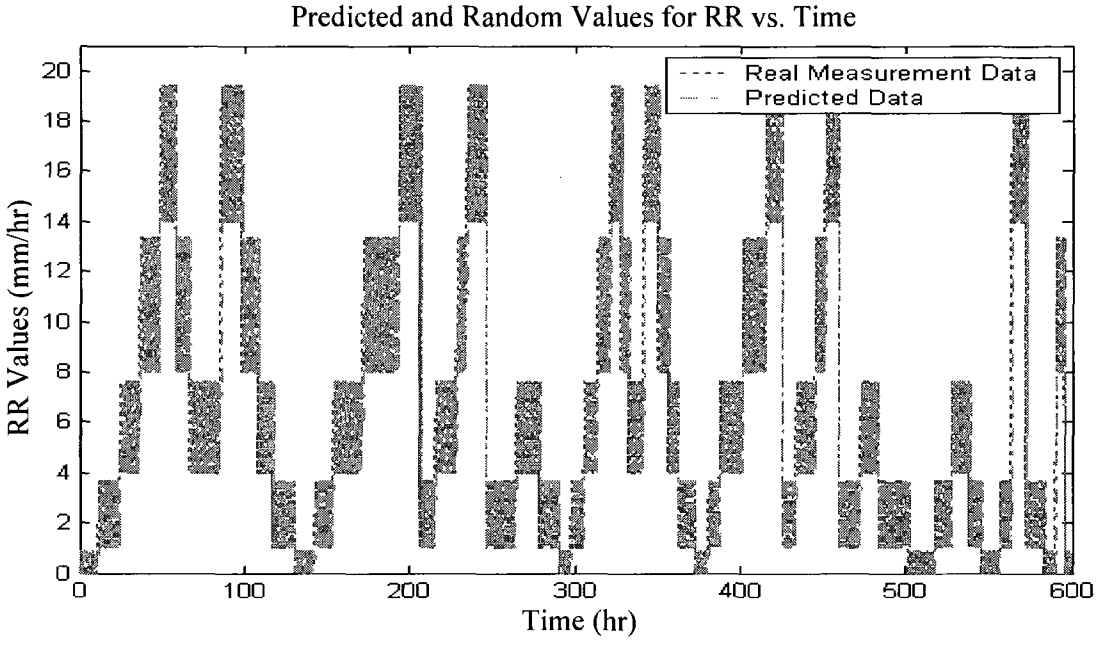


**Figure 4.4:** Comparison of random data and predicted rainfall rate values.

samples are presented in the table to keep it readable and the prediction matches closely with the measured results.

We conclude that, the Markov Chain has promising application in effectively predicting the future weather result in statistical terms. The results are astoundingly accurate. Therefore, our methodology for predicting rainfall rate can be applied under different weather conditions at any given location on earth.

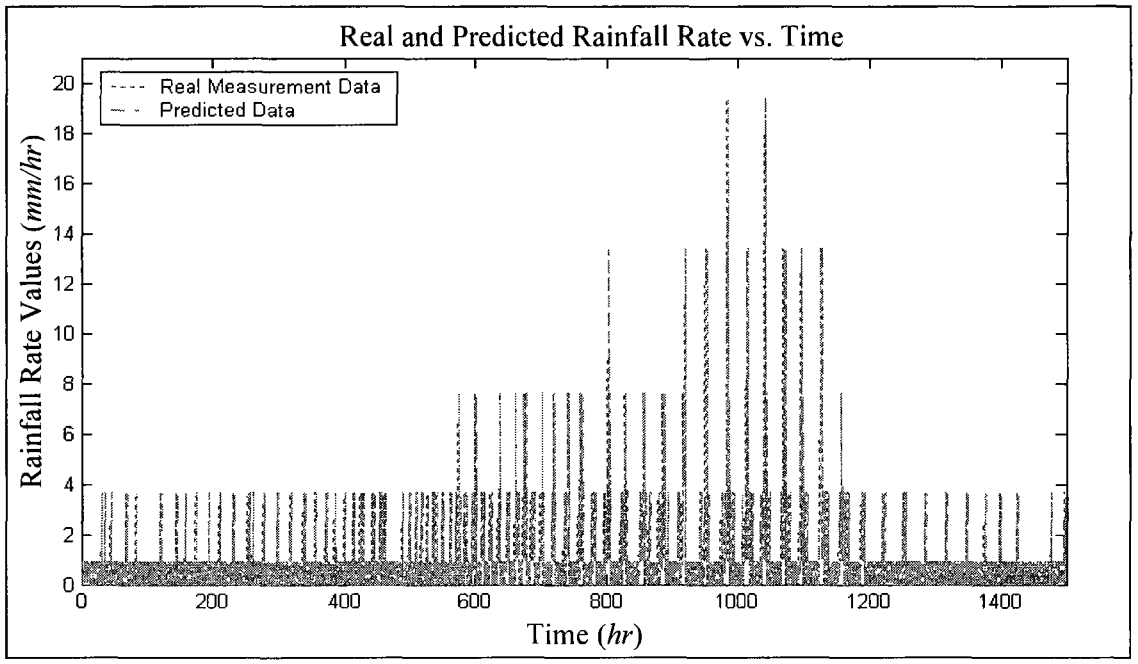


**Figure 4.5:** Comparison of actual and predicted rainfall rate values at South West of King City.

**Table 4.1:** Comparison of Accurate and Predicted Rainfall Rate Data at Different Time.

| Time [hr] | Accurate Time Data [mm/hr] | Predicted Data [mm/hr] | Different Between Both Results [mm/hr] |
|---|---|---|---|
| 1 | 0 | 0 | 0 |
| 3 | 0 | 0 | 0 |
| 4 | 0 | 0 | 0 |
| 80 | 0 | 0 | 0 |
| 170 | 0 | 0 | 0 |
| 200 | 0 | 0 | 0 |
| 210 | 1 | 0 | 1 |
| 220 | 0 | 0 | 0 |
| 330 | 0 | 0 | 0 |
| 338 | 1 | 1 | 0 |
| 350 | 0 | 0 | 0 |
| 510 | 1 | 1 | 0 |
| 610 | 1 | 1 | 0 |
| 620 | 0 | 0 | 0 |
| 640 | 0 | 0 | 0 |
| 650 | 1 | 1 | 0 |
| 780 | 1 | 1 | 0 |
| 790 | 0 | 0 | 0 |
| 880 | 1 | 1 | 0 |
| 890 | 0 | 0 | 0 |
| 970 | 0 | 0 | 0 |
| 1071 | 8 | 8 | 0 |
| 1098 | 4 | 4 | 0 |
| 1103 | 0 | 1 | 1 |
| 1104 | 1 | 1 | 0 |
| 1126 | 8 | 4 | 4 |
| 1127 | 8 | 8 | 0 |
| 1137 | 1 | 1 | 0 |
| 1148 | 0 | 0 | 0 |
| 1152 | 0 | 0 | 0 |
| 1155 | 1 | 1 | 0 |
| 1190 | 1 | 1 | 0 |
| 1192 | 1 | 1 | 0 |
| 1429 | 0 | 0 | 0 |

### 4.2.4 The Values of Weights and Transition Probabilities

The values of the weight matrix as defined in (4.1) and the transition probabilities as defined in (4.2), (4.3), and (4.4) were obtained through an extensive exercise of iterative adjustments and their test of validity on rainfall rate data. In the end, the study not only revealed a set of workable values but also the following behavior in them revealed the following behaviors.

1- For a given set of transition probabilities, there is a corresponding weight that gives the best prediction of rainfall rate in Markov Chain theory.

2- Studies done over actual rain data revealed that the five states model developed here gives extremely reliable prediction of rain with the following values of weights ($W$'s) are:

$$W = \begin{bmatrix} 0.495 & 0.335 & 0.170 \end{bmatrix}, \tag{4.8}$$

and transition probabilities ($P$'s) are:

$$P_0 = \begin{bmatrix} 0.35 & 0.25 & 0.2 & 0.1 & 0.1 \end{bmatrix}, \tag{4.9}$$

$$P_1 = \begin{array}{c} \\ A \\ : \\ E \end{array} \begin{array}{c} \begin{array}{ccccc} A & B & C & D & E \end{array} \\ \begin{bmatrix} 0.43 & 0.33 & 0.2 & 0.04 & 0 \\ : & : & : & : & : \\ P_{EA} & P_{EB} & P_{EC} & P_{ED} & P_{EE} \end{bmatrix} \end{array}, \tag{4.10}$$

and

$$P_2 = \begin{array}{c} \\ AA \\ : \\ EE \end{array} \begin{array}{c} \begin{array}{ccccc} A & B & C & D & E \end{array} \\ \begin{bmatrix} 0.45 & 0.37 & 0.14 & 0.03 & 0.01 \\ : & : & : & : & : \\ P_{EEA} & P_{EEB} & P_{EEC} & P_{EED} & P_{EEE} \end{bmatrix} \end{array}. \tag{4.11}$$

The full set of values could be obtained by contacting the author.

3- When rain rate classification as done in 4.2.1 is altered to better suite different locations on earth, the coefficients mentioned above will change. However, the values listed here will give good starting values for the iterative process of finding the new values.

Notice that, the weights and the transition probability matrices values are selected initially based on the statistical investigation of historical field data collected over several years. We discovered that the coefficient of the matrices and the weights remain relatively stable although weather conditions vary significantly. Nevertheless, some severe weather conditions not recorded by the data analyzed for this research could require some adjustments.

We acknowledge that the depending of Markov theory in stochastic assumptions and the potential errors in estimating the weights and coefficients of transition probability matrices. Especially for the fact that the method assumes stationary weather within one discrete time period, its prediction is nothing more than a practical approximation. Nevertheless, the test on the fields data demonstrated highly respectable results, yielding prediction values to contain low relative percentage error of ($\leq 11.9\%$) for the presented fifteen hundred hours rainfall rate data stated in Figure 4.5.

## 4.3 Summary

The proposed method, based on Markov theory, is flexible and can be presented in a given number of states that are chosen for the test environment. Through experiments it was concluded that five states yielded a good compromise between accuracy of results and computational efficiency. In practical systems, the number of states as well as the width of time-slice used for state observation can be changed, even dynamically if desired, to better reflect the weather pattern of a given location. It should also be noted that increasing the number of states to represent the weather spectrum increase the accuracy of prediction. Note that, when increasing the number of states, the compu-

tational complexity increases significantly. The predicted rainfall rate will be applied directly for atmospheric attenuations as it will be shown in the following chapter.

# Chapter 5

# Calculation of Atmospheric Attenuation

## 5.1 Introduction

The aim of this chapter is to describe a method to calculate signal attenuations due to rain, gaseous absorption, cloud, fog, and tropospheric scintillation with the aid of estimated weather condition. Our method presented here is a major enhancement over ITU – R methods as it improves computational efficiency in estimating atmospheric attenuations in the presence of both changing weather and frequencies. In addition, we have presented a three dimensional relationship for atmospheric attenuations in relation to rainfall rate and propagation angle at a given frequency, location and propagation parameters. Similarly, a three dimensional relationship is also established between atmospheric attenuation with rainfall rate and frequency for a specific propagation angle at a given location and propagation parameters [9, 15, 16, 50].

Relationship is also established between weather attenuations, propagation angle, and predicted rainfall rate for different operational frequencies given the geographic location of ground terminals. Therefore, we propose new results presented in three dimensional relationships for different atmospheric attenuations, predicted rainfall rate, and propagation angle for a selected operational frequency, which can be any value up to $55\ GHz$.

Thus, the above mentioned results will be an immense asset for the satellite's controller to have a clear view of channel characteristics that are related to a given location based on different propagation angles, frequencies, and other satellite parameters.

## 5.2 Migrating ITU − R Model from the Design Domain to the Operational Domain

ITU − R model for estimating environmental attenuations based on the weather data that was collected over a decade and a half have served well in knowing average operating conditions and the boundary conditions that a communication system would be subjected to. ITU − R provides the geographic parameters of a location, such as the height above sea level and average rain height as shown in Figure 3.2 and weather factors like the probability of precipitation. Further, the ITU − R provides mathematical formula for estimating rainfall rate, and subsequently estimating signal attenuation to be caused by rain, gas, cloud and fog, and scintillation. The ITU − R techniques have been serving useful purpose in selecting the optimal combination of frequency, modulation, coding, and other transmission and reception parameters when designing satellite communication systems.

The research work reported in this thesis stemmed from an interest that, if these techniques were to be extended to estimate the attenuations in a real-time environment, they would have greatly served the purpose of optimally operating those designed systems by allowing to select proper combination of controllable parameters. Therefore, the ITU − R methodology was studied and extended to solve the problem of adapting the control systems with the instantaneous variations of weather. Markov theory has been utilized to estimate the weather condition for the immediately following time-period based on the actual data from the immediately preceding time-periods and the statistical probability of state changes. Subsequent experiment demonstrated that inclusion of Markov prediction technique and its resulting data as an input to ITU − R techniques resulted in

highly accurate estimation for rainfall rate, rain, gaseous, fog and cloud, and scintillation attenuations. The improvement in the ability to predict weather attenuation in real-time would thus help significantly to improve the real-time control by enhancing the ability to select the signal parameters not only during system design but also during system operation.

The following are the key benefits achieved by the proposed technique:

1. Use of Markov model for real-time estimation of rainfall rate. The prediction of rainfall rate is made by viewing the time series of weather data. The impending rain rate is estimated based on current rate, previous rate, and previous to previous rate.

2. Calculation of attenuations based on the predicted rainfall rate based on measured data.

3. Actual signal adaptation to weather variation. It is facilitated by selecting appropriate frequency, modulation, coding, and transmission rate.

## 5.3 Fusing ITU − R Method with Markov Model

A new model of representing satellite channel has been devised such that it not only gives better estimation of channel characteristics, but is also conducive for efficient software implementation. In doing that, various constituent contributors of total attenuation are estimated separately and extended to give good approximations for a wide range of signal frequency, propagation angle, and predicted rainfall rate. The model uses ITU − R coefficients as shown in Figure 3.2 while estimating the attenuation at grid locations in weather collection map that is used by ITU − R. In cases where the location of concern does not fall on the grid, a bi-linear interpolation technique is then used to get the parameters [3,9].

Most of the formulas and variables presented in the following section are derived from ITU − R model and are adapted to handle actual data of the present window and Markov prediction of the data for the following period. Next section is devoted to predict constituent contributors of channel

attenuation due to different weather variants. The total attenuation due to all the factors combined is then determined. Also, in the following chapter, SNR calculation based on the estimated attenuations is presented.

## 5.4 Calculating Atmospheric Attenuation Using Historical and Predicted Data

### 5.4.1 Calculating Rain Attenuation

#### i- Using Historical Data

Rain attenuation is the single greatest weather factor in signal attenuation, which occurs in satellite networks largely due to signal absorption and scattering of incoming signal. Note that rain forms only in the troposphere that extends around sixteen kilometers from sea level and the satellites are located in geostationary orbit at $35,800\ km$ above earth. Nevertheless free space loss alone would be very substantial when the transmitting and receiving entities are at great distances.

It is due to this need that determining signal attenuation from rain became as important as those from other climatic-variations and free-space loss in satellite communication systems. Therefore, modeling rain attenuation from predicted rainfall rate at regional or individual sites were found to be important for improved control of satellite channel parameters especially when higher transmission frequencies were adopted to achieve greater transmission rate through communication channels [44–47].

Usually, control of transmit power is used to compensate for the change in signal attenuation. This extra power that is reserved to compensate for rain attenuation is called rain fade margin [22]. However, this measure is not always sufficient to achieve desired level of link

quality. For this reason, the fade margin is used along with other factors such as different coding, modulation, frame size, and transmission rate. Also, with home satellite dishes, when the loss of signal strength due to rain is less than the rain fade margin, television can still be watched while raining and signal will be lost when its loss exceeds the rain fade margin.

In most situations, this measure is supplemented with limiting of up-link power to increase the availability, the performance of satellite links [39, 68–70] and the control of other parameters such as coding, modulation, frame size, and transmission rate. That is why satellite control systems become complex.

Thus, a new method for extracting rain attenuation as a function of propagation angle and rainfall rate is presented below. The calculation of rain attenuation is performed in few steps. First, rain attenuation is the multiple of specific attenuations and the effective path length as follows [9,30]:

Obtain the specific attenuation using:

$$\gamma_R(\theta,\ RR_{ep}) \ = \ K_\tau(\theta) \ \cdot \ (RR_{ep})^{\alpha_\tau(\theta)} \ \ dB/km, \tag{5.1}$$

where the frequency-dependent coefficients $K_\tau$ and $\alpha_\tau$ as a function of propagation angle $(\theta)$ can be computed as:

$$K_\tau(\theta) \ = \ \left[K_H + K_V + (K_H - K_V)\cos^2\theta\cos 2\tau\right]/2 \tag{5.2}$$

and

$$\alpha_\tau(\theta) \ = \ \left[K_H\alpha_H + K_V\alpha_V + (K_H\alpha_H - K_V\alpha_V)\cos^2\theta\cos 2\tau\right]/2k, \tag{5.3}$$

where $K_V, \alpha_V$ and $K_H, \alpha_H$, are constant coefficients of vertical and horizontal polariza-

tions [7], and the effective path length is calculated as:

$$L_E(\theta,\ RR_{ep}) \ = \ L_R(\theta,\ RR_{ep}) \ \cdot \ v(\theta,\ RR_{ep}) \ \ km. \tag{5.4}$$

The above variables $K_\tau, \gamma_R, \alpha_\tau, L_E$, and $L_R$ are described in Section (3.4). The difference in this Section is that we represent these variables as function of rainfall rate ($RR_{ep}$) and propagation angle ($\theta$). Calculate the rain attenuation by multiplying the specific attenuation with the effective path length as:

$$A_{Rain}(\theta,\ RR_{ep}) \ = \ \gamma_R(\theta,\ RR_{ep}) \ \cdot \ L_E(\theta,\ RR_{ep}) \ \ dB. \tag{5.5}$$

The $A_{Rain}(\theta,\ RR_{ep})$, which is a function of propagation angle ($\theta$), rainfall rate ($\mathrm{RR_{ep}}$), location, polarization, and frequency, has been plotted in Figure 5.1 for a weather at Hazelton Station in Canada. The figure shows that rain attenuation increases exponentially with the increase of rainfall rate and with the decrease of propagation angle. Rain attenuation values are collected at the station ranging from 0 to 21 $dB$ when rainfall rate ranges from 0 to 12 $mm/hr$ and propagation angle ranges from 50 to 0 $degrees$ for a given frequency equal to 20 $GHz$.

As mentioned, rain attenuation is considered a dominant factor among other atmospheric attenuations and strongly affects wireless signal propagation. In the previous chapter, rain attenuation was presented as a function of frequency by:

$$A_{Rain}(f_n) \ = \ \gamma_R(f_n) \ \cdot \ L_E(f_n) \ \ dB. \tag{5.6}$$

Another way is then proposed for extracting rain attenuation (RA) as a function of frequency

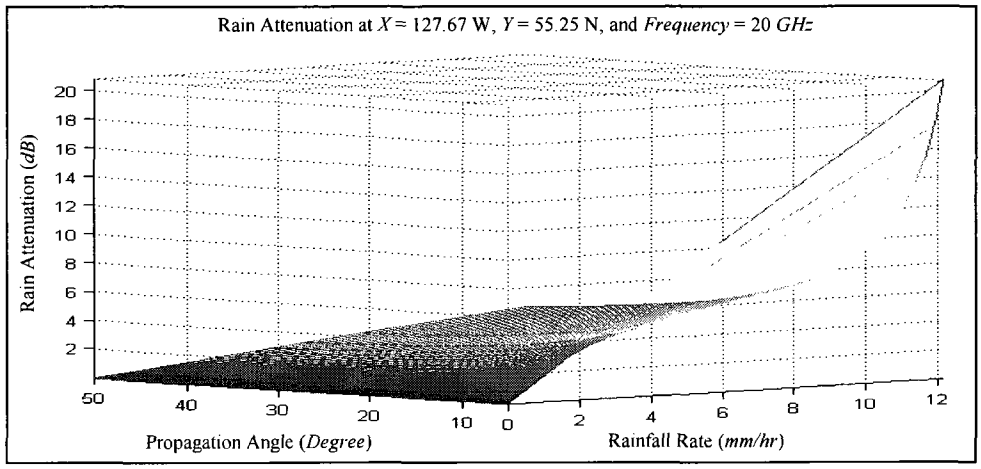


**Figure 5.1:** Rain attenuation – function of rainfall rate and propagation angle at Hazelton Station, Canada.

and rainfall rate by combining several functions [9, 29]. Therefore, RA computed in (5.5) can be reformulated for different frequencies and rainfall rate values as per (5.7). The RA of an average year for different frequencies ranging from 7 to 55 $GHz$, and for different rainfall rate values ranging form 0 $mm/hr$ to higher values, can be obtained from:

$$A_{Rain}\,(f,\ RR_{ep}) \ = \ \gamma_R\,(f,\ RR_{ep}) \cdot L_E\,(f,\ RR_{ep}) \ \ dB, \tag{5.7}$$

where $A_{Rain}(f,\ RR_{ep})$ represents RA at a given frequency and given rainfall rate. Series of $A_{Rain}$ values calculated for a range of frequencies and rainfall rate. Figure 5.2 shows that rain attenuation increases widely with the increase of rainfall rate and operational frequency. The rain attenuation values ranged from 0 to 25 $dB$ when rainfall rate ranged from 0 to 12 $mm/hr$, frequency ranged from 0 to 50 $GHz$ for a given propagation angle of 25 $degrees$ placed at Atlin Station, Canada.

The foundational work of this technique and variables are explained in [3, 6, 7]. Here, it is

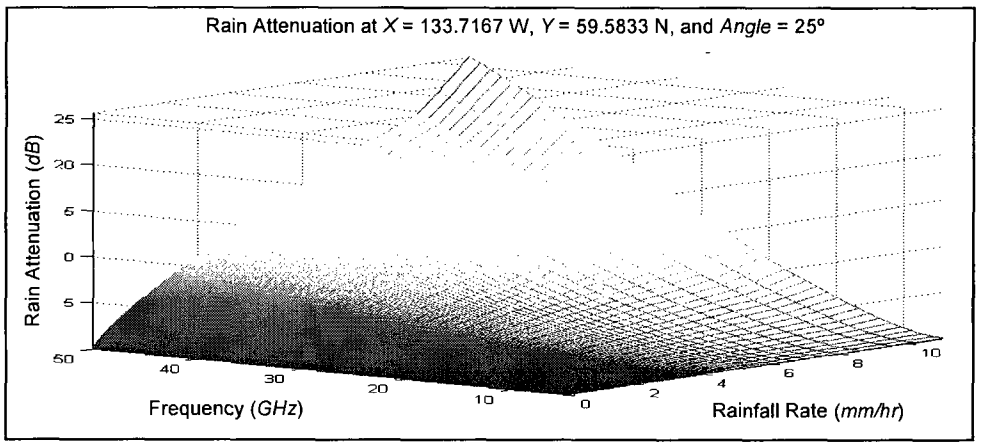


**Figure 5.2:** Rain attenuation – function of rainfall rate and frequency at Atlin Station, Canada.

emphasized that in this technique we start with an attenuation value at a known frequency $(f_n)$ and then estimate the attenuation at one higher frequency $(f_{n+1})$ increment. Then using the attenuation at $(f_{n+1})$, we find attenuation at $(f_{n+2})$, and so on. That is, once we have rain attenuation at a lower selected frequency, we can then compute rain attenuation at a higher frequency and we continue the process until we reach the maximum desired frequency. Similar approach is used when the sample frequency $(F_s)$ is found at a higher frequency and we traverse towards lower frequencies.

**ii- Using Predicted Data**

The technique developed for historical data works equally well for actual data. However, we use a notation $RR_{pr}$ to denote the predicted rainfall rate from actual data. The rain attenuation thus obtained from actual scenario would be as follows [3,6]:

$$A_{Rain}\left(f_n, RR_{pr}\right) \;=\; \gamma_R\left(f_n, RR_{pr}\right) \;\cdot\; L_E\left(f_n, RR_{pr}\right)\; dB, \tag{5.8}$$

where based on previous definition for $\gamma_R$ and $L_E$, we found that we can present these two

variables as a function of predicted rainfall rate and frequency, thereby making it useful for the operation of the control system. The historical data only helped in design but not in operation. The derivation of the above variables were explained in Section (3.4).

Here the rain attenuation is calculated as a function of frequency and rainfall rate. Unlike existing ITU − R method, this method provides high CPU efficiency as it avoid reparative calculation for each frequency. The different in CPU time consumption between Original ITU − R Method and IAM increases with the degree of variation in weather. As the weather varies the saving obtained through the IAM becomes more and more significant. Also with the increase in the range of frequency of operation, the saving from IAM increase. In discrete frequency of $n$ steps, the calculation in ITU − R Original Method is made $n$ times. But with IAM only one major calculation and one more calculation to extrapolate the value in required. Moreover, IAM eliminates the accumulated error in comparison with existing Approximated ITU − R solution [9,30].

Also, the rain attenuation (RA) is calculated as a function of propagation angle ($\theta$), predicted rainfall rate ($\mathrm{RR_{pr}}$), effective path length, and frequency coefficient, as:

$$A_{Rain}\left(\theta, RR_{pr}\right) = \gamma_R\left(\theta, RR_{pr}\right) \cdot L_E\left(\theta, RR_{pr}\right) \quad dB, \tag{5.9}$$

where $A_{Rain}(\theta, RR_{pr})$ represents RA for a given value of predicted rainfall rate ($\mathrm{RR_{pr}}$), and propagation angle ($\theta$). Figure 5.3 plots RA versus $\theta$ and $\mathrm{RR_{pr}}$, and the variables $L_E$ and $\gamma_R$ are described in Section (3.4.1). The figure shows that rain attenuation increases exponentially with the increase in rainfall rate and decrease in propagation angle. The rain attenuation values, collected at South West of King City Station, Canada, ranged from 0 to 55 $dB$ when rainfall rate ranged from 0 to 15 $mm/hr$, propagation angle ranged from 45 to 5 $degrees$ for a given frequency that equals to 20 $GHz$.

Thus far we discussed prediction of rain attenuation at a desired location for different prop-

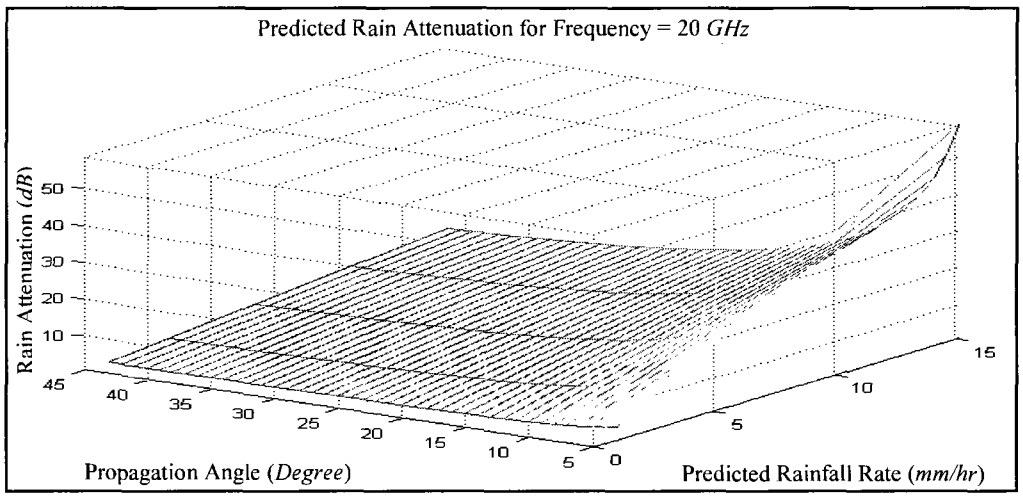


**Figure 5.3:** Predicted rain attenuation – function of predicted rainfall rate and propagation angle at South West of King City Station, Canada.

agation angles, predicted rainfall rate values, and channel frequencies. However, in order to control the satellite channels efficiently, we also need to factor other parameters like gaseous, cloud, fog, and scintillation attenuations as described below.

### 5.4.2 Calculating Gaseous Attenuation

#### i- Using Historical Data

In this section, we extend the analytical methods for estimating gaseous attenuation presented in ITU – R Recommendation P. 676. This method had been discussed in great deal in our papers [3, 31] to present the variations of gaseous attenuation with the changing of rainfall rate, propagation angle, and frequency for a given temperature, pressure, location, etc. The key point is that gaseous attenuation depends on meteorological conditions created by the distribution of temperature, pressure, and humidity along the transmission path. Also,

the effective path length varies with location, month of the year, height of the station above sea level and the propagation angle. Essentially the calculation is done by summing the effects of all of the significant resonance lines given in ITU − R Recommendation P. 676 "Attenuation by atmospheric gases". The calculation requires the following parameters:

1. *Specific Attenuation for Dry Air ($\gamma_\tau$).*
2. *Specific Attenuation for Water Vapor ($\gamma_v$).*
3. *Equivalent Path Length for Dry Air ($h_\tau$).*
4. *Equivalent Path Length for Water Vapor ($h_v$).*

The ITU − R mathematical equations for obtaining the values of these parameters are given below.

1. *Specific Attenuation for Dry Air ($\gamma_\tau$)*

   For dry air, the attenuation $\gamma_\tau$ $(dB/km)$ for the frequency $(f \leq 54\ GHz)$ is given as [2,50,53]:

$$\gamma_\tau = \left[\frac{7.2 \cdot r_t^{2.8}}{f^2 + 0.34 \cdot r_{ph}^2 \cdot r_t^{1.6}} + \frac{0.62 \cdot \xi_3}{(54 - f)^{1.16 \cdot \xi_1} + 0.83 \cdot \xi_2}\right] f^2 \cdot r_{ph}^2 \cdot 10^{-3}, \quad (5.10)$$

   with

$$\xi_1 = \varphi(r_{ph}, r_t, 0.0717, -1.8132, 0.0156, -1.6515), \quad (5.11)$$

$$\xi_2 = \varphi(r_{ph}, r_t, 0.5146, -4.6368, -0.1921, -5.7416), \quad (5.12)$$

$$\xi_3 = \varphi(r_{ph}, r_t, 0.3414, -6.5851, 0.2130, -8.5854), \quad (5.13)$$

   and

$$\varphi(r_{ph}, r_t, a, b, c, d) = r_{ph}^a \cdot r_t^b \cdot \exp[c(1 - r_{ph}) + d(1 - r_t)]. \quad (5.14)$$

2. *Specific Attenuation for Water Vapor ($\gamma_v$)*

For water vapour, the attenuation $\gamma_v$ $(dB/km)$ is given as:

$$\begin{aligned}\gamma_v = \{ & \tfrac{3.98\cdot\eta_1\cdot\exp[2.23(1-r_t)]}{(f-22.235)^2+9.42\cdot\eta_1^2}\cdot g(f,22) + \tfrac{11.96\cdot\eta_1\cdot\exp[0.7(1-r_t)]}{(f-183.31)^2+11.14\cdot\eta_1^2}\cdots \\ \cdots & + \tfrac{0.081\cdot\eta_1\cdot\exp[6.44(1-r_t)]}{(f-321.226)^2+6.29\cdot\eta_1^2} + \tfrac{3.66\cdot\eta_1\cdot\exp[1.6(1-r_t)]}{(f-325.153)^2+9.22\cdot\eta_1^2}\cdots \\ \cdots & + \tfrac{25.37\cdot\eta_1\cdot\exp[1.09(1-r_t)]}{(f-380)^2} + \tfrac{17.4\cdot\eta_1\cdot\exp[1.46(1-r_t)]}{(f-448)^2}\cdots \\ \cdots & + \tfrac{844.6\cdot\eta_1\cdot\exp[0.17(1-r_t)]}{(f-557)^2}\cdot g(f,557) + \tfrac{290\cdot\eta_1\cdot\exp[0.41(1-r_t)]}{(f-752)^2}\cdot g(f,752)\ \},\end{aligned} \tag{5.15}$$

with

$$\eta_1 = 0.955\cdot r_{ph}\cdot r_t^{0.68} + 0.006\cdot\rho, \tag{5.16}$$

$$\eta_2 = 0.735\cdot r_{ph}\cdot r_t^{0.5} + 0.0353\cdot r_t^4\cdot\rho,$$

and

$$g\,(f,f_i) = 1+\left(\frac{f-f_i}{f+f_i}\right)^2, \tag{5.17}$$

where $ph$: pressure $(hPa)$, $r_{ph} = ph/1013$, $r_t = 288/(273+t)$, $\rho$: water-vapour density $(g/m^3)$, $f$: frequency $(GHz)$, and $t$: mean temperature values $(^\circ C)$, can be obtained from ITU − R Recommendation P. 1510 when no adequate temperature data is available.

3. *Equivalent Path Length for Dry Air ($h_\tau$)*

The equivalent height for the dry air is given by:

$$h_\tau = \frac{6.1}{1+0.17\cdot r_{ph}^{-1.1}}\cdot(1+t_1+t_2+t_3), \tag{5.18}$$

where

$$t_1 = \frac{4.64}{1+0.066\cdot r_{ph}^{-2.3}}\cdot\exp\left[-\left(\frac{f-59.7}{2.87+12.4\cdot\exp(-7.9\cdot r_{ph})}\right)^2\right], \tag{5.19}$$

$$t_2 = \frac{0.14 \cdot \exp(2.12 \cdot r_{ph})}{(f - 118.75)^2 + 0.031 \cdot \exp(2.2 \cdot r_{ph})}, \tag{5.20}$$

and

$$t_3 = \frac{0.0114}{1 + 0.14 \cdot r_{ph}^{-2.6}} \cdot f \cdot \frac{-0.0247 + 10^{-4} \cdot f + 1.61 \cdot 10^{-6} \cdot f^2}{1 - 0.0169 \cdot f + 4.1 \cdot 10^{-5} \cdot f^2 + 3.2 \cdot 10^{-7} \cdot f^3}, \tag{5.21}$$

with the constraint that:

$$h_\tau \leq 10.7 \cdot r_{ph}^{0.3}, \tag{5.22}$$

when $f < 70\,GHz$.

4. *Equivalent Path Length for Water Vapour ($h_v$)*

For water vapour, the equivalent height for $f \leq 350\,GHz$ is:

$$h_v(RR_{ep}) = 1.66 \cdot \cdots$$
$$\cdots \cdot \left(1 + \frac{1.39 \cdot \sigma_v}{(f-22.235)^2+2.56 \cdot \sigma_v} + \frac{3.37 \cdot \sigma_v}{(f-183.31)^2+4.69 \cdot \sigma_v} + \frac{1.58 \cdot \sigma_v}{(f-325.1)^2+2.89 \cdot \sigma_v}\right) km, \tag{5.23}$$

where

$$\sigma_v = \frac{1.013}{(1 + \exp[-8.6\,(r_{ph} - 0.57)])}. \tag{5.24}$$

## • *Calculating Total Gaseous Attenuation*

The total gaseous attenuation based on surface meteorological data using the cosecant law for a given propagation angle and rainfall rate ($RR_{ep}$) could be obtained from:

$$A_{Gas}(\theta, RR_{ep}) = \frac{A_\tau + A_v(RR_{ep})}{\sin\theta} \quad dB, \tag{5.25}$$

where $A_\tau = h_\tau \cdot \gamma_\tau\ dB$, $A_v(RR_{ep}) = h_v(RR_{ep}) \cdot \gamma_v\ dB$, and $\theta \geq 5\ degrees$. This equation estimates gaseous values at desired locations, for all ranges of propagation angle, rainfall rate, and for a given frequency. Figure 5.4 shows the gaseous attenuation

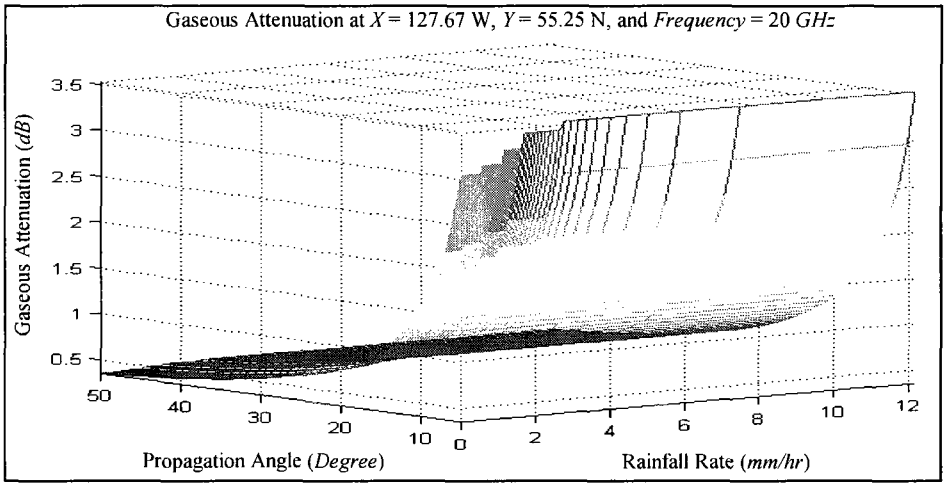


**Figure 5.4:** Gaseous attenuation – function of rainfall rate and propagation angle at Hazelton Station, Canada.

calculated for a Hazelton Station in Canada. The figure shows that gaseous attenuation increase exponentially with the increase in rainfall rate and decrease in propagation angle. The gaseous attenuation values, collected at the station ranged from 0 to 3.5 $dB$ when rainfall rate ranged from 0 to 12 $mm/hr$, and propagation angle ranged from 50 to 0 $degree$ for a given frequency that equals to 20 $GHz$.

Note that, gaseous attenuation can also be presented as a function of rainfall rate and frequency for a specific propagation angle as:

$$A_{Gas}\,(f,\ RR_{ep}) \ = \ \frac{A_{\tau} \ + \ A_{v}(RR_{ep})}{\sin\theta} \ dB. \tag{5.26}$$

Based on equation (5.26) and its derivatives, water vapour has resonance of $(22.235\ GHz)$, $(183.31\ GHz)$, and $(325.1\ GHz)$, respectively and that attenuation changes with the amount of water vapour in the atmosphere. Note that $\sigma_v$ is a function of predicted rainfall rate [53].

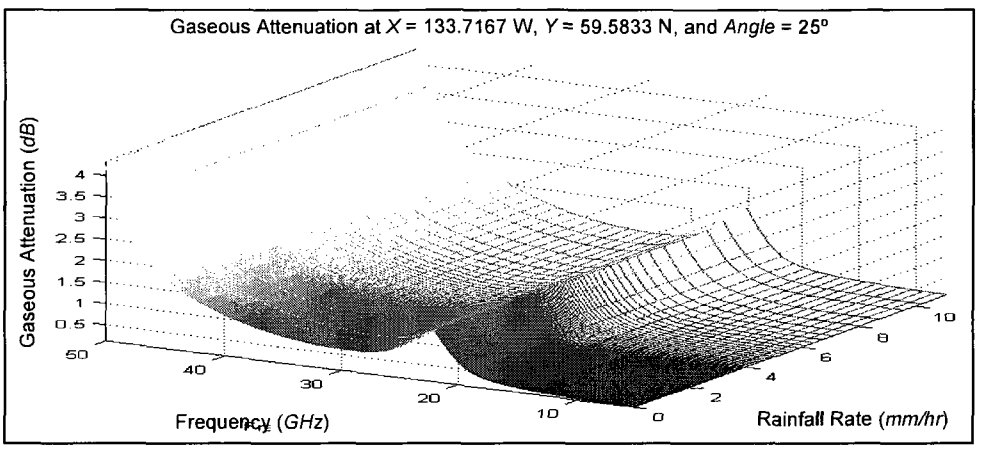


**Figure 5.5:** Gaseous attenuation – function of rainfall rate and frequency at Atlin Station, Canada.

Gaseous attenuation is calculated at the experimental location. We can notice from Figure 5.5 that the attenuation increases at operating frequency near $(22.235\ GHz)$ for all given rainfall rate values (0 to 12 $mm/hr$) signaling greater absorption of signal at this frequency. Therefore, satellite's controller should avoid the operation at and around this operational frequency to avoid high attenuation due to resonance effect [50, 53].

**ii- Using Predicted Data**

In this section, the gaseous attenuation is calculated by deploying actual prediction [34]. Let us replace the historical rainfall rate ($\mathrm{RR_{ep}}$) with the predicted rainfall rate ($\mathrm{RR_{pr}}$) in equation (5.25) as in the following:

$$A_{Gas}\left(\theta, RR_{pr}\right) = \frac{A_\tau + A_v(RR_{pr})}{\sin\theta} \quad dB, \tag{5.27}$$

where

$$A_\tau = h_\tau \cdot \gamma_\tau \quad dB \tag{5.28}$$

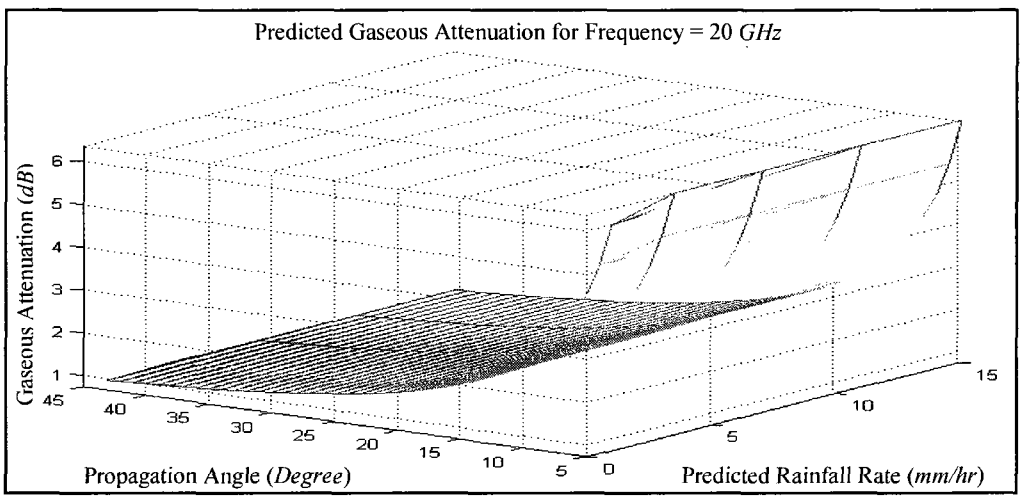


**Figure 5.6:** Predicted gaseous attenuation – function of predicted rainfall rate and propagation angle at South West of King City Station, Canada.

and

$$A_v(RR_{pr}) = h_v(RR_{pr}) \cdot \gamma_v \quad dB. \tag{5.29}$$

Figure 5.6 shows that the gaseous attenuation increase with the increase in rainfall rate and decrease in propagation angle. The gaseous attenuation values, ranged from 0 to 6.5 $dB$ when rainfall rate ($\mathrm{RR_{pr}}$) ranged from 0 to 15 $mm/hr$ and propagation angle ranged from 45 to 5 $degrees$ for a given frequency that equals to 20 $GHz$ at South West of King City Station, in this example.

### 5.4.3 Calculating Clouds and Fog Attenuations

Cloud and fog can be described as a collection of smaller rain droplets or alternatively, as different interactions from rain since the water droplet size in fog and cloud are smaller than the wavelength of 3 – 30 $GHz$ signals.

**i- Using Historical Data**

In this section, we extend analytical method in [16] for estimating clouds and fog attenuations. This method has also been discussed in papers [3,31,54].

We compute the attenuation due to clouds and fog using the following equation for propagation angle ranging between $5 \leq \theta \leq 90\ degrees$ using the following relationship:

$$A_{Cloud\&Fog}\,(\theta,\ RR_{ep}) \ = \ \frac{L_w \cdot K_t}{\sin\theta}\ dB, \tag{5.30}$$

where

$$K_t \ = \ (0.819 \cdot f)/(D_{p2}\cdot(1+\eta^2)) \quad (dB/km)/(g/m^3)\ , \tag{5.31}$$

$$\eta \ = \ (2 + D_{p1})/D_{p2}\ , \tag{5.32}$$

$$D_{p1} \ = \ \left((\varepsilon_0 - \varepsilon_1)\,/\,\left(1 + (f/f_p)^2\right)\right) + \left((\varepsilon_1 - \varepsilon_2)\,/\,\left(1 + (f/f_{sc})^2\right)\right) + \varepsilon\ , \tag{5.33}$$

and

$$D_{p2} \ = \ \left(f \cdot (\varepsilon_0 - \varepsilon_1)\,/\,\left(f_p \cdot \left(1 + (f/f_p)^2\right)\right)\right) + \left(f \cdot (\varepsilon_1 - \varepsilon_2)\,/\,\left(f_{sc} \cdot \left(1 + (f/f_{sc})^2\right)\right)\right)\ , \tag{5.34}$$

where $K_t$ represents attenuation coefficients. And $\varepsilon_0,\ \varepsilon_1$, and $\varepsilon_2$ are the complex dielectric permittivities of water as:

$$\begin{aligned} \varepsilon_2 \ &= \ 3.51, \\ \varepsilon_1 \ &= \ 5.48, \\ \varepsilon_0 \ &= \ 77.6 + 103.3(\mathrm{t}_1 - 1), \end{aligned} \tag{5.35}$$

where

$$t_1 \ = \ 300\ /\ t_k\ , \tag{5.36}$$

$$f_p \;=\; 20.09 - 142(t_1{-}1) + 294(t_1{-}1)^2\,, \tag{5.37}$$

and

$$f_{sc} \;=\; 590 - 1500(t_1{-}1)\,, \tag{5.38}$$

where $t_k$ represents temperatures in $Kelvin$. $f_p$ and $f_{sc}$ represent the principal and the secondary relaxation frequencies, respectively.

To obtain the estimated attenuation due to clouds for a given rainfall rate value, the statistics of the total columnar content of liquid water $L_w$ $(kg/m^2)$ is to be known. The latter, however, is an integration of liquid water density, $M$ $(kg/m^3)$, along a cross section of 1 $m^2$ from surface to top of clouds for a given site.

The clouds and fog attenuations $A_{Cloud\&Fog}$ can be expressed in terms of rainfall rate, and propagation angle, for a specific frequency and temperature values. Figure 5.7 shows that cloud and fog attenuation increases exponentially with the increase in rainfall rate and with decrease in propagation angle. The cloud and fog attenuation values, collected at Hazelton Station, Canada, ranged from 0 to 1.9 $dB$ when rainfall rate ranged from 0 to 12 $mm/hr$ and propagation angle ranged from 50 to 0 $degree$, for a frequency of 20 $GHz$.

Also, cloud and fog attenuations can also be expressed after mathematical manipulation in terms of wide range of frequency ($f$) and rainfall rate ($\mathrm{RR_{ep}}$) for a given propagation angle as:

$$A_{Cloud\&Fog}\,(f,\; RR_{ep}) \;=\; \frac{L_w \cdot K_t}{\sin\theta}\;\; dB. \tag{5.39}$$

The result of equation (5.39) is plotted in Figure 5.8. This figure shows that cloud and fog attenuations increases with the increase of rainfall rate and operational frequency. The cloud and fog attenuation values ranged from 0 to 2.8 $dB$ when rainfall rate ranged from 0 to 12 $mm/hr$ and frequency ranged from 0 to 50 $GHz$ for a given propagation angle of 25 $degrees$ placed at Atlin Station, Canada.

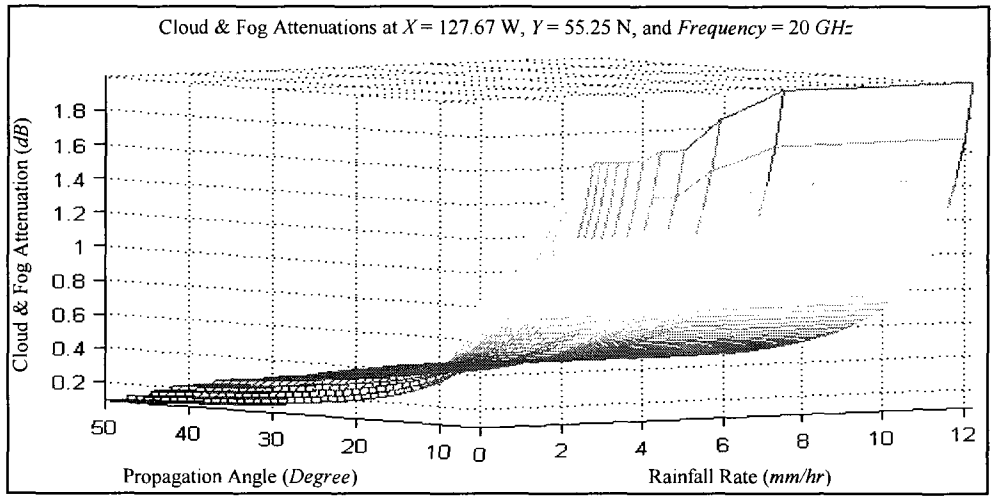


**Figure 5.7:** Clouds and fog attenuations – function of rainfall rate and propagation angle at Hazelton Station, Canada.

The difference between equation (5.30) and equation (5.39) is that: The former is a function of propagation angle and rainfall rate for a fixed frequency value, and the later is a function of frequency and rainfall rate for a fixed propagation angle value.

### ii- Using Predicted Data

The predicted cloud and fog attenuations can be expressed by replacing the historical rainfall rate ($\mathrm{RR_{ep}}$) in equation (5.30) with the predicted rainfall rate ($\mathrm{RR_{pr}}$). These attenuations are estimated in terms of predicted rainfall rate and propagation angle for a specific frequency and temperature values $t_k$ $(Kelvin)$ as follows:

$$A_{Cloud\&Fog}\,(\theta, RR_{pr}) \;=\; \frac{L_v(pr)\cdot K_t}{\sin\theta}\;dB, \tag{5.40}$$

where $A_{Cloud\&Fog}(\theta, RR_{pr})$ represents predicted cloud and fog attenuations. $L_v$ $(kg/m^2)$ is the statistics of the total columnar content of liquid water and the integration of liquid water

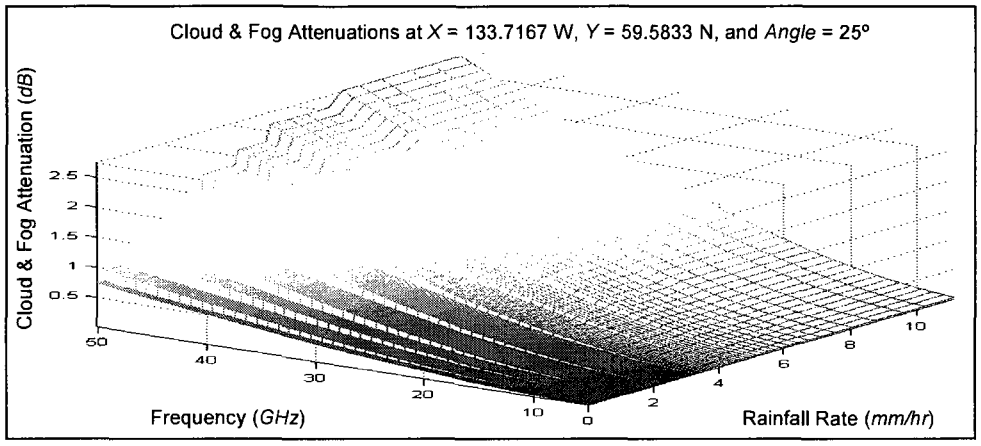


**Figure 5.8:** Cloud and fog attenuations – function of rainfall rate and frequency at Atlin Station, Canada.

density, $M$ $(kg/m^3)$, along a cross section of 1 $m^2$ from surface to top of clouds for a given site. The $L_v$ is provided from ITU – R for the exceed percentage probability ($pr$) based on predicted rainfall rate. The reader is referred to Section 3.2 to obtain the relation between $pr$ and predicted rainfall rate ($\mathrm{RR_{pr}}$). In all cases the value of $pr$ based on the predicted rainfall rate has been found to be in the range of 0.001% to 50%. Figure 5.9 shows the clouds and fog attenuations as a function of propagation angle ($\theta$) and predicted rainfall rate ($RR_{pr}$) for the station at King City, Canada. The figure shows that cloud and fog attenuations increases exponentially with the increase in rainfall rate and decrease in propagation angle. The cloud and fog attenuation values ranged from 0 to 5.5 $dB$ when rainfall rate ranged from 0 to 15 $mm/hr$, propagation angle ranged from 45 to 5 $degrees$ for a given frequency that equals to 20 $GHz$.

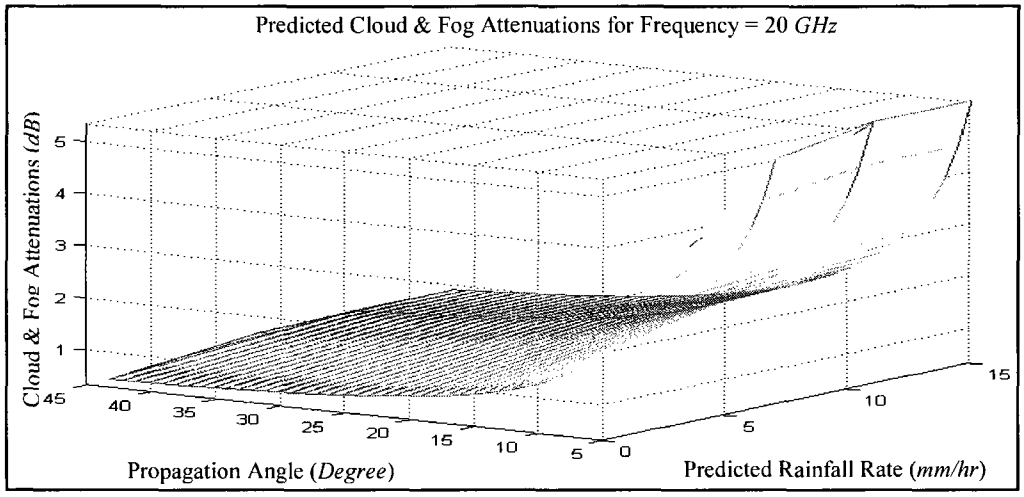


**Figure 5.9:** Predicted cloud and fog attenuations – function of predicted rainfall rate and propagation angle at South West of King City Station, Canada.

### 5.4.4 Calculating Scintillation Attenuation

In satellite communications, scintillation attenuation results from rapid variations in the signal's amplitude and phase due to changes in the refractive index of the earth's atmosphere. In the following Subsection, we present a general technique for estimating and predicting the scintillation attenuation as a function of rainfall rate and propagation angle [29].

#### i- Using Historical Data

The cumulative distribution of tropospheric scintillation is based on monthly or longer average ambient temperature $t$ $(Celsius)$. This distribution reflects the specific climate conditions of the site [3, 31, 57]. The following is a general technique for estimating scintillation attenuation as a function of rainfall rates and propagation angles.

1)- Calculate the standard deviation of the signal amplitude $\sigma_{ref}$:

$$\sigma_{ref} = 3.6 \cdot 10^{-3} + 10^{-4} \cdot N_{wet} \ dB, \tag{5.41}$$

where $N_{wet}$ is the radio refractivity, given in ITU − R Recommendation P. 453.

2)- Calculate the effective path length $L_{Scintillation}$ as:

$$L_{Scintillation} = \frac{2 \cdot h_L}{\sqrt{\sin^2\theta + 2.35 \cdot 10^{-4}} + \sin\theta} \quad m, \tag{5.42}$$

where $h_L$ is the height of the turbulent layer equal to 1000 $m$.

3)- Estimate the effective antenna diameter, $D_{eff}$, from the geometrical diameter of the earth-station antenna ($D$), and the antenna efficiency ($\eta$) (if unknown, use $\eta = 0.5$):

$$D_{eff} = \sqrt{\eta} \cdot D \quad m. \tag{5.43}$$

4)- Calculate the antenna-averaging factor from:

$$g(x) = \sqrt{3.86 \cdot (x^2+1)^{11/12} \cdot \sin\left[\frac{11}{6}\arctan\frac{1}{x}\right] - 7.08 \cdot x^{5/6}}, \tag{5.44}$$

with

$$x = 1.22 \cdot D^2{}_{eff} \cdot (f \ / \ L_{Scintillation}), \tag{5.45}$$

and

$$\sigma(\theta) = \sigma_{ref} \cdot f^{(7/12)} \cdot \frac{g(x)}{(\sin\theta)^{1.2}}. \tag{5.46}$$

5)- Calculate the time percentage factor, $a(RR_{ep})$, where $RR_{ep}$ is the rainfall rate for ex-

ceed percentage probability ($ep$) ranges from $0.001\%$ to $50\%$:

$$a(RR_{ep}) = -0.061 \cdot (\log \text{ep})^3 \cdot 0.072 \cdot (\log \text{ep})^2 - 1 . 71 \cdot (\log \text{ep}) + 3.0 . \tag{5.47}$$

6)- Calculate the scintillation fade depth using the procedure that can be found in [3]:

$$A_{Scintillation}(\theta, RR_{ep}) = a(RR_{ep}) \cdot \sigma(\theta) \ dB. \tag{5.48}$$

The scintillation attenuation $A_{Scintillation}$ is presented in terms of rainfall rate ($\text{RR}_{\text{ep}}$) and propagation angle ($\theta$), for a specific frequency ($f$). Figure 5.10 shows that scintillation attenuation increases with the increase of rainfall rate and decrease of propagation angle. The scintillation attenuation values ranged from 0 to 0.45 $dB$ when rainfall rate ranged from 0 to 12 $mm/hr$ and propagation angle ranged from 0 to 50 $GHz$ for a frequency equal to 20 $GHz$ placed at Hazelton Station, Canada.

Note that, scintillation attenuation estimated in equation (5.48) can also be presented as a function of $\text{RR}_{\text{ep}}$ and frequency for a specific propagation angle as:

The scintillation attenuation calculated at experimental location using the above equation (5.49). The resulting relationship among the attenuation, rainfall rate, and frequency is shown in Figure 5.11. This shows that scintillation attenuation increases with the increase of rainfall rate and slightly operational frequency. The scintillation attenuation values ranged from 0 to 0.17 $dB$ when rainfall rate ranged from 0 to 12 $mm/hr$ and frequency ranged from 0 to 50 $GHz$ for a propagation angle of 25 $degrees$ placed at Atlin Station, Canada.

$$A_{Scintillation}(f, \ RR_{ep}) = a(RR_{ep}) \cdot \sigma(f) \ dB, \tag{5.49}$$

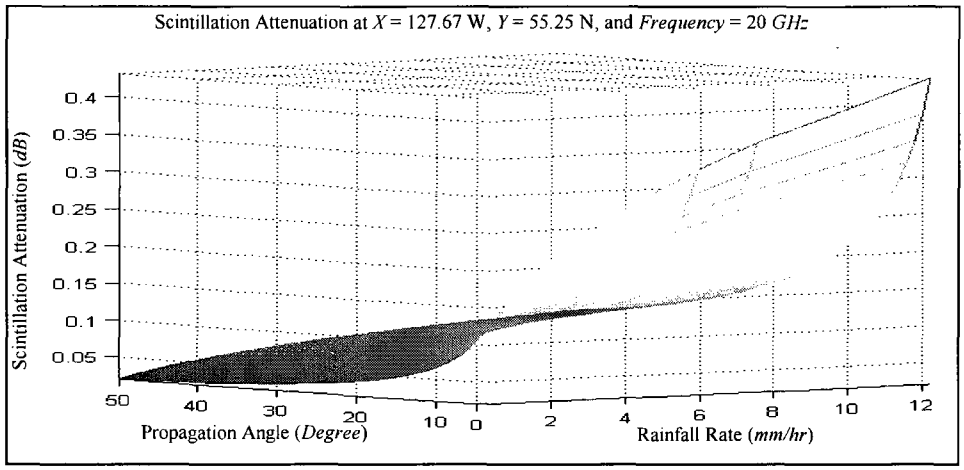


**Figure 5.10:** Scintillation attenuation – function of rainfall rate and propagation angle at Hazelton Station, Canada.

where

$$\sigma\left(f\right) = \sigma_{ref} \cdot f^{(7/12)} \cdot \frac{g(x)}{(\sin\theta)^{1.2}} \,. \tag{5.50}$$

The model we present for different attenuations provide controllers with a perceptible view of approximate channel attenuation, based on ITU – R Recommendation, and by estimating different weather attenuations at desired locations, for different propagation angles, for a given rainfall rate, and for a wide range of uplink or downlink frequencies. Also, as mentioned above, it can be computed for different frequencies, for different rainfall rate values, and for any specific operation propagation angle [29]. The original version of this method was developed by ITU – R [29] to work with historical data. We adapted it for predicted weather conditions. Its ultimate application in SNR prediction was found to be close to field measured data in TELESAT experiments. However, we do not have access to those experimental values to present here in this document.

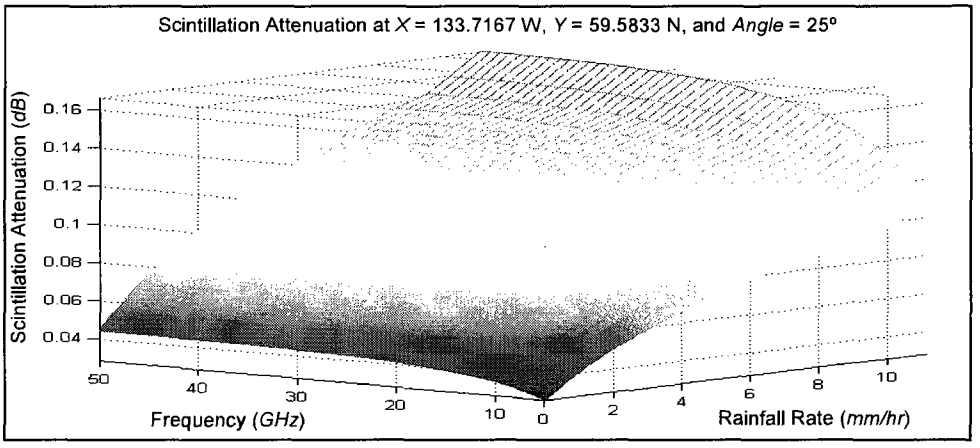


**Figure 5.11:** Scintillation attenuation – function of rainfall rate and frequency at Atlin Station, Canada.

### ii- Using Predicted Data

Let us calculate time percentage factor, $a(RR_{pr})$, where $RR_{pr}$ is the predicted rainfall rate for the predicted probability of precipitation ($pr$) as follows:

$$a(RR_{pr}) = -0.061 \cdot (log\,(pr))^3 \cdot 0.072 \cdot (log\,(pr))^2 - 1.71 \cdot log\,(pr) + 3.0. \tag{5.51}$$

Thus,

$$A_{Scintillation}(\theta, RR_{pr}) = a(RR_{pr}) \cdot \sigma(\theta) \quad dB. \tag{5.52}$$

The scintillation attenuation calculated by using (5.52) resulted in a set of $A_{Scintillation}$ values in relation to propagation angle ($\theta$), prediction rainfall rate ($\mathrm{RR_{pr}}$), frequency ($f$), and location as shown in Figure 5.12. The figure shows that scintillation attenuation increases exponentially with the increase in rainfall rate and decrease in propagation angle. The scintillation attenuation values, collected at South West of King City Station, Canada, ranged

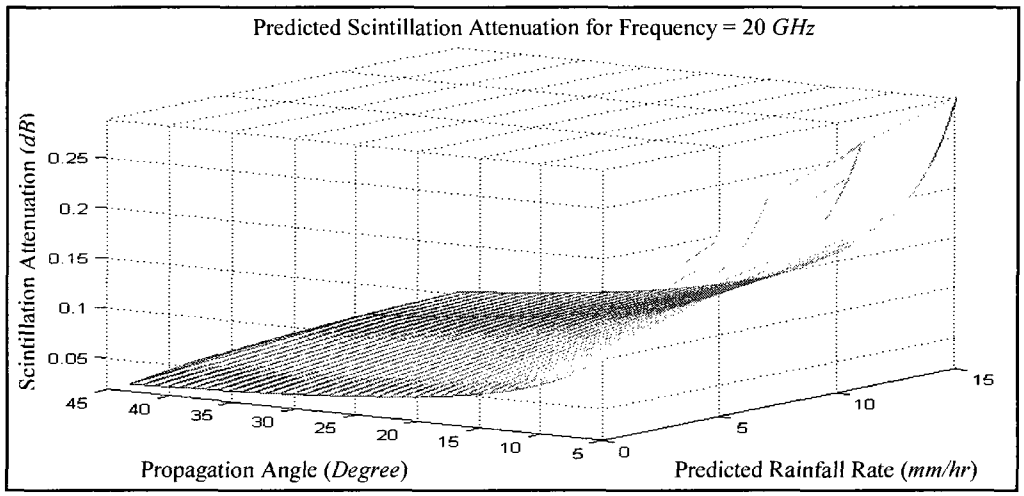


**Figure 5.12:** Predicted scintillation attenuation – function of predicted rainfall rate and propagation angle at South West of King City Station, Canada.

from 0 to 0.25 $dB$ when rainfall rate ranged from 0 to 15 $mm/hr$, propagation angle ranged from 45 to 5 $degrees$ for a given frequency that equals to 20 $GHz$.

## 5.5 Summary

In this chapter, we presented techniques to calculate rain, gaseous, cloud, fog, and scintillation attenuations based on historical weather data as well as with the hourly rainfall rate data captured by weather stations. The new method presented in this chapter better support the satellite system's controller with an improved view of the channel at any specific location with the use of actual predictions before weather deteriorates the operational function of the system.

In the following chapter, total attenuation is computed based on these attenuations and we

will present how it could be utilized to improve SNR estimation. The estimated SNR values for different combinations of propagation parameters are used by the intelligent weather aware control system (IWACS) for selecting the right combination to achieve the desired quality in the communication channels.

# Chapter 6

# Signal Attenuation Prediction and Intelligent Weather Aware Control System

## 6.1 Introduction

In this chapter, total effect of all four types of attenuation, that were calculated in the previous chapter, are used to determine atmospheric attenuation and is combined with free space attenuation to determine total attenuation. Also, we describe an intelligent weather aware control system (IWACS) to better control channel parameters and queuing characteristics.

A three dimensional relationship is introduced among total attenuation, estimated rainfall rate, and propagation angle on one hand, and among total attenuation, predicted rainfall rate, and propagation angle on the other. Similar relationship is established among SNR, transmit power, and both of estimated and predicted total attenuation [3,9,30,31]. These relationships are then used as decision aid by IWACS for control purposes. A set of channel parameters are selected based on the value of total attenuation to facilitate the decision support system. Such control includes adjusting satellite signal power, modulation, and coding schemes as countermeasures for degradation of signal quality.

The algorithm also able to receive heuristic and SLA inputs from the DSS and the SNR feedback from the neighboring terminals. The selection of appropriately weighted modulation/codepoint for impending weather conditions, configuration settings and tolerance/safety margins for honoring SLA is the prime objective of this chapter.

## 6.2 Calculating Total Attenuation from Historical Data and Predicted Data

### 6.2.1 Calculating Atmospheric Attenuations Using Historical Data

In this section atmospheric attenuations are calculated based on rain, gas, cloud, fog, and scintillation attenuations.

The required input parameters for the above attenuations are:

$A_{Rain}(\theta,\ RR_{ep})$: attenuation due to rain, as estimated in (5.5).

$A_{Gas}(\theta,\ RR_{ep})$: gaseous attenuation due to water vapour and oxygen, as estimated in (5.25).

$A_{Cloud\&Fog}(\theta,\ RR_{ep})$: cloud and fog attenuations, as by (5.30).

$A_{Scintillation}(\theta,\ RR_{ep})$: attenuation due to tropospheric scintillation, as estimated in (5.48).

Here, $A_{Rain}(\theta,\ RR_{ep})$, $A_{Gas}(\theta,\ RR_{ep})$, $A_{Cloud\&Fog}(\theta,\ RR_{ep})$, and $A_{Scintillation}(\theta,\ RR_{ep})$ represent atmospheric attenuations for a wide range of rainfall rates and propagation angles.

A general method for calculating the updated atmospheric attenuations $A_W(\theta, RR_{ep})$, is given by [3,9]:

$$\begin{aligned} A_W(\theta, RR_{ep}) &= A_{Gas}(\theta, RR_{ep}) + \cdots \\ \cdots &+ \sqrt{(A_{Rain}(\theta, RR_{ep}) + A_{Cloud\&Fog}(\theta, RR_{ep}))^2 + (A_{Scintillation}(\theta, RR_{ep}))^2}, \end{aligned} \tag{6.1}$$

where

$$A_{cloud\&Fog}(\theta,\ RR_{ep}) \cong A_{cloud\&Fog}(\theta, RR_{ep=1\,\%}) \quad \text{for} \quad ep \leq 1.0\,\% \tag{6.2}$$

and

$$A_{Gas}(\theta, RR_{ep}) \cong A_{Gas}(\theta, RR_{\text{ep=1 \%}}) \quad \text{for} \quad ep \leq 1.0\,\%\,. \tag{6.3}$$

Equation (6.2) and (6.3) take into consideration that large parts of clouds and gaseous attenuations are already included in the prediction of rain attenuation below 1 % [16]. $RR_{ep}$ is the rainfall rate for exceeded percentage probability ($ep$) in the range between 0.001 % to 50 %. This method was tested using contour rain map presented in [15], using procedures set out in ITU – R Recommendation P. 311. The results were found to be in good agreement with the available measurement data for all latitudes, and for the prediction of wide rainfall rate ranges as shown in Figures 5.1, Figure 5.4, Figure 5.7, Figure 5.10, and Figure 6.1.

### 6.2.2 Calculating Atmospheric Attenuation Using Predicted Data

The aim of this section is to estimate different atmospheric attenuations such as rain, snow, gaseous, cloud, fog, and scintillation using our adaptive scheme. This combines predicted rainfall rate with ITU – R propagation models and interpolation methods to do this estimation. A three dimensional relationship for this attenuation with respect to propagation angle and predicted rainfall rate ($\text{RR}_{\text{pr}}$) is shown in Figure 6.2 [1,3,7,9].

We first calculate $A_{Rain}(\theta, RR_{pr})$, $A_{Gas}(\theta, RR_{pr})$, $A_{Cloud\&Fog}(\theta, RR_{pr})$, and $A_{Scintillation}(\theta, RR_{pr})$ using equations (5.9), (5.27), (5.40), and (5.52), respectively. Then, we obtain the predicted atmospheric attenuations $A_W(\theta, RR_{pr})$, from the following equation [3,9]:

$$\begin{aligned} A_W(\theta, RR_{pr}) &= A_{Gas}(\theta, RR_{pr}) + \cdots \\ \cdots &+ \sqrt{(A_{Rain}(\theta, RR_{pr}) + A_{Cloud\&Fog}(\theta, RR_{pr}))^2 + (A_{Scintillation}(\theta, RR_{pr}))^2}. \end{aligned} \tag{6.4}$$

The results were found to be in good agreement, according to ITU – R standards [7,15,16,29], with the available measurement data for all latitudes for wide range of predicted rainfall rate as calculated in Chapter 4, propagation angle, and other selected propagation parameters as shown in

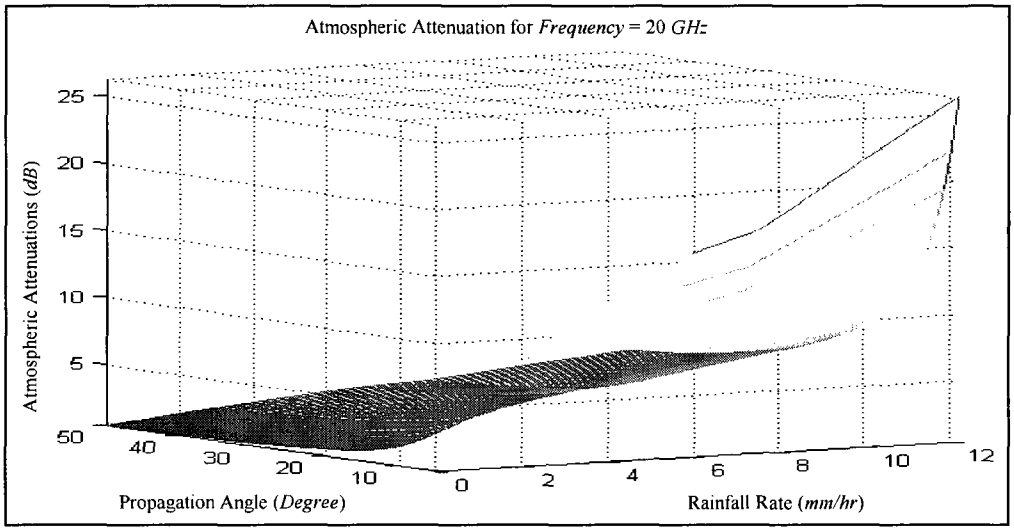


**Figure 6.1:** Atmospheric attenuations – function of rainfall rate and propagation angle at Hazelton Station, Canada.

Figure 5.3, Figure 5.6, Figure 5.9, Figure 5.12, and Figure 6.2.

### 6.2.3 Free Space Calculation

By definition free space is a space with nothing inside it. The most important four features of free space are its uniformity everywhere, absence of electrical charge, no current flowing through it, and its infinite extent in all directions. Since such phenomenon does not exist in the known universe, it is a common practice to assume interstellar space as a good approximation [38,41]. The free space attenuation, $A_0(\theta)$, is obtained as follows:

$$A_0(\theta) = (4 \cdot \pi \cdot d(\theta) / \lambda)^2, \tag{6.5}$$

with $d(\theta)$ being the distance between transmitter and receiver and the wavelength $\lambda = c/f$.

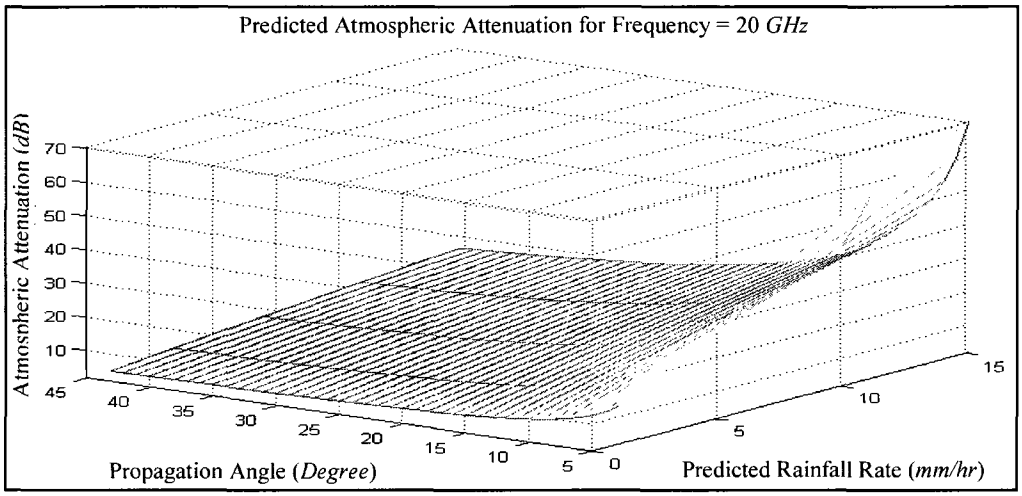


**Figure 6.2:** Predicted atmospheric attenuation – function of predicted rainfall rate and propagation angle at South West of King City Station, Canada.

### 6.2.4 Calculating Total Attenuation

The total attenuation is calculated based on both atmospheric and free space attenuations. As a result, we could calculate the total attenuation ($A_t$) from the following relation:

$$A_t(\theta, RR_{pr}) = A_W(\theta, RR_{pr}) + A_0(\theta), \tag{6.6}$$

where, $A_t(\theta, RR_{pr})$ is the total attenuation, $A_W(\theta, RR_{pr})$ is the atmospheric attenuation described in (6.4), and $A_0(\theta)$ is the free space attenuation described in (6.5).

Figure 6.3 shows a three dimensional relationship of total attenuations in terms of propagation angle and predicted rainfall rate [34]. From the operational point of view, it is important to consider the effect of these attenuation, especially for systems running at frequencies above $10\ GHz$ – with low propagation angles [29, 57]. Knowing different weather attenuations' behavior will be

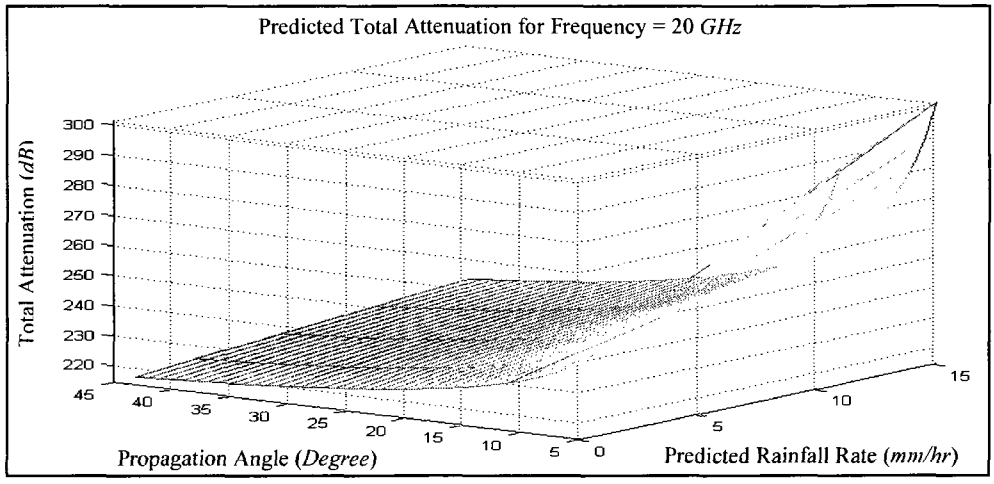


**Figure 6.3:** Predicted total attenuation – function of predicted rainfall rate and propagation angle at South West of King City Station, Canada.

an immense asset to support analysis for budgeting the operational satellite networking parameters around the world under different weather conditions.

Prediction of total attenuation becomes a key factor in diagnosing, adjusting and improving satellite signal power, modulation and coding schemes.

We verified that prediction of total attenuation using the above method, improves the accuracy of the results. The total attenuation is used to calculate SNR. IWACS uses the calculated SNR to determine the channel quality and subsequently adjust satellite propagation parameters. We will describe this in the next section.

## 6.3 Intelligent Weather Aware Control System

In order to put all of the principles and methods discussed thus far in this thesis, we designed an intelligent weather aware control system (IWACS). The main function of IWACS is sensing

the health of the communication nodes and links and improve them continuously. However, our primary objective in using IWACS, is to improve SNR in weather impacted networks.

The improvements are achieved by controlling parameters like power, modulation, coding, and data rate. The IWACS uses a broad set of general and specialized knowledge representations, reasoning mechanisms, on problem solving and search algorithms, and on machine learning techniques [3, 39, 68].

The IWACS continuously strives to maximize SNR and therefore the throughput of the network. It also maintains the SLAs by adaptively adjusting signal power, channel rate, location, propagation angle, frequency, modulation, coding, and queuing schemes to adapt with the operation of changing weather conditions by the use of predicted weather knowledge. The proposed IWACS adjusts transmission parameters before the rain problems actually manifest by minimizing estimated attenuation effect, maximizing channel robustness and efficiency, and improving SNR as well as QoS. IWACS is also similar to generally available control systems except that it is extended to factor various weather affected parameters separately to achieve better optimization of the service. The core architecture of the IWACS, as shown in Figure 6.4, where it may be noted that it consists of four control blocks along with a special module called decision support system (DSS).

The first control block, estimates SNR. SNR is a function of signal parameters, such as estimated data, propagation angle, frame size, frequency, signal transmitted power, and atmospheric attenuation.

The second control block compares the differences between the estimated SNR and its threshold value set by the system's controller. This will lead to one of three different possible outcomes $\{A$, $B$, and $C\}$ as shown in Figure 6.4. For the first outcome $\{A\}$, where SNR value is smaller than the threshold level, the DSS increases transmit power up to a maximum limit of $-30\ dB$ $(0\ dBm)$. For the second outcome $\{B\}$, where SNR value is equal to or greater than the threshold level, the DSS take no action and jumps to the last block. For the third outcome $\{C\}$, where SNR is smaller

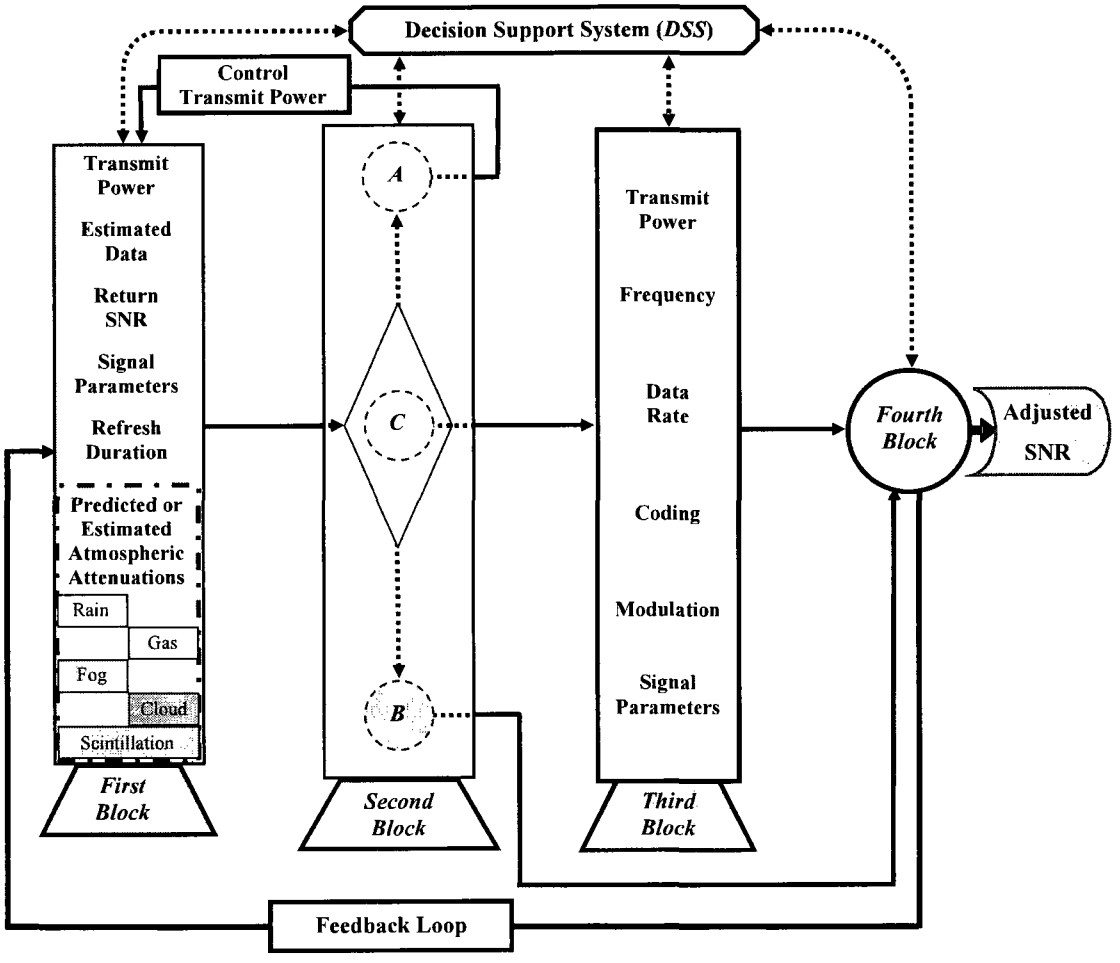


**Figure 6.4:** Intelligent weather aware control system for satellite networks.

than the threshold level even after increasing the transmit power to its maximum value, the DSS goes to the next block for more diagnostics.

In the third control block, the DSS will opt for the adjustment of other parameters such as data rate, transmit power, frequency, modulation, and coding schemes based on weather variations so as to keep the SNR within a tolerable range. In doing that, DSS relies on a combination of modulation and coding schemes and transmit power predetermined to give optimal results for a given frequency and propagation angle subjected to different atmospheric attenuations. One such set for a specific transmission frequency and propagation angle has been shown in Table 6.3. Therefore, the DSS will compromise among different SNR achieved outputs and will make the optimum decision based on the intelligent controller according to available parameters and requirements. It will then pass the selected SNR to next block.

In the fourth control block, if satisfactory SNR is not achieved through different combinations, the control system goes back to first control block through feedback to re-adjust the parameters as explained earlier and comes to re-work with the tables according to DSS decision, until a satisfactory value is reached at which the procedure will stop. In case significant improvement is not achieved it abandons the process after a set number of iterations and gives the warning to the operator.

The DSS utilizes the predicted weather knowledge and other signal parameters for control. It is constructed from specific classes of computerized algorithms that support satellite signal decision-making activities to control and monitor SNR with signal propagation values during operation. This system searches for different combinations of input variables in order to minimize the estimated attenuation effect and maximize the channel robustness and efficiency by improving SNR. The DSS utilizes system parameters like atmospheric attenuation, propagation angle, location, and antenna gain, to adaptively adjust signal power, transmission rate, coding, and modulation under different weather conditions in a way to honor the desired levels of QoS and SLA. Typical information that a DSS might gather and present would be to sense the environment by accessing

current information assets, such as knowledge base, channel and transmission parameters, and periodic querying for the variable parameter values, which keeps updating the knowledge based input to the DSS [39, 68, 70]. The model is made to deal with ITU − R collected data as well as actual weather data.

The next task of IWACS is to improve SNR, availability of links, and QoS by adaptively controlling the system in response to changing weather conditions. To achieve that, IWACS relies on knowledge representations, problem solving, search algorithms, and signal parameter adjustment schemes.

In IWACS, the said improvements are much noticeable compared to ISs that we have come to know thus far. It proficiently searches for different combinations of input control variables such as transmit power level, modulation schemes, channel coding, transmission rates, etc. to minimize estimated attenuations effect and maximize channel robustness and efficiency by improving SNR using the technique presented in Figure 6.4.

The major difference between IWACS and models known thus far is that the IWACS acquires rain, cloud and fog, scintillation, and gaseous attenuation separately and tunes the controllable parameters to get the optimal result. Whereas the traditional techniques did not treat them separately. Signal attenuation is calculated by factoring these four major impairment factors separately as well as parts of total attenuation for an improved control of channel parameters especially at higher transmission frequencies.

### 6.3.1 Decision Support System

The derived parameter values, being fed through IWACS to improve the estimated SNR, will enable the DSS block to maintain QoS and SLAs by adaptively adjusting satellite signal power, modulation, coding, and data rate at frequent storms and precarious weather conditions. The DSS and its network optimization blocks are depicted in Figure 6.5. The work fits in the data prediction module, and the interface to the core computing intelligence model of the DSS. The periodically-

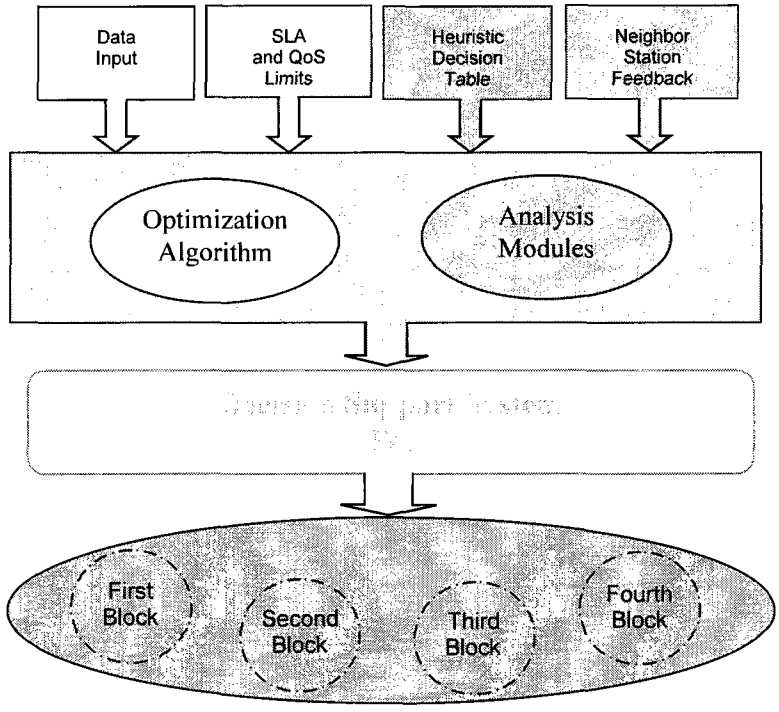


**Figure 6.5:** Network optimization decision support system

computed attenuation will keep updating our knowledge input to the DSS.

The DSS is constructed from specific classes of algorithms that takes experiential decision inputs from the user so that they could be factored in decision-making activities. Typical information that a DSS might gather and present would be:

- Accessing current information assets, such as knowledge base, satellite parameters, and triggering of periodic query
- Maintaining different combinations of channel parameters known to give acceptable system performance
- Monitoring SNR values during operation and learning new combination of parameters when they become known.

The DSS takes in the predicted weather database as shown in Figure 6.4 and proficiently searches for different combinations of controllable input variables such as transmit power level, modulation schemes, channel coding rates, etc. to minimize the estimated attenuation effect and maximize the channel robustness and efficiency by improving SNR. The ability to better predict attenuation for different weather conditions allows for adjust propagation parameters such that the attenuation could be lowered, SNR be improved thereby achieve improved QoS.

## 6.4 Relating Total Attenuation with Signal to Noise Ratio

In this section, we describe the effect of total attenuation on SNR. Estimating the channel attenuation would be an important support to determine the appropriate value for SNR, and to help satellite provider to make the necessary improvement to the system according to the presented situation before weather deteriorate the signal. SNR is usually measured in decibels $(dB)$ [41]. The signal energy $(E_s)$ to noise power spectral density $(N_0)$ per symbol is calculated from the

knowledge that $E_s = C \cdot T_s = C / R_s$, where $C$ is signal power, $T_s$ is symbol duration, and $R_s$ transmission rate.

$$\frac{E_s}{N_0} = \frac{C}{N_0} \cdot T_s = \frac{C}{N_0} \cdot \frac{1}{R_s}. \tag{6.7}$$

Note that thermal noise power spectral density $N_0 = K_b \cdot T$, and $K_b$ (Boltzman constant) $= 1.38 \cdot 10e-23$ Ws/K $= -228.6$ dB Ws/K. The $T$ is effective noise temperature and it is the sum of noise temperatures of both the antenna and the receiver.

$$T\ (effective\ noise\ temperature) = T_a + T_r, \tag{6.8}$$

where $T_a$ noise temperature of the antenna as represented in Table 6.1, and

$$T_r\ (noise\ temperature\ of\ the\ receiver) = (10^{(N_r\ /\ 10)} - 1) \cdot 290. \tag{6.9}$$

In the above equation the noise figure ($N_r$) for a low-noise amplifier is found to be in the range of 0.7 to 2 $dB$. The above equations can now be combined as:

$$\frac{C}{N_0} = \frac{C}{K_b \cdot T} = \frac{P_r}{K_b \cdot T} = \frac{P_t \cdot G_t}{A_t} \cdot \frac{G_r}{K_b \cdot T}, \tag{6.10}$$

where $P_t$ and $P_r$ are transmitter and receiver power, respectively. $G_t$ and $G_r$ are antenna gain at transmitter and receiver sides, respectively. Now expressing (6.10) in $dB$, we find:

$$\frac{C}{N_0} = P_t + G_t - A_t + G_r - K_b - T \quad dBHz \tag{6.11}$$

As

$$E_s\ (\text{symbol energy}) = \text{C} \cdot \text{T}_\text{s} = \text{C} / \text{R}_\text{s}, \tag{6.12}$$

where transmission rate $R_s\ (symbol/sec)$ is inversely equivalent to symbol duration $T_s$ and energy-

**Table 6.1:** Noise Temperature in Antenna.

| **Antenna Noise Temperature *Ta*** | | ***Kelvin*** |
|---|---|---|
| Directional satellite antenna | Earth from space | 290 |
| Directional terminal antenna | Space from earth at 90° elevation | $3 - 10$ |
| | Space from earth at 10° elevation | $\approx 80$ |
| | Sun $(1...10\ GHz)$ | $10^5...10^4$ |
| Hemispherical terminal antenna | At night | 290 |
| | Cloudy sky | 360 |
| | Clear sky with sunshine | 400 |

to-noise power density per symbol is:

$$\frac{E_s}{N_0} = \frac{C}{N_0} \cdot T_s = \frac{C}{N_0} \cdot \frac{1}{R_s} \tag{6.13}$$

or

$$\left.\frac{E_s}{N_0}\right|_{dB} = \frac{C}{N_0} - R_s\ , \tag{6.14}$$

and SNR is expressed as:

$$\frac{E_s}{N_0}(A_t,\ P_t) = P_t + G_t - A_t + G_r - T - K_b - R_s \quad dB. \tag{6.15}$$

It should be noted that the SNR estimation of (6.10) will be optimized by the virtue of having better estimation of $A_t$ through (6.15). Figure 6.6 and Figure 6.7 show SNR values before adjustment as a function of total attenuation and transmit power. These figures represent the estimated and predicted weather data at Vancouver Station and at South West of King City Station, respectively.

The SNR calculation contributes to optimization of channel throughput, because, keeping other

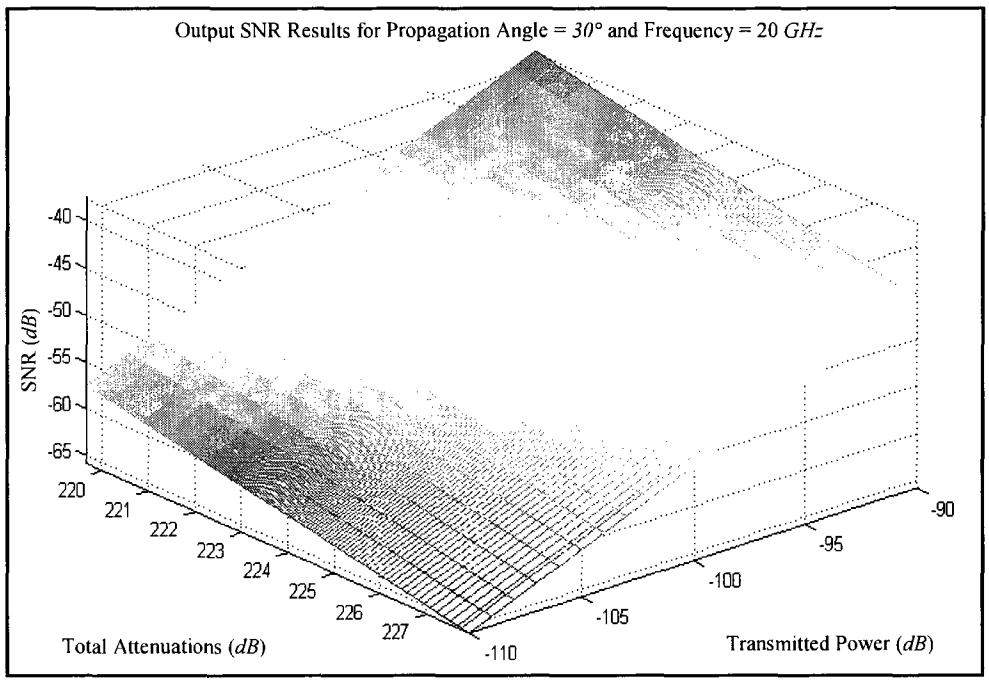


**Figure 6.6:** Output SNR at Vancouver Station, Canada.

factors as they are, improvement in SNR results in indirect improvement in throughput. Therefore, the control system to be included in the real section works continuously to maximize the value of SNR.

Real-time channel measurements such as SNR and BER can also serve as a feedback tuning control for our DSS by adaptively modifying the input control variables for clear channel optimization.

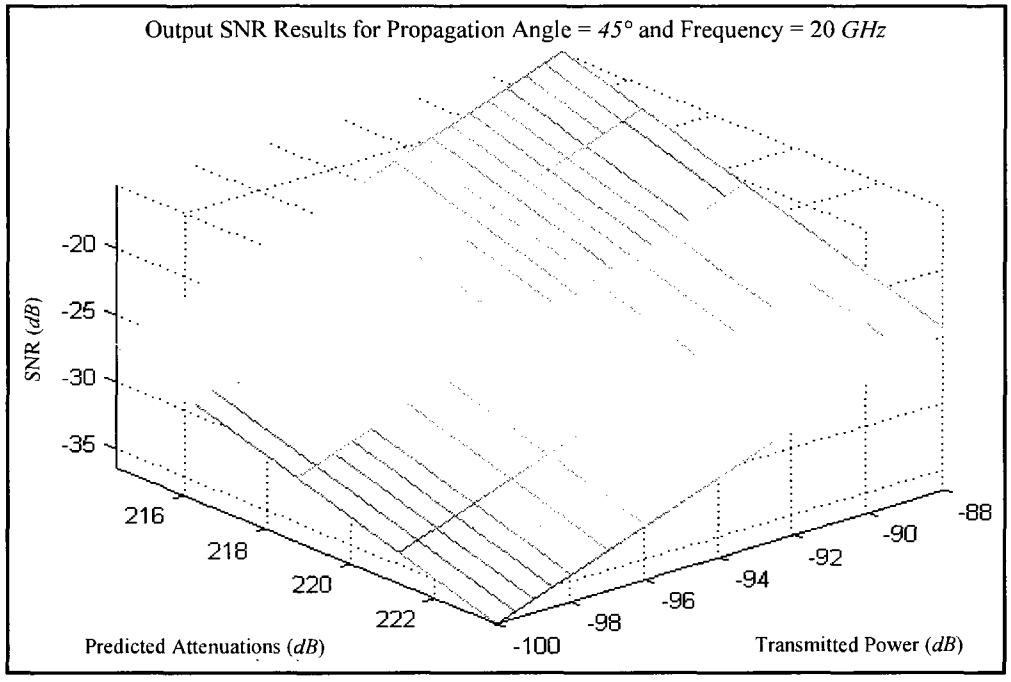


**Figure 6.7:** Output SNR at South West of King City Station, Canada.

## 6.5 Signal to Noise Ratio Adjustment

Several factors such as power, modulation, etc. could be adjusted in order to improve SNR and to maximize system's throughput and availability of links. The adjustment of these parameters ultimately results in the adjustment of SNR. In this section, it is demonstrated how SNR is related to attenuation along with other parameters.

We propose that, by controlling the supplying factors of the IWACS, a path is given to allow for an efficient mechanism to better estimate satellite's networking parameters. These derived parameters would enable the IWACS to maintain SNR by adaptively adjusting signal power, transmission rate, coding, and modulation under severe weather conditions.

Equation (6.15) can be used to determine BER of a digital transmission scheme. Figure 6.4 illustrates a manner for changing parameters of the communication system in order to overcome the deteriorating effect of atmospheric impairments, and to increase reliability of the data transmitted throughout the channel.

Figure 6.6, Figure 6.7, Figure 6.8, and Figure 6.11 show a comparison for the outputs of SNR ranges before and after modification for estimated and predicted measured weather data at Vancouver Station and at South West of King City Station, respectively.

These results are also presented in 2-D relationships at a given value of the third variable for clarity. Figure 6.9 and Figure 6.12 represent the adjusted output SNR with adjusted transmission power for given values of estimated and predicted attenuations. Also, Figure 6.10 and Figure 6.13 represents the adjusted output SNR with total estimated and predicted attenuations for given values of transmission power. These results are taken at Vancouver Station and at South West of King City Station, respectively.

Consequently Figure 6.8, Figure 6.9, Figure 6.10, Figure 6.11, Figure 6.12, Figure 6.13, Table 6.2, and Table 6.3 show throughput enhancements for wireless communication systems. These results also create a robust IWACS by allowing service provider to work with flexible ranges by

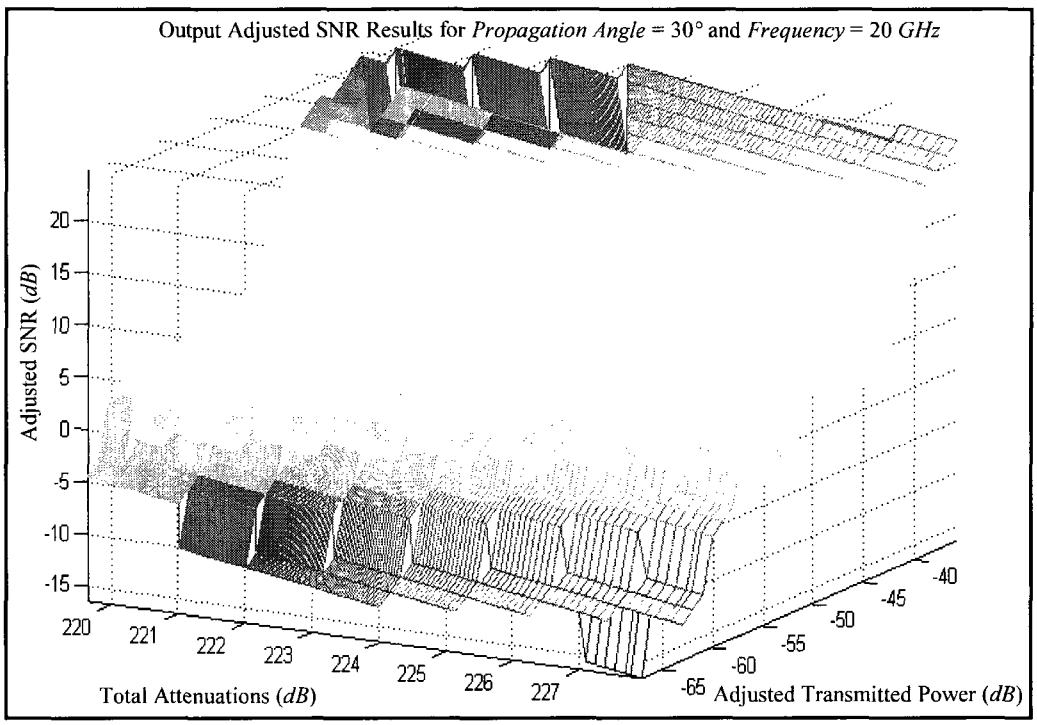


**Figure 6.8:** Output Adjusted SNR at Vancouver Station, Canada.

applying various combinations of satellite's signal parameters under different weather conditions as discussed in the following section.

## 6.6 Simulation Results and Discussions

In the previous sections, the estimated and predicted atmospheric attenuations are calculated at any specific location on earth for different rainfall rate values, with a range of given operational frequency and propagation angle. These schemes provide appropriate results up to high frequency

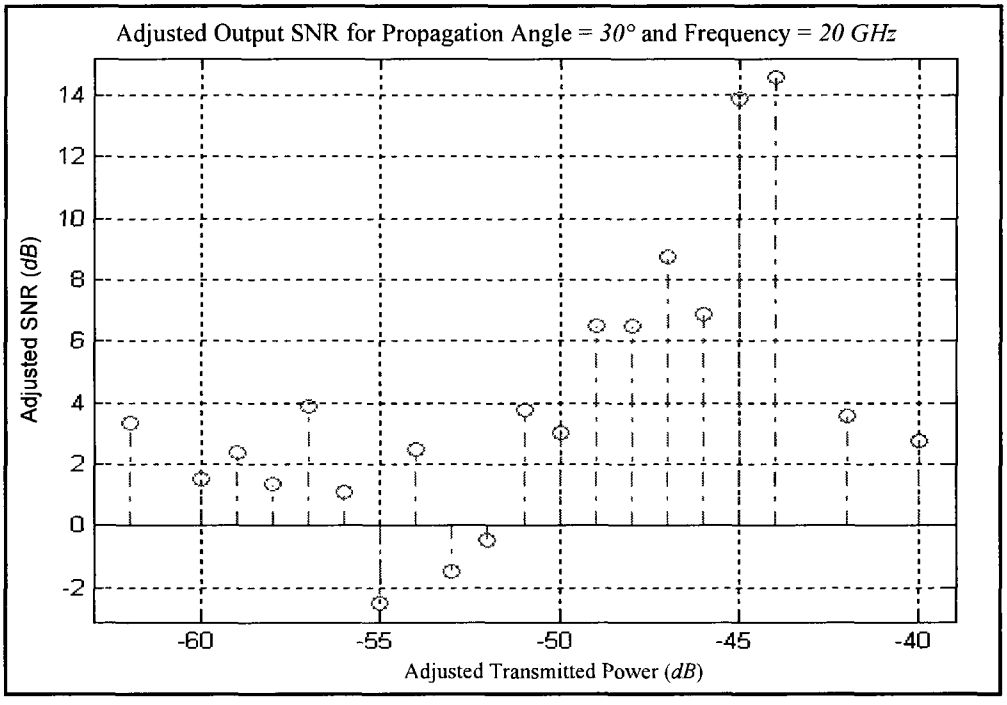


**Figure 6.9:** Output SNR at Vancouver Station, Canada.

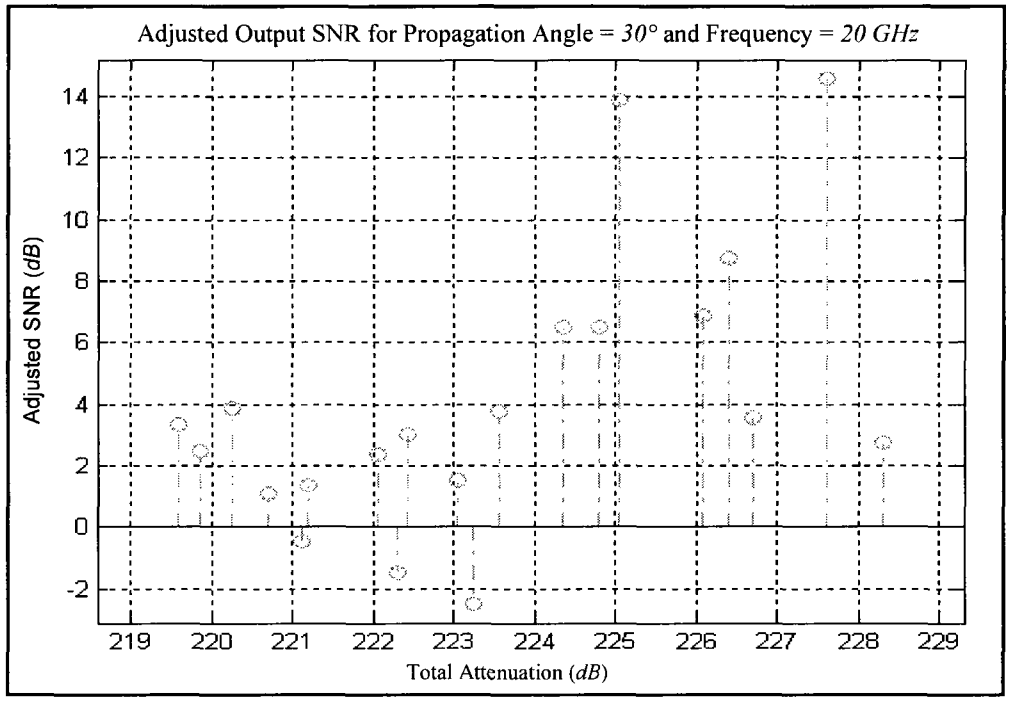


**Figure 6.10:** Output SNR at Vancouver Station, Canada.

**Table 6.2:** Forward Link Modes and Performance at Vancouver Station for Propagation Angle $= 30\ Degrees$ and Frequency of Operation $= 20\ GHz$.

| **Modulation** | **LPC Code Identifier** | SNR **Adjusted Values** $[dB]$ | **Transmit Power** $[dB]$ | **Total Attenuation** $[dB]$ |
|---|---|---|---|---|
| **QPSK** | 1/4 | 2.73 | -40 | 228.30 |
| **QPSK** | 1/3 | 3.56 | -42 | 226.70 |
| **QPSK** | 2/5 | -0.47 | -52 | 221.13 |
| **QPSK** | 1/2 | -1.47 | -53 | 222.30 |
| **QPSK** | 3/5 | -2.51 | -55 | 223.25 |
| **QPSK** | 2/3 | 2.47 | -54 | 219.86 |
| **QPSK** | 3/4 | 1.10 | -56 | 220.70 |
| **QPSK** | 4/5 | 3.02 | -50 | 222.42 |
| **QPSK** | 5/6 | 3.76 | -51 | 223.57 |
| **QPSK** | 8/9 | 6.52 | -48 | 224.80 |
| **8PSK** | 3/5 | 6.90 | -46 | 226.08 |
| **8PSK** | 2/3 | 6.49 | -49 | 224.35 |
| **8PSK** | 3/4 | 3.89 | -57 | 220.25 |
| **8PSK** | 5/6 | 1.34 | -58 | 221.19 |
| **8PSK** | 8/9 | 13.89 | -45 | 225.04 |
| **16PSK** | 2/3 | 8.73 | -47 | 226.40 |
| **16PSK** | 3/4 | 2.38 | -59 | 222.05 |
| **16PSK** | 4/5 | 1.51 | -60 | 223.04 |
| **16PSK** | 5/6 | 3.35 | -62 | 219.59 |
| **16PSK** | 8/9 | 14.61 | -44 | 227.61 |

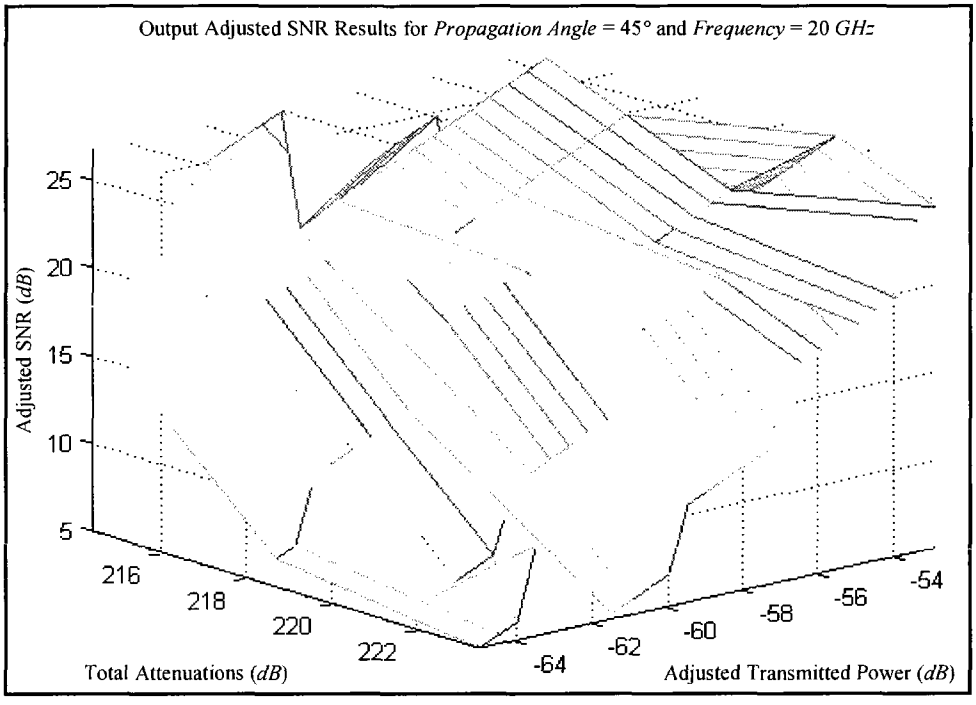


**Figure 6.11:** Adjusted output SNR at South West of King City Station, Canada.

**Table 6.3:** Forward Link Modes and Performance at South West of King City Station for Propagation Angle $= 45\ Degrees$ and Frequency $= 20\ GHz$.

| Modulation | LPC Code Identifier | SNR Adjusted Values $[dB]$ | Transmitted Power $[dB]$ | Total Attenuation $[dB]$ |
|---|---|---|---|---|
| **QPSK** | 2/3 | 12.37 | -55 | 214.36 |
| **QPSK** | 4/5 | 5.90 | -60 | 223.46 |
| **8PSK** | 2/3 | 1.2 | -62 | 221.13 |
| **8PSK** | 8/9 | 4.86 | -58 | 218.69 |
| **16PSK** | 8/9 | 21.10 | -57 | 216.23 |

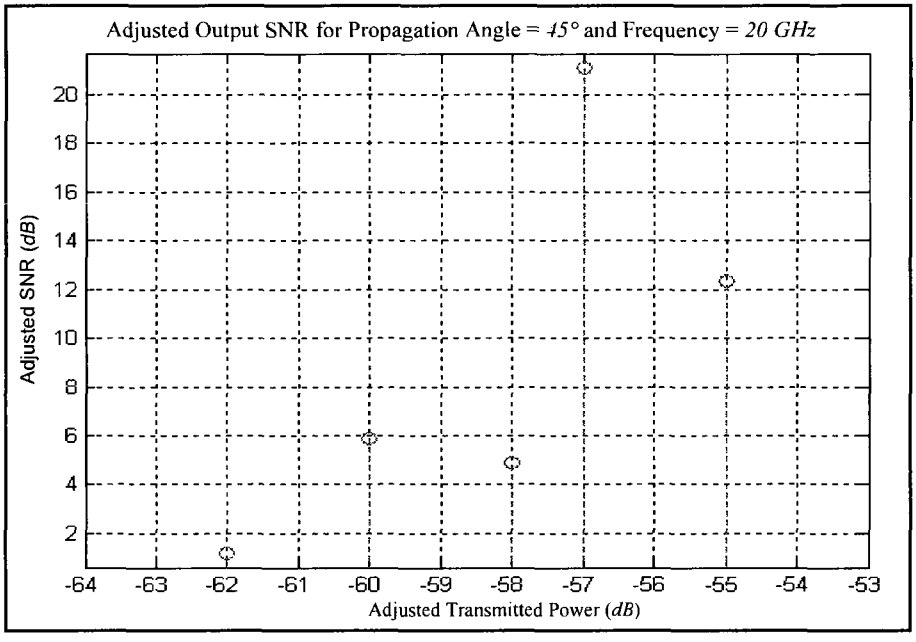


**Figure 6.12:** Output SNR at South West of King City Station, Canada.

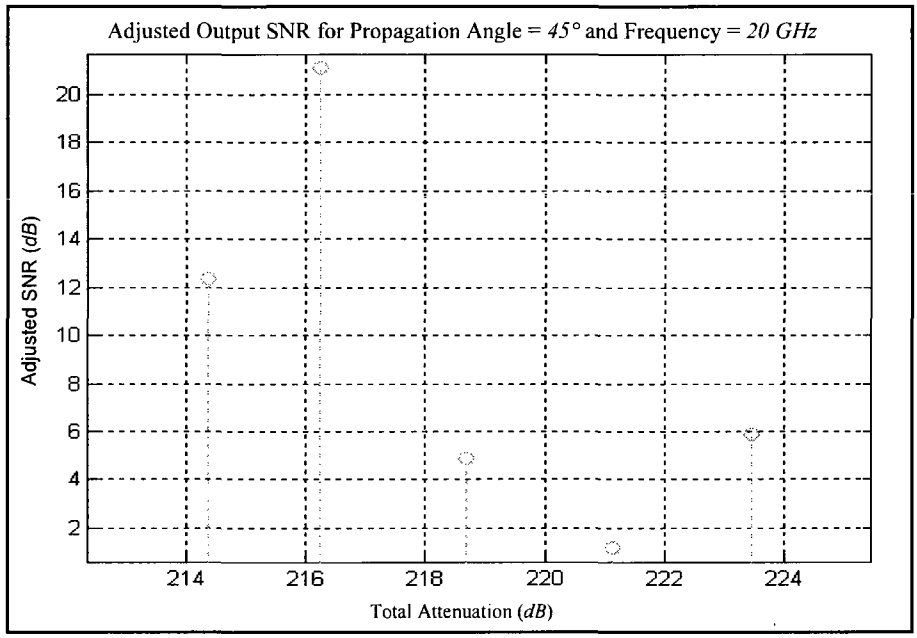


**Figure 6.13:** Output SNR at South West of King City Station, Canada.

of operations for historical data for rain, gas, cloud and fog, and scintillation attenuations as shown in Figures 5.1, Figure 5.4, Figure 5.7, and Figure 5.10, and for the same weather attenuations with predicted data as shown in Figure 5.3, Figure 5.6, Figure 5.9, and Figure 5.12, respectively. Moreover, these results are key factors in implementing an enhanced intelligent engine that act to improve end-to-end wireless communications for different weather conditions.

The IWACS was simulated in Matlab simulations version 7.1 running on Intel Centrino Pentium M 1.6 $GHz$ CPU, 512 $MB$ RAM. A special module was written to read weather data from Environment Canada supplied in a specially formatted text stream. It then converted it into a three hour sliding window of moving weather data always proceeding the present moment. Software modules were written to extract propagation related parameters shown in Figure 3.2 and Table 3.3 for the location from ITU $-$ R supplied data. Algorithm for predicting the rainfall rate based on Markov theory with fixed-duration weather data was written. The main IWACS module took the above mentioned data, along with transmit power and other signal propagation parameters, as inputs, calculated predicted signal attenuations, and heuristically searched right combination of controllable parameters for the input conditions, while learning to adapt. The improvement in SNR values experienced in receiving stations due to the adjustments made by IWACS were then evaluated. These are explained below.

IWACS checked various combinations of input parameters based on the given threshold signal level at receiver's end. It searched for a blend of available power, frequency, propagation angle, coding, transmission rate, and modulation in response to predicted channel attenuations and by attempting to maintain a desired level of SNR as shown in Figure 6.6, Figure 6.7, Figure 6.8, Figure 6.9, Figure 6.10, Figure 6.11, Figure 6.12, Figure 6.13, Table 6.2, and Table 6.3 for the estimated SNR requirements.

Figure 6.6, Figure 6.7, Figure 6.8, and Figure 6.11 compare the SNR before and after the adjusted techniques discussed in this thesis. They are put to use for making improvements to the system performance. Also, for having a close view of the output SNR results, we provide

relationships between SNR and either of adjusted transmit power or total attenuation as shown in Figure 6.9, Figure 6.10, Figure 6.12, and Figure 6.13.

The cases of SNR before and after adjustment, using IWACS for satellite networks, based on estimated and predicted data are:

**Case 1:** For estimated data, Figures 6.6 and Figure 6.8 represent cases when SNR fell between $(-66 \sim -38)\ dB$ and transmit power from $(-110 \sim -90)\ dB$ before intelligent decision mechanism was turned on. The improvements made in SNR and transmit power levels were significant after the IWACS was allowed to operate in the same condition. In presence of IWACS based propagation parameter control, the SNR improved to $(-16 \sim 25)\ dB$ and transmit power level ranged from $(-63 \sim -37)\ dB$. Both cases were subjected to identical weather conditions where total attenuation due to weather ranged from $(219 \sim 228)\ dB$ for a frequency of 20 $GHz$ at 30 $degrees$ propagation angle and transmission rate in the range of 40 $dB$.

**Case 2:** For predicted data, Figures 6.7 and Figure 6.11 represent cases when SNR fell between $(-37 \sim -15)\ dB$, transmit power from $(-100 \sim -88)\ dB$ before intelligent decision mechanism was turned on. The improvement made in SNR and transmit power level were significant after the IWACS was allowed to operate in the same condition. In presence of IWACS based propagation parameter control, the SNR improved to $(5 \sim 27)\ dB$ and transmit power level ranged from $(-63 \sim -52)\ dB$. Both cases were subjected to identical weather conditions where total attenuation due to weather ranged from $(214 \sim 224)\ dB$ for a frequency of 20 $GHz$ at 45 $degrees$ propagation angle and transmission rate in the range of 45 $dB$.

Note that IWACS was able to bring the upper limit for transmit power to less than the maximum allowed of $-30\ dB$. Any time this limit is reached, signal parameters are re-adjusted to prevent uncontrolled signal transmission as shown in Figure 6.8 and Table 6.2, similarly for actual data in

Figure 6.11 and Table 6.3. It could be noted that the improvements in channel performance made by the scheme is significant.

The cases of SNR presentation in 2-D after adjustment, using IWACS for satellite networks, based on estimated and predicted data are:

**Case 1:** For estimated data, Figure 6.9 shows that adjusted SNR takes different values from approximately $(-3 \sim 15)\ dB$ when adjusted transmit power have values between $(-62 \sim -40)\ dB$ for given estimated total weather attenuation, modulation, coding, transmission rate, frequency equal to 20 $GHz$, and propagation angle equal to 30 $degrees$. Also, Figure 6.10 shows that adjusted SNR takes different values from approximately $(-3 \sim 15)\ dB$ when total weather attenuation have values between $(219 \sim 229)\ dB$ for given adjusted transmitted power, modulation, coding, transmission rate, frequency equal to 20 $GHz$, and propagation angle equal to 30 $degrees$. Both Figure 6.9 and Figure 6.10 took place at Vancouver Station, Canada.

**Case 2:** For predicted data, Figure 6.12 shows that adjusted SNR takes different values from approximately $(1 \sim 22)\ dB$ when adjusted transmit power have values between $(-62 \sim -55)\ dB$ for given total predicted weather attenuation, modulation, coding, transmission rate, frequency equal to 20 $GHz$, and propagation angle equal to 45 $degrees$. Also, Figure 6.13 shows that adjusted SNR takes different values from approximately $(1 \sim 22)\ dB$ when total predicted weather attenuation have values between $(214 \sim 224)\ dB$ for given adjusted transmitted power, modulation, coding, transmission rate, frequency equal to 20 $GHz$, and propagation angle equal to 45 $degrees$. Both Figure 6.12 and Figure 6.13 took place at South West of King City, Canada.

These results help in understanding the SNR behavior with respect to adjusted power from one side and total attenuations from the other.

This simulation provides a feedback algorithm and a refresh duration for different satellite

signal parameters that are used to iteratively tune the intelligent controller technique as shown in Figure 6.4. The results are done by using Matlab simulations, where different programs were written to collect database information from different sources such as ITU − R, to implement the two and three dimensional relationships for predicted rainfall rate, different weather attenuations, total attenuation, and SNR, and to run the intelligent engine in order to present the desired output for the communication satellite systems.

## 6.7 Summary

In this chapter, the total effect for all of rain, gas, cloud and fog, and scintillation attenuations are used to determine the atmospheric attenuation. This attenuation is combined with free space attenuation to calculate total attenuation. Also, an IWACS is implemented to demonstrate how the system performance could be improved by providing suitable estimates for different weather attenuations that leads to adjust estimated SNR output in lieu of a wide range of rainfall rate and transmitted power, for any specific frequency, propagation angle, transmission rate, gain, and location. Hence, this mechanism gives system's controllers the flexibility to apply various combinations of modulation, coding, and transmit power for a given atmospheric condition in order to maximize system's throughput as well as QoS.

# Chapter 7

# Conclusions and Future Works

## 7.1 Conclusions

Rain, gaseous, cloud, fog, scintillation, and other atmospheric properties can have a distorting effect on communication signals. The signal fading caused by different weather attenuations directly affect the QoS in satellite links and, hence, affect system availability especially at frequencies above $Ku-$ band. Such attenuation makes it difficult to provide agreed upon QoS by satellite networks unless special mitigation measures are devised to counter weather effects. Thus, control systems could be made to be the most effective if we had the best possible technique for predicting channel attenuation due to weather related factors. Especially at high frequency bands the relative effect of atmospheric attenuation is so great that an efficient and dependable method for estimating these attenuations was considered essential for designing efficient and intelligent control systems. This thesis studies QoS improvement by providing estimated results for atmospheric attenuations in lieu of a wide range of rainfall rates, frequencies, propagation angles, and other propagation parameters at any specific location on earth.

This work stemmed from the idea that the ability to predict channel attenuation due to atmospheric conditions can enable mitigation of channel fading condition by adaptively selecting

appropriate propagation parameters. In this thesis, not only a new technique to calculate different atmospheric attenuations such as rain, gas, cloud and fog, and scintillation for any specific location based on ITU − R database has been presented, but also, an intelligent weather aware control system (IWACS) was established to bring noticeable improvements in the SNR on satellite communication channels. This is done by utilizing the atmospheric attenuation estimations and free space attenuation in the decision support algorithms. The ability to better estimate these attenuations has resulted in a significant opportunity to channel modeling such that we are able to improve SNR by better tuning of parameters like transmit power, modulation, coding, propagation angle, frequency, and transmission rate. The ultimate benefit of this work would be in realizing tolerance/safety margins for SLA commitment by achieving optimal QoS.

In this thesis, we presented a method to estimate rain attenuation and other atmospheric attenuations using the weather database from using bi-linear interpolation and frequency extrapolation. We also demonstrated that the calculation of rain attenuation is better done by some improvements made over ITU − R Original Method and ITU − R Approximation Method. The improved technique is named as Iterative Approximation Method (IAM). Simulation results clearly showed that IAM is very effective and computationally efficient. A three dimensional model of rain attenuation as well as other atmospheric attenuations with both propagation angle and rainfall rate from one side, and the atmospheric attenuations with both frequency and rainfall rate from other side, are also the result of this work.

This thesis presents a technique for predicting channel attenuation based on actual weather data and the use of Markov theory. The results of predicted rainfall rate obtain is found to be able to make significant improvement over the control techniques known thus far. The technique positively contributes to QoS maintenance by allowing for better tuning and adaptation of signal propagation parameters such as frequency, power, propagation angle, modulation, coding, and transmission rate with changing weather conditions.

The work also introduces a three dimensional relationship model between attenuation, propa-

gation angle, and predicted rainfall rate with an implication that for a given atmospheric condition, the signal attenuation could be predicted with much improved accuracy than the techniques in use thus far.

The IWACS described here and that is used to select appropriate combination of controllable channel characteristics is able to demonstrate that SNR could be maximized for a given weather condition in presence of techniques presented here. The IWACS successfully controlled modulation, coding, transmission power, frequency, propagation angle, and transmission rate, to improve channel robustness and, consequently, maximizing the throughput of the satellite network by preparing for the next weather period with predicted data. The algorithm uses the weighted modulation/codepoint optimal values that tune with predicted weather conditions, configuration settings, and tolerance/safety margins for SLA commitment and improve QoS under variant weather conditions.

## 7.2 Future Works

Several avenues for future works that could be launched based on the foundation of this work. These avenues include:

1. Take the implementation from simulation environment and apply it in practical systems and demonstrate its efficiency through physical systems by comparing the estimated and predicted results with the actual results.

2. Study of Markov model for weather conditions at different locations in the world, and research the possibility of having an optimal model for places having different weather patterns.

3. Investigate to control the time period for measuring rainfall rate when dealing with high variations on weather states and locations.

4. Build up a flexible IWACS based on neuro-fuzzy systems with optimized algorithms and core computing intelligence model that would be controlled by predicted weather knowledge in order to minimize their impact on the QoS in satellite networks.

# References


[1] R. K. Crane, "Prediction of the effects of rain on satellite communication systems," *Proc. of the IEEE*, vol. 65, no. 3, pp. 456–474, 1977.

[2] F. Haidara, A. Dissanayake, and J. Allnutt, "A prediction model that combines rain attenuation and other propagation impairments along earth-satellite paths," *IEEE Trans. on Antennas & Propagation*, vol. 45, no. 10, pp. 1546–1558, 1997.

[3] K. Harb, A. Srinivasan, B. Cheng, and C. Huang, "Intelligent weather aware scheme for satellite systems," *Proc. of IEEE International Conference on Communications (ICC)'08*, pp. 1930–1936, May 2008.

[4] L. J. Ippolito, "Propagation effects and system performance considerations for satellite communications above 10 GHz," *Proc. of the IEEE*, vol. 1, no. 302, pp. 86–91, 1990.

[5] T. S. Rappaport, *Wireless communications, principles and practice (2nd Edition).* Upper Saddle River, NJ: Prentice Hall PTR, 2002.

[6] K. Harb, F. R. Yu, P. Dakhal, and A. Srinivasan, "An intelligent QoS control system for satellite networks based on Markovian weather," *Proc. of IEEE Vehicular Technology Conference (VTC)'10*, Sep. 2010.

[7] ITU-R, "Specific attenuation model for rain for use in prediction methods," *Radio wave propagation, International Telecommunication Union Recommendation ITU-R P.838-3*, 2003.

[8] D. V. Rogers, L. J. I. Jr., and F. Davarian, "System requirements for ka-band Earth-satellite propagation data," *Proc. of the IEEE*, vol. 85, no. 6, pp. 810–820, 1997.

[9] K. Harb, A. Srinivasan, B. Cheng, and C. Huang, "Prediction method to maintain QoS in weather impacted wireless and satellite networks," *Proc. of Systems, Man and Cybernetics (SMC)'07*, pp. 4008–4013, Oct. 2007.

[10] ITU-R, "Attenuation due to clouds and fog," *Radio wave propagation, International Telecommunication Union Recommendation ITU-R P.840-3*, 1999.

[11] J. Goldhirsh, "Prediction methods for rain attenuation statistics at variable path angles and carrier frequencies between 13 and 100 GHz," *IEEE Trans. on Antennas & Propagation*, vol. 23, no. 6, pp. 786–791, 1975.

[12] L. Tsang, J. Kong, E. Njoku, D. Staelin, and J. Waters, "Theory for microwave thermal emission from a layer of cloud or rain," *IEEE Trans. on Antennas & Propagation*, vol. 25, no. 5, pp. 650–657, 1977.

[13] A. A. Aboudebra, K. Tanaka, T. Wakabayashi, S. Yamamoto, and H. Wakana, "Signal fading in land-mobile satellite communication systems: statistical characteristics of data measured in Japan using ETS-VI," *Proc. of the IEEE - Microwave, Antennas & Propagation*, vol. 146, no. 5, pp. 349–354, 1999.

[14] L. J. I. Jr. and T. A. Russell, "Propagation considerations for emerging satellite communications applications," *Proc. of the IEEE*, vol. 81, no. 6, pp. 923–929, 1993.

[15] ITU-R, "Characteristics of precipitation for propagation modeling," *Radio wave propagation, International Telecommunication Union Recommendation ITU-R P.837-4*, 2001.

[16] ITU-R, "Rain height model for prediction methods," *Radio wave propagation, International Telecommunication Union Recommendation ITU-R P.837-4*, 2001.

[17] M. S. J. Singh, S. I. S. Hassan, and M. F. Ain, "Rainfall attenuation and rainfall rate measurements in Malaysia comparison with prediction models," *American Journal of Applied Sciences*, vol. 4, no. 1, pp. 5–7, 2007.

[18] M. Richharia, *Satellite Communication Systems, Design Principles*. McGraw-Hill, New York, 1999.

[19] T. Boonchuk, N. Hemmakorn, P. Supnithi, M. Lida, K. Tanaka, K. Igarashi, and Y. Moriya, "Rain attenuation of satellite link in Ku-band at Bangkok," *Information, Communications and Signal Processing, Fifth International Conference*, pp. 1093–1096, Dec. 2005.

[20] J. A. García-López, J. M. Hernando, and J. M. Selga, "Simple rain attenuation prediction method for satellite radio links," *IEEE Trans. on Antennas & Propagation*, vol. 36, no. 3, pp. 444–448, 1988.

[21] H. Fukuchi and P. A. Watson, "Statistical stability of cumulative distributions of rainfall rate in the UK," *Proc. of the IEEE*, vol. 136, no. 2, pp. 105–109, 1989.

[22] A. Safaai-Jazi, H. Ajaz, and W. L. Stutzman, "Empirical models for rain fade time on Ku and Ka-band satellite links," *IEEE Trans. on Antennas & Propagation*, vol. 43, no. 12, pp. 1411–1415, 1995.

[23] U.-C. Fiebig, "Modeling rain fading in satellite communications links," *Proc. of IEEE Vehicular Technology Conference (VTC)'99*, vol. 3, no. 9, pp. 1422–1426, 1999.

[24] C. I. Christodoulou, S. C. Michaelides, M. Gabella, and C. S. Pattichis, "Prediction of rainfall rate based on weather radar measurements," *Proc. of International Joint Conference on Neural Networks (IJCNN)'04*, vol. 2, no. 4, pp. 1393–1396, 2004.

[25] J.-C. Hsieh, H.-P. Lin, and C. Yang, "A two-level, multi-state Markov model for satellite propagation channels," *Proc. of IEEE Vehicular Technology Conference (VTC)'01*, vol. 4, no. 4, pp. 3005–3009, 2001.

[26] E. E. Altshuler, M. A. Gallop, Jr., and L. E. Telford, "Atmospheric attenuation statistics at 15 and 35 GHz for very low elevation angles," *Radio Science*, vol. 13, no. 5, pp. 839–852, 1978.

[27] S. D. Slobin, "Microwave noise temperature and attenuation of clouds: Statistics of these effects at various sites in the United States, Alaska and Hawaii," *Radio Science*, vol. 17, no. 6, pp. 1443–1454, 1982.

[28] Y. Karasawa and T. Matsudo, "Characteristics of fading on low-elevation angle earth-space paths with concurrent rain attenuation and scintillation," *IEEE Trans. on Antennas & Propagation*, vol. 39, no. 5, pp. 657–661, 1991.

[29] ITU-R, "Propagation data and prediction method required for the design of earth-space telecommunication systems," *Radio wave propagation, International Telecommunication Union Recommendation ITU-R P.618-8*, 2001.

[30] K. Harb, A. Srinivasan, B. Cheng, and C. Huang, "QoS in weather impacted satellite networks," *Pacific Rim Conference on Communications, Computers and Signal Processing*, pp. 178 – 181, Aug. 2007.

[31] K. Harb, A. Srinivasan, B. Cheng, and C. Huang, "Intelligent weather systems with fuzzy logic controller for satellite networks," *Proc. of IEEE Wireless Communications and Networking Conference (WCNC)'08*, pp. 3069–3074, March 2008.

[32] H. Fujii, T. Asai, Y. Okumura, R. Kawauchi, I. Hiradate, H. Akazawa, and T. Sotoyama, "Capacity achievable by spectrum sharing with adaptive transmit power control: Based on field measurements," *Proc. of 4th International Conference on Cognitive Radio Oriented Wireless Networks and Communications (CROWNCOM)'09*, pp. 1–6, Aug. 2009.

[33] S. Haykin, "Cognitive radio: brain empowered wireless communications," *IEEE Journal on Selected Areas of Communications*, vol. 23, no. 2, pp. 210–220, 2005.

[34] K. Harb, F. R. Yu, P. Dakhal, and A. Srinivasan, "Performance improvement in satellite networks based on Markovian weather prediction," *Proc. of IEEE GlobCom*, Dec. 2010.

[35] D. J. Whalen, *The Origins of Satellite Communications, 1945-1965.* Washington, D.C.: Smithsonian Institution Press, 2002.

[36] Neets, "Naval electrical engineering training series." website: http://www.tpub.com/neets, last accessed date August 2010.

[37] D. Smith, *Digital Communication via Satellite: A Vision in Retrospect.* Boston: A.W. Sijthoff, 1976.

[38] G. Maral and M. Bousquet, *Satellite Communications Systems.* John Wiley & Sons Ltd, UK, 1993.

[39] Telesat, "ISS (Intelligent Satellite Service) research and development." website: http://www.telesat.ca/en, last accessed date August 2010.

[40] J. Pelton, "The start of commercial satellite communications [History of communications]," *IEEE Communications Magazine*, vol. 48, no. 3, pp. 24–31, 2010.

[41] E. Lutz, M. Werner, and A. Jahn, *Satellite Systems for Personal and Broadband Communications.* Springer, New York, 2000.

[42] T. peng Mao, D. fang Zhou, and Z. xia Niu, "The calculation model of the attenuation due to clouds or fog and the analysis of its characteristic," *Proc. of Asia-Pacific'04*, pp. 332–334, Aug. 2004.

[43] C. Communications, "About VSAT." website: http://www.crystalcommunications.net, last accessed date August 2010.

[44] D. Chakraborty, "VSAT communications networks - An overview," *Communication Magazine*, vol. 26, no. 5, pp. 10–24, 1988.

[45] L. P. Seidman, "Satellites for wideband access," *Communication Magazine*, vol. 34, no. 10, pp. 108–111, 1996.

[46] Comsys, "The comsys VSAT report, 11th edition." website: http://www.comsys.co.uk/vsatnets.htm, last accessed date August 2010.

[47] K. M. S. Murthy, J. Alan, J. Barry, B. G. Evans, N. Miller, R. Mullinax, P. Noble, B. O'Neal, J. J. Sanchez, N. Seshagiri, D. Shanley, J. Stratigos, and J. W. Warner, "VSAT user network examples," *Communication Magazine*, vol. 27, no. 5, pp. 50–57, 1989.

[48] L. A. Hoffman, H. J. Wintroub, and W. A.Garber, "Propagation observations at 3.2 millimeters," *Proc. of the IEEE*, vol. 54, no. 4, pp. 449–454, 2005.

[49] W. J. Vogel and J. Goldhirsh, "Multipath fading at L band for low elevation angle, land mobile satellite scenarios," *IEEE Journal on selected areas in communications*, vol. 13, no. 2, pp. 197–204, 1995.

[50] ITU-R, "Attenuation by atmospheric gases," *Radio wave propagation, International Telecommunication Union Recommendation ITU-R P.676-6*, 2005.

[51] S. J. Shellhammer, "Estimation of packet error rate caused by interference using analytic techniques - A coexistence assurance methodology," *IEEE P802.19-05/0028r1, Qualcomm Inc.*, Sept. 2005.

[52] B. Sklar, *Digital Communications: Fundmentals and Applications (2nd Edition).* Prentice Hall PTR, NJ, 2001.

[53] M. Willis, "Absorption by atmospheric gases." website: http://www.mike-willis.com/Tutorial/gases.htm, last accessed date August 2010.

[54] H. J. Liebe, T. Manabe, and G. A. Hufford, "Millimeter-wave attenuation and delay rates due to fog/cloud conditions," *IEEE Trans. on Antennas & Propagation*, vol. 37, no. 12, pp. 1617–1623, 1989.

[55] L.-I. Lo, B. M. Fannin, and A. W. Straiton, "Attenuation of 8.6 and 3.2 mm radio waves by clouds," *IEEE Trans. on Antennas & Propagation*, vol. 23, no. 6, pp. 782–786, 1975.

[56] E. R. Westwater, "The accuracy of water vapor and cloud liquid determination by dual-frequeny ground-based microwave radiometry," *Radio Science*, vol. 13, no. 4, pp. 677–685, 1978.

[57] Y. Karasawa, K. Yasukawa, and M. Yamada, "Tropospheric scintillation in the 14/11-GHz bands on earth-space paths with low elevation angles," *IEEE Trans. on Antennas & Propagation*, vol. 36, no. 4, pp. 563–569, 1988.

[58] R. McLeod and M. L. Baart, *Geometry and Interpolation of Curves and Surfaces*. Cambridge University Press, July 1998.

[59] V. Network, "Bilinear interpolation definition." website: http://www.pcmag.com, last accessed date August 2010.

[60] I. T. Union, "Radiocommuniation sector (ITU-R) home." website: http://www.itu.int/ITU-R, last accessed date August 2010.

[61] M. van Vuuren and E. Winands, "Iterative approximation of k-limited polling systems," *Source Queueing Systems: Theory and Applications archive*, vol. 55, no. 3, pp. 161–178, 2006.

[62] R. Wangkeeree, "An iterative approximation method for a countable family of nonexpansive mappings in hilbert spaces," *Applied Mathematics and Computation*, vol. 186, no. 2, pp. 1551–1558, 2007.

[63] L. Castanet, T. Deloues, and J. Lemorton, "Channel modelling based on n-state Markov Chains for satcom systems simulation," *IEEE Trans. on Antennas & Propagation*, vol. 1, no. 491, pp. 119–122, 2003.

[64] D. A. Sanchez-Salas and J. L. Cuevas-Ruiz, "N-states channel model using Markov Chains," *Proc. of Electronics, Robotics and Automotive Mechanics Conference*, pp. 342 – 347, Oct. 2007.

[65] W. Suozhu, L. Haifang, and H. Zhaohui, "Application of Markov Chains prediction model in product layout optimization," *International Forum on Computer Science-Technology and Applications (IFCSTA)'09*, vol. 3, no. 10, pp. 243–246, 2009.

[66] L. Saloff-Coste, *Lectures on Finite Markov Chains. In lectures on probability theory and statistics (Saint-Flour, 1996)*. Springer, Berlin, 1997.

[67] K. Harb, F. R. Yu, P. Dakhal, and A. Srinivasan, "A decision support scheme to maintain QoS in weather impacted satellite networks," *Proc. of Atmospheric and Space Environments Conference (AIAA)'10*, Aug. 2010.

[68] Y. Leung, *Intelligent Spatial Decision Support Systems*. Springer Verlag, New York, 1997.

[69] D. J. Power, *Decision Support Systems: Concepts and Resources for Managers*. Quorum, Greenwood, 2002.

[70] L. J. Bannon, "Group decision support systems: An analysis and critique," *Proceedings of 5th European Conference on Information Systems*, pp. 526–539, June 1997.

# Appendix

# Appendix A

# Rainfall Rate Calculation and Bi-Linear Interpolation Code

The following code is used to calculate rainfall rate combined with bi-linear interpolation. Also, it is computed other factors such as the level of satellite position according to sea level, height above mean sea level of earth station, and Mean $0°$ $C$ isotherm height above mean sea level for the input specific location x and y.

**function** [**rainfallrate**] = **Rainfall_Rate_Calculation**,

% Define Variables

global x y ep Rk h0 hs hr ceta1

% x: Longitude

% y: Latitude

% h0 : Mean 0° C isotherm height above mean sea level

% hs: Height above mean sea level of earth station

```
% hr: Mean rain height above mean sea level
% ceta1: Propagation angle
% Longitude axis matrix size = [1 X 241];
xx = [0:1.5:360];
% Latitude axis matrix size = [121 X 1];
yy = [90: - 1.5: - 90];
% Matrix size = [121 X 241] for Pr6 values;
Pr6 = FafoPr6;
% Matrix size = [121 X 241] for Mc values;
Mc = FafoMc;
% Matrix size = [121 X 241] for Ms values;
Ms = FafoMs;
% Matrix size = [121 X 241] for h0 values;
HH0 = FafoH0;
% Matrix size = [121 X 241] for hs values;
HHS = FafoHS15;
Y1 = size(yy);
uu = 1;
% Space distance among grid is 1.5 degrees
Ak = 1.5;
% Variables initialization
xb = 0; xc = 0;
yb = 0; yc = 0;
i1a = 0; i1b = 0;
i1c = 0; i1d = 0;
xk = 0; yk = 0;
```

```
x = 0; y = 0;
xb1 = 0; xc1 = 0;
yb1 = 0; yc1 = 0;
i1a1 = 0; i1b1 = 0;
i1c1 = 0; i1d1 = 0;
% Input x value:
x = input ('Please note that x ranges from [0 to + 360] degrees, Input x = ');
xx1 = x;
while x > 360 | x < 0,
x = input ('Please note that x ranges from [0 to + 360] degrees, Input x = ');
xx1 = x;
end
xa = xx1;
% Input y value:
y = input ('Please note that y ranges from [ - 90 to + 90] degrees, Input y = ');
yy1 = y;
while y > 90 | y < - 90,
y = input ('Please note that y ranges from [ - 90 to + 90] degrees, Input y = ');
yy1 = y;
end
% Start bi-linear interpolation function
ya = yy1;
xx(1) = 0;
% Interpolation for x axis
ikx = 0;
xab3 = 0;
```

```
if xa >  = xx(i11x - 1) & xa <  = xx(i11x),
xab1 = xa;
xab2 = xa + Ak;
xb = xx(i11x - 1);
xc = xb + Ak;
ikx1 = i11x - 1;
ikx2 = i11x;
ikx = i11x;
i1a = i11x - 1;
i1b = i11x;
if xa == xx(i11x - 1) | xa == xx(i11x),
if xa == xx(i11x),
ikx2 = i11x;
ikx = i11x;
ikx1 = i11x;
else
ikx2 = i11x - 1;
ikx = i11x - 1;
ikx1 = i11x - 1;
end
xab1 = xa;
xab2 = xa;
xab3 = xa;
end
xb1 = xab1;
xc1 = xab2;
```

```
i1a1 = ikx1;
i1b1 = ikx2;
break;
end
end
yy(1) = 90;
% Interpolation for y axis
for i11y = 2: 121,
iky = 0;
yab3 = 0;
if (ya < = yy(i11y - 1) & ya > = yy(i11y)),
yab1 = ya;
yab2 = ya - Ak;
yb1 = yab1;
yc1 = yab2;
yc = yy(i11y);
yb = yy(i11y - 1);
iky1 = i11y - 1;
iky2 = i11y;
iky = i11y;
i1c1 = iky1;
i1d1 = iky2;
i1c = i11y - 1;
i1d = i11y;
if ya == yy(i11y - 1) | ya == yy(i11y),
if ya == yy(i11y - 1),
```

```
iky = i11y - 1;
iky2 = i11y - 1;
iky1 = i11y - 1;
yb = ya;
i1c = i11y - 1;
yc = ya - Ak;
i1d = i11y;
elseif ya == yy(i11y)
iky = i11y;
iky2 = i11y;
iky1 = i11y;
yb = ya + Ak;
i1c = i11y - 1;
yc = ya;
i1d = i11y;
elseif ya == - 90,
iky = i11y;
iky2 = i11y;
iky1 = i11y;
i1d = i11y;
yb = ya + Ak;
i1c = i11y - 1;
yc = ya;
end
yab1 = ya;
yab2 = ya;
```

```
yab3 = ya;
yb1 = yab1;
yc1 = yab2;
i1c1 = iky1;
i1d1 = iky2;
end
break;
end
end
% End of bi-linear interpolation function
% Print out the four closed points of x and y axis location
if (xa == xab3)  & (ya == yab3),
KK1 = sprintf('x1 = %1.2f degrees, xa1 = %1.1f degrees, ···
··· xb1 = %1.1f degrees, and y1 = %1.2f degrees, ya1 = %1.2f degrees, ···
··· yb1 = %1.1f degrees', xa, xb1 , xc1, ya , yb1, yc1);
disp(KK1)
else
KK1 = sprintf('x = %1.2f degrees, xa = %1.1f degrees, xb = %1.1f degrees, ···
··· and y = %1.2f degrees, ya = %1.2f degrees, ···
··· yb = %1.1f degrees', xa, xb , xc, ya , yb, yc);
disp(KK1)
end
x = xa;
x1 = xb;
x2 = xc;
y = ya;
```

```
y1 = yb;
y2 = yc;
i1 = i1a; i2 = i1b; % for x axis
j1 = i1c; j2 = i1d; % for y axis
% Bi-linear interpolation in the x and y direction yield to:
% Check if the location (x, y) falls on one of the grid points
xk = mod(x, Ak);
yk = mod(y, Ak);
% xk and yk are equal to zero their values fall on the grid
if xk == 0 & yk == 0,
FT_Pr6e = Pr6(iky, ikx);
FT_Mc = Mc(iky, ikx);
FT_Ms = Ms(iky, ikx);
FT_H0 = HH0(iky, ikx);
T_HS15 = HHS(iky, ikx);
else
% First variable Pr6,
F_Pr6e1 = [(x - x2) / (x1 - x2)] * Pr6(j1, i1) + [(x - x1) / (x2 - x1)] * Pr6(j1, i2);
F_Pr6e2 = [(x - x2) / (x1 - x2)] * Pr6(j2, i1) + [(x - x1) / (x2 - x1)] * Pr6(j2, i2);
FT_Pr6e = [(y - y2) / (y1 - y2)] * F_Pr6e1 + [(y - y1) / (y2 - y1)] * F_Pr6e2;
% Second variable Mc,
F_Mc1 = [(x - x2) / (x1 - x2)] * Mc(j1, i1) + [(x - x1) / (x2 - x1)] * Mc(j1, i2);
F_Mc2 = [(x - x2) / (x1 - x2)] * Mc(j2, i1) + [(x - x1) / (x2 - x1)] * Mc(j2, i2);
FT_Mc = [(y - y2) / (y1 - y2)] * F_Mc1 + [(y - y1) / (y2 - y1)] * F_Mc2;
% Third variable Ms,
F_Ms1 = [(x - x2) / (x1 - x2)] * Ms(j1, i1) + [(x - x1) / (x2 - x1)] * Ms(j1, i2);
```

```
F_Ms2 = [(x - x2) / (x1 - x2)] * Ms(j2, i1) + [(x - x1) / (x2 - x1)] * Ms(j2, i2);
FT_Ms = [(y - y2) / (y1 - y2)] * F_Ms1 + [(y - y1) / (y2 - y1)] * F_Ms2;
% Fourth variable h0: 0'C above mean sea level
FT_H0_1 = [(x - x2) / (x1 - x2)] * HH0(j1, i1) + [(x - x1) / (x2 - x1)] * HH0(j1, i2);
FT_H0_2 = [(x - x2) / (x1 - x2)] * HH0(j2, i1) + [(x - x1) / (x2 - x1)] * HH0(j2, i2);
FT_H0 = FT_H0_1 + FT_H0_2;
% Fifth variable hs: Height above mean sea level
FT_HS_1 = [(x - x2) / (x1 - x2)] * HHS(j1, i1) + [(x - x1) / (x2 - x1)] * HHS(j1, i2);
FT_HS_2 = [(x - x2) / (x1 - x2)] * HHS(j2, i1) + [(x - x1) / (x2 - x1)] * HHS(j2, i2);
FT_HS15 = FT_HS_1 + FT_HS_2;
end
x = xa;
x1 = xb;
x2 = xc;
y = ya;
y1 = yb;
y2 = yc;
% Calculation of average annual convective rainfall amount Mc
MC = FT_Mc;
% Calculation of average annual stratiform rainfall amount Ms
MS = FT_Ms;
% Calculate hr: Mean rain height above mean sea level
hr = FT_H0 + 0.36;
% Derive the percentage probability of rain in an average year P0:
% Check for P0 and P
if (isnan(FT_Pr6e) | FT_Pr6e == 0),
```

```
P0a = 0;
ep = 0;
Rp_Lat_Lon = 0;
else
% Calculation of rainfall rate
P0_Lat_Lon = FT_Pr6e * (1 - exp( - 0.0117 * (FT_Ms) / FT_Pr6e));
P0a = P0_Lat_Lon;
% Enter exceed percentage probability (ep) for rainfall rate:
% Note that P should be less than P0 otherwise result will be zero
rrpa = sprintf('Notice that %ep should be smaller or equal to P0 = %3.4f and ···
··· different from zero otherwise rainfall rate will be equal to Zero', P0a);
disp(rrpa)
ep = input ('Please enter the percentage rate ep = % ');
if (ep > P0a | ep == 0),
P0a = 0;
Rp_Lat_Lon = 0;
else
a = 1.11;
b = (FT_Mc + FT_Ms) / (22932 * P0_Lat_Lon);
c = 31.5 * b;
A = a * b;
B = a + c * log(ep / P0_Lat_Lon);
C = log(ep / P0_Lat_Lon);
% Rainfall rate value will be:
Rp_Lat_Lon = ( - B + sqrt(B^2 - 4 * A * C)) / (2 * A);
end
```

```
end
% The rainfall rate is equal to:
rainfallrate = Rp_Lat_Lon;
Rk = rainfallrate
```

# Appendix B

# Rain Attenuation Calculation Code Using Historical Data

Calculation of rain attenuation using ITU−R Original Method, ITU−R Approximation Method, and Iterative Approximation Method (IAM).

The rain attenuation values are calculated for different propagation angles and frequencies at any location on earth.

**function [atten1] = atten_P2_AF,**

global x y ep Rk h0 hs hr ceta1 P00

APp001 = 0;

% Collect different propagation parameters according to the specific location

sab = Rainfall_Rate_Calculation; % Presented in Appendix A

x = sab(1);

y = sab(2);

P = sab(3);

P0 = sab(4);

```
Rain_rate = sab(5);
h0 = sab(6);
hs = sab(7);
% Calculation of rain attenuation using ITU − R Original Method
% The following steps are as presented in Chapter 3
% Step 1:
% Satellite position over mean sea level
hr = sab(8);
R001 = Rain_rate;
Rk = Rain_rate;
% Effective raduis of the earth in Re
Re = 8500;
rr10 = sprintf(' x y P P0 Rain_rate h0 hs hr');
disp(rr10)
tapa = sprintf('%g %g %2.2g %2.2g %2.5g  ...
...  %2.4g %2.4g %2.4g', x, y, P, P0, Rain_rate, h0, hs, hr);
disp(tapa)
P001 = 0;
A001 = 0;
Pf = 0;
ApS = sprintf(' For P = %g %, Attenuation due to rain  ...
...  A(%g) = %g', PPf, PPf, Aps);
disp(ApS)
% Step 2:
else
ceta1 = input ('Please enter the propagation angle Ceta(degrees), Input Ceta = ');
```

```
if ceta1 >  = 5,
ceta1d = ceta1 * pi / 180;
% Calculate slant-path length Ls as:
Ls = (hr - hs) / sin(ceta1d);
else
Ls = (2 * (hr - hs)) / ((((sin(ceta1d))^2) + ...
... (2 * (hr - hs) / Re))^(1 / 2) + sin(ceta1d));
end
Ls = abs (Ls);
% Step 3:
% Calculate horizontal projection Lg as:
Lg = abs (Ls) * abs (cos(ceta1d));
% Step 4:
Rain_rate = sab(5);
% Step 5: Calculate rain attenuation at different frequencies:
uu = 0;
for F1 = 7: 55,
uu = uu + 1;
fkv = KalfaFreq(F1);
F_actual = fkv(1);
fe = fkv(2);
% Call frequency - dependent coefficients and constant coefficients of horizontal and
vertical polarizations
Kh = fkv(3);
Kv = fkv(5);
Alfah = fkv(4);
```

```
Alfav = fkv(6);
taw = 45 * pi / 180;
% Constant coefficients of vertical and horizontal polarizations K:
K = (Kh + Kv + (Kh - Kv) * ((cos(ceta1d))^2) * cos(2 * taw)) / 2;
K = abs (K);
Alfa = (Kh * Alfah + Kv * Alfav + (Kh * Alfah - Kv * Alfav) ...
... * ((cos(ceta1d))^2) * cos(2 * taw)) / (2 * K);
Alfa = abs (Alfa);
% Calculate specific attenuation GamaR as:
GamaR = K * (R001)^(Alfa);
f = fe * 1e9;
% Step 6: Calculate the horizontal adjustment r001:
r001 = 1 / (1 + 0.78 * sqrt((Lg * GamaR) / f) - (0.38 * (1 - exp( - 2 * Lg))));
% Step 7: Calculate the vertical adjustment factor V001:
Phi = abs (y);
% Calculate vertical adjustment factor Fita as:
Fita = atan((hr - hs) / (Lg * r001));
if Fita > ceta1,
% Calculated the actual slant-path length Lr as:
Lr = Lg * r001 / (cos(ceta1d));
else
Lr = (hr - hs) / (sin(ceta1d));
end
if Phi < 36,
xeso = 36 - Phi;
else
```

```
xeso = 0;
end
Lr = (Lr);
V001 = 1 / (1 + sqrt(sin(ceta1d)) ...
... * (31 * (1 - exp( - ceta1 / (1 + xeso))) * (sqrt(Lr * GamaR) / f^2) - 0.45));
V001 = (V001);
% Step 8: The effective path length is:
Le = Lr * V001;
% Step 9: Rain attenuation using ITU - R Original Method:
AT(uu) = GamaR * Le;
FF1(uu) = F1;
end
atten1 = [FF1' AT'];
end
```

This program calculates rain attenuation for different frequency sample ($Fs$) as per ITU − R Approximation Method.

```
function atten = atten_P_Freq(Fs),
global x y ep Rk h0 hs hr ceta1
% Fs: Input sample frequency
APp001 = 0;
% Call for rainfall rate and other propagation parameters
sab = Rainfall_Rate_Calculation; % Presented in Appendix A
x = sab(1);
y = sab(2);
P = sab(3);
```

```
P0 = sab(4);
Rain_rate = sab(5);
h0 = sab(6);
% Satellite position over mean sea level hs:
hs = sab(7);
hr = sab(8);
R001 = Rain_rate;
Rk = Rain_rate;
F_actual = Fs;
Re = 8500;
rr10 = sprintf(' x y P P0 Rain_rate h0 hs hr');
disp(rr10)
tapa = sprintf('%g %g %2.2g %2.2g %2.5g ...
... %2.4g %2.4g %2.4g', x, y, P, P0, Rain_rate, h0, hs, hr);
disp(tapa)
% Calculation of rain attenuation using ITU - R as explained in Chapter 3
GamaR = 0;
Le = 0;
if ((hr - hs) < = 0 | Rain_rate == 0),
rain_att = 0;
P001 = 0;
A001 = 0;
Pf = 0;
else
ceta1 = input ('Please enter the propagation angle Ceta(degrees), Input Ceta = ');
ceta1d = ceta1 * pi / 180;
```

```
if ceta1 > = 5,
Ls = (hr - hs) / sin(ceta1d);
else
Ls = (2 * (hr - hs)) / ((((sin(ceta1d))^2) + (2 ...
... * (hr - hs) / Re))^(1 / 2) + sin(ceta1d));
end
Lg = (Ls) * abs (cos(ceta1d));
% Calculation of rainfall rate
Rain_rate = sab(5);
fkv = KalfaFreq(Fs);
F_actual = fkv(1);
fe = fkv(2);
Kh = fkv(3);
Kv = fkv(5);
Alfah = fkv(4);
Alfav = fkv(6);
taw = 45 * pi / 180;
f = fe;
K = (Kh + Kv + (Kh - Kv) * ((cos(ceta1d))^2) * cos(2 * taw)) / 2;
Alfa = (Kh * Alfah + Kv * Alfav + (Kh * Alfah - Kv * Alfav) ...
... * ((cos(ceta1d))^2) * cos(2 * taw)) / (2 * K);
GamaR = K * (R001)^(Alfa);
r001 = 1 / (1 + 0.78 * sqrt((Lg * GamaR) / f) - (0.38 * (1 - exp( - 2 * Lg))));
Phi = abs (y);
Fita = atan((hr - hs) / (Lg * r001));
if Fita > ceta1,
```

```
Lr = Lg * r001 / (cos(ceta1d));
else Lr = (hr - hs) / (sin(ceta1d));
end
if Phi < 36,
xeso = 36 - Phi;
else
xeso = 0;
end
V001 = 1 / (1 + sqrt(sin(ceta1d)) * (31 * (1 - exp( - ceta1 / (1 + xeso))) ...
... * (sqrt(Lr * GamaR) / f^2) - 0.45));
Le = Lr * V001;
end
% The rain attenuation values using ITU - R Approximation Method is:
A001 = GamaR * Le;
APp001 = sprintf(' For P = %g %, Attenuation due to rain A(%g) = %g dB', P, P, A001);
disp(APp001)
atten = [F_actual P A001];
```

This program is used to calculate the rain attenuation based on Iterative Approximation Method (IAM) and compare the results with the ITU - R Original Method.

```
function [tato1] = Comp_ApF2(),
global x y ep Rk h0 hs hr ceta1
% Get the rain attenuation values using ITU - R Original Method
[Faro] = atten_P_AFreq2;
F_actual = Faro(:, 1);
A1 = Faro(:, 2); % A1 at different frequencies
```

```
f1 = 0;
Phi1(1) = 0;
u = 0;
for ff = 7: 55,
f1 = ff;
fw = (ff + 1);
u = u + 1;
Phi1(u) = (f1^2) / (1 + (10^-4) * (f1^2));
Phi2(u) = (fw^2) / (1 + (10^(-4)) * (fw^2));
Hh(u) = 1.12 * (10^(-3)) * ((Phi2(u) / Phi1(u))^0.5) * ((Phi1(u) * A1(u))^0.55);
ff2(u) = fw;
A2(u) = A1(u) * (Phi2(u) / Phi1(u))^(1 - Hh(u));
A22(u) = A2(u);
end
% Rain attenuation values using IAM is:
Ai = A22';
tato1 = [F_actual A1 ff2' Ai];
```

This program is used to calculate the rain attenuation using ITU − R Original Method for different frequencies,

```
function [atten15] = atten_P_AFreq2,
global x y ep Rk h0 hs hr ceta1
APp001 = 0;
Rain_rate = Rk;
R001 = Rain_rate;
Re = 8500;
```

```
Ffa = [7 : 55];
zz1 = length(Ffa);
ceta1d = ceta1 * pi / 180;
if ((hr - hs) < = 0 | Rain_rate == 0),
rain_att = 0;
P001 = 0;
A001 = 0;
Pf = 0;
FF1(zz1) = 0;
AT(zz1) = 0;
else
if ceta1 > = 5,
Ls = (hr - hs) / sin(ceta1d);
else
Ls = (2 * (hr - hs)) / ((((sin(ceta1d))^2) + ...
... (2 * (hr - hs) / Re))^(1 / 2) + sin(ceta1d));
end
Lg = (Ls) * abs (cos(ceta1d));
Rain_rate = Rk;
uu = 0;
for F1 = 7: 55,
uu = uu + 1;
% Call frequency dependent variables: Kh Alfah Kv Alfav
fkv = KalfaFreq(F1);
F_actual = fkv(1);
fe = fkv(2);
```

```
Kh = fkv(3);
Kv = fkv(5);
Alfah = fkv(4);
Alfav = fkv(6);
taw = 45 * pi / 180;
K = (Kh + Kv + (Kh - Kv) * ((cos(ceta1d))^2) * cos(2 * taw)) / 2;
K = abs (K);
Alfa = (Kh * Alfah + Kv * Alfav + (Kh * Alfah - Kv * Alfav) ...
... * ((cos(ceta1d))^2) * cos(2 * taw)) / (2 * K);
Alfa = abs (Alfa);
GamaR = K * (R001)^(Alfa);
f = fe;
r001 = 1 / (1 + 0.78 * sqrt((Lg * GamaR) / f) - (0.38 * (1 - exp( - 2 * Lg))));
Phi = abs (y);
Fita = atan((hr - hs) / (Lg * r001));
if Fita > ceta1,
Lr = Lg * r001 / (cos(ceta1d));
else
Lr = (hr - hs) / (sin(ceta1d));
end
if Phi < 36,
xeso = 36 - Phi;
else
xeso = 0;
end
Lr = abs (Lr);
```

```
V001 = 1 / (1 + sqrt(sin(ceta1d)) * (31 * (1 - exp( - ceta1 / (1 + xeso))) ...
... * (sqrt(Lr * GamaR) / f^2) - 0.45));
V001 = abs (V001);
Le = Lr * V001;
% Rain attenuation
AT(uu) = GamaR * Le;
FF1(uu) = F1;
end
end
atten15 = [FF1' AT'];
```

# Appendix C

# Total Attenuation Calculation Code Using Historical Data

```
Calculation of total attenuation using historical weather data
function [rajo] = P_Att_Rain_Angle_Static(Ceta_Min, Ceta_Step, Ceta_Max, fw, pu,Ptt,dd),
global x y h0 hs hr ceta1 Le Nwet P00 fwi
global TempKa TempCa IWV1 IWV2 IWV3 IWV5 WVD1
global WVD2 WVD3 WVD5 pz Vt1 Pk101 Rain_Pred101
fwi = fw;
% Ptt: Represents transmit power value
% dd: Represents antenna diameter at transmit station
% The following function collects the required propagation parameters
that are used to calculate rain, gas, cloud, fog, and scintillation attenuations.
It is similar to Rainfall_Rate_Calculation function presented in Appendix A,
which collects only the rain related parameters
Rain_Gas_Cloud_Scint;
```

```
hsat = 35880; % Satellite height above sea level
% This function is used to get the rainfall rate
Rain_Prob(pu);
% Le: Distance between earth station and rain height above sea level
% Rain attenuation calculation
L_RAINdB = Atten_Rain(Ceta_Min, Ceta_Step, Ceta_Max);
% Gaseous attenuation calculation
L_GASEOUSdB = Atten_Gaseous(Ceta_Min, Ceta_Step, Ceta_Max);
% Cloud attenuation calculation
L_CLOUD_FOGdB = Atten_Cloud(Ceta_Min, Ceta_Step, Ceta_Max);
% Antenna efficiency at receiver ranging from: 0.55 to 0.65
Mu_r = 0.55;
Mu_rmax = 0.65;
Dia = dd; % Antenna diameter at transmitter side
Mu = Mu_rmax;
D_S = Dia;
% Scintillation attenuation calculation
L_SCINTdB = Atten_Scintillation(Ceta_Min, Ceta_Step, Ceta_Max, D_S, Mu);
% Calculation of atmospheric attenuation:
R = size(L_RAINdB);
G = size(L_GASEOUSdB);
C = size(L_CLOUD_FOGdB);
S = size(L_SCINTdB);
% Calculation of total loss due to atmospheric attenuation
Lt_exact1 = L_GASEOUSdB + ...
... sqrt((L_RAINdB + L_CLOUD_FOGdB).^2 + (L_SCINTdB).^2);
```

```
Lt_exact = Lt_exact1;
xw = 360 - x;
% Calculation of total power:
P1 = Ptt;
Pt = P1 * ones(size(Lt_exact));
% Speed of light c:
c = 2.998 * 1e + 8;
% Wavelength Lamda:
Lamda = c / fwi;
Gmax = Mu * (pi * Dia / Lamda)^2;
Gmax_dB = db(Gmax, 'power');
Gt1 = Gmax_dB; Gr1 = 100;
% Transmitter and receiver gain
Gt = Gt1 * ones(size(Lt_exact));
Gr = Gr1 * ones(size(Lt_exact));
% Total Power after adding all attenuations:
Pr_dB = Pt + Gt + Gr - Lt_exact;
% Propagation angle ranges Ceta
Ceta = [Ceta_Min:Ceta_Step:Ceta_Max];
rainfall = Rain_Pred101;
rain_Max = max(rainfall);
rainfall1 = rainfall;
% Total attenuation calculation
Lt_min = min(min(Lt_exact));
Lt_max = max(max(Lt_exact));
Figure
```

```
mesh(Ceta, rainfall1, Lt_exact)
grid on
uuu1 = sprintf('Total Attenuation at X = %4.4f W, Y = %4.4f N', xw, y);
title(uuu1),
uuu = sprintf('Total Attenuation(dB)');
xlabel('Propagation Angle(Degree)'),
ylabel('Rainfall Rate(mm / hr)'),
zlabel(uuu)
axis([Ceta_Min Ceta_Max 0 rain_Max Lt_min Lt_max])
% Rain attenuation
L_RAINdB_Max = max(max(L_RAINdB));
L_RAINdB_Min = min(min(L_RAINdB));
Figure
mesh(Ceta, rainfall1, L_RAINdB) grid on
uuu1 = sprintf('Rain Attenuation at X = %4.4f W, Y = %4.4f N', xw, y);
title(uuu1),
uuu = sprintf('Rain Attenuation(dB)');
xlabel('Propagation Angle(Degree)'),
ylabel('Rainfall Rate(mm / hr)'),
zlabel(uuu),
axis([Ceta_Min Ceta_Max 0 rain_Max L_RAINdB_Min L_RAINdB_Max])
% Gaseous attenuation
L_GASEOUSdB_Max = max(max(L_GASEOUSdB));
L_GASEOUSdB_Min = min(min(L_GASEOUSdB));
Figure
mesh(Ceta, rainfall1, L_GASEOUSdB) grid on
```

```
uuu1 = sprintf('Gaseous Attenuation at X = %4.4f W, Y = %4.4f N', xw, y);
title(uuu1),
uuu = sprintf('Gaseous Attenuation(dB)');
xlabel('Propagation Angle(Degree)'),
ylabel('Rainfall Rate(mm / hr)'),
zlabel(uuu),
axis([Ceta_Min Ceta_Max 0 rain_Max L_GASEOUSdB_Min L_GASEOUSdB_Max])
% Cloud & Fog attenuations
L_CLOUD_FOGdB_Max = max(max(L_CLOUD_FOGdB));
L_CLOUD_FOGdB_Min = min(min(L_CLOUD_FOGdB));
Figure
mesh(Ceta, rainfall1, L_CLOUD_FOGdB) grid on
uuu1 = sprintf('Cloud & Fog Attenuations at X = %g, Y = %g', xw, y);
title(uuu1),
uuu = sprintf('Cloud and Fog Attenuations(dB)');
xlabel('Propagation Angle(Degree)'),
ylabel('Rainfall Rate(mm / hr)'),
zlabel(uuu)
axis([Ceta_Min Ceta_Max 0 rain_Max L_CLOUD_FOGdB_Min L_CLOUD_FOGdB_Max])
% Scintillation attenuation
L_SCINTdB_Max = max(max(L_SCINTdB));
L_SCINTdB_Min = min(min(L_SCINTdB));
Figure
mesh(Ceta, rainfall1, L_SCINTdB) grid on
uuu1 = sprintf('Scintillation Attenuation at X = %4.4f W, Y = %4.4f N', xw, y);
title(uuu1),
```

```
uuu = sprintf('Scintillation Attenuation(dB)');
xlabel('Propagation Angle(Degree)'),
ylabel('Rainfall Rate(mm / hr)'),
zlabel(uuu),
axis([Ceta_Min Ceta_Max 0 rain_Max L_SCINTdB_Min L_SCINTdB_Max])
```

# Appendix D

# Total Attenuation Calculation Code Using Predicted Data

This program returns the total attenuation using real-time data.

function [rajo] = P_Att_Rain_Angle_Dynamic(Ceta_Min, Ceta_Step,

Ceta_Max, fw, Ptt, dd, gg),

global x y h0 hs hr ceta1 Le Nwet P00 fwi TempKa TempCa

global IWV1 IWV2 IWV3 IWV5 WVD1 WVD2 WVD3

global WVD5 pz Vt1 Pk101 Rain_Pred101

% Ceta: Represents propagation angle

fwi = fw; % Frequency of operation

% Ptt: Represents transmit power value

% dd: Represents antenna diameter at transmit station

% gg: Represents antenna gain

% This function is similar to Rainfall_Rate_Calculation presented in Appendix A

Rain_Gas_Cloud_Scint;

```
hsat = 35880;
% This function calls Markov Model presented in Chapter 4
Markovk_L5;
% Actual distance between earth and satellite station
% Le: Distance between earth station and rain height above sea level
% Rain attenuation calculation
L_RAINdB = Atten_Rain(Ceta_Min, Ceta_Step, Ceta_Max);
% Gaseous attenuation calculation
L_GASEOUSdB = Atten_Gaseous(Ceta_Min, Ceta_Step, Ceta_Max);
% Cloud attenuation calculation
L_CLOUD_FOGdB = Atten_Cloud(Ceta_Min, Ceta_Step, Ceta_Max);
% Antenna efficiency at receiver range: 0.55 to 0.65
Mu_r = 0.55; Mu_rmax = 0.65;
% Antenna diameter(m) at transmitter side
Dia = dd;
Mu = Mu_rmax;  D_S = Dia;
% Scintillation attenuation calculation
L_SCINTdB = Atten_Scintillation(Ceta_Min, Ceta_Step, Ceta_Max, D_S, Mu);
% Calculation of Total Loss:
R = size(L_RAINdB);
G = size(L_GASEOUSdB);
C = size(L_CLOUD_FOGdB);
S = size(L_SCINTdB);
Lt_exact1 = L_GASEOUSdB ...
... + sqrt((L_RAINdB + L_CLOUD_FOGdB).^2 + (L_SCINTdB).^2);
Lt_exact = Lt_exact1;
```

```
xw = 360 - x;
% Calculation of Total Power:
% Power balance:
Pr = 0 at: Zeroe_Received_Power = Lt - Gr - Gt;
% uk = sprintf('Transmit power required to assure 0 dB received power = %g dB', Zeroe)
P1 = Ptt; Pt = P1 * ones(size(Lt_exact));
c = 2.998 * 1e + 8;
Lamda = c / fwi;
Gmax = Mu * (pi * Dia / Lamda)^2;
Gmax_dB = db(Gmax, 'power');
Gt1 = Gmax_dB; Gr1 = gg;
Gt = Gt1 * ones(size(Lt_exact));
Gr = Gr1 * ones(size(Lt_exact));
% Received power
% Pr = (Pt * Gt * Gr) / Lt;
% Received power after adding all attenuation: Pr_dB = Pt + Gt + Gr - Lt_exact;
Ceta = [Ceta_Min:Ceta_Step:Ceta_Max];
rainfall = Rain_Pred101;
rain_Max = max(rainfall);
% Total attenuation calculation
Lt_min = min(min(Lt_exact));
Lt_max = max(max(Lt_exact));
figure
mesh(Ceta, rainfall, Lt_exact) grid on
uuu1 = sprintf('Total Attenuation at X = %g, Y = %g and Freq. = %g GHz', xw, y, fw);
title(uuu1), uuu = sprintf('Total Attenuation(dB)');
```

```
xlabel('Propagation Angle(Degree)'),
ylabel('Rainfall Rate(mm / hr)'),
zlabel(uuu)
axis([Ceta_Min Ceta_Max 0 rain_Max Lt_min Lt_max])
% Rain attenuation
L_RAINdB_Max = max(max(L_RAINdB)); L_RAINdB_Min = min(min(L_RAINdB));
figure
mesh(Ceta, rainfall, L_RAINdB) grid on
uuu1 = sprintf('Rain Attenuation at X = %g, Y = %g and Freq. = %g GHz', xw, y, fw);
title(uuu1), uuu = sprintf('Rain Attenuation(dB)');
xlabel('Propagation Angle(Degree)'),
ylabel('Rainfall Rate(mm / hr)'),
zlabel(uuu),
axis([Ceta_Min Ceta_Max 0 rain_Max L_RAINdB_Min L_RAINdB_Max])
% Gaseous attenuation
L_GASEOUSdB_Max = max(max(L_GASEOUSdB));
L_GASEOUSdB_Min = min(min(L_GASEOUSdB));
figure
mesh(Ceta, rainfall, L_GASEOUSdB) grid on
uuu1 = sprintf('Gaseous Attenuation at X = %g, Y = %g and Freq. = %g GHz', xw, y, fw);
title(uuu1), uuu = sprintf('Gaseous Attenuation(dB)');
xlabel('Propagation Angle(Degree)'),
ylabel('Rainfall Rate(mm / hr)'),
zlabel(uuu),
axis([Ceta_Min Ceta_Max 0 rain_Max L_GASEOUSdB_Min L_GASEOUSdB_Max])
% Cloud & Fog attenuations
```

```
L_CLOUD_FOGdB_Max = max(max(L_CLOUD_FOGdB));
L_CLOUD_FOGdB_Min = min(min(L_CLOUD_FOGdB));
figure
mesh(Ceta, rainfall, L_CLOUD_FOGdB) grid on
uuu1 = sprintf('Cloud & Fog Attenuations at X = %g, Y = %g and Freq. = %g GHz', xw, y, fw);
title(uuu1), uuu = sprintf('Cloud and Fog Attenuations(dB)');
xlabel('Propagation Angle(Degree)'),
ylabel('Rainfall Rate(mm / hr)'),
zlabel(uuu)
axis([Ceta_Min Ceta_Max 0 rain_Max L_CLOUD_FOGdB_Min L_CLOUD_FOGdB_Max])
% Scintillation attenuation
L_SCINTdB_Max = max(max(L_SCINTdB));
L_SCINTdB_Min = min(min(L_SCINTdB));
figure
mesh(Ceta, rainfall, L_SCINTdB) grid on
uuu1 = sprintf('Scintillation Attenuation at X = %g, Y = %g and Freq. = %g GHz', xw, y, fw);
title(uuu1),
uuu = sprintf('Scintillation Attenuation(dB)');
xlabel('Propagation Angle(Degree)'),
ylabel('Rainfall Rate(mm / hr)'),
zlabel(uuu),
axis([Ceta_Min Ceta_Max 0 rain_Max L_SCINTdB_Min L_SCINTdB_Max])
```

# Appendix E

# Signal to Noise Ratio Calculation Code

This program is used to calculate SNR after calculating atmospheric attenuation and free space loss. The output of SNR is presented using both total attenuation and transmit power for Geosynchronous Earth Orbit (GEO) where satellite height is 35880 km above sea level

function [rajo] = SNR_Total_Power_Adjust_Fuzzy ...

... (P_Start, P_Step, Inv_P_End, Pw_min, Pw_step, Pw_max, Ceta_A, fw, SnR, dd, rr, gg),

% fw: Represents the lower and upper frequency

% Pw: Represents transmit power

% P: Represents Rainfall Rate for exceed percentage probability

% Ceta: Represents the lower and upper propagation angle

% SnR: Signal to Noise Ratio

% dd: Represents antenna diameter at transmit station

% rr: Represents transmission rate

% gg: Represents antenna gain

global x y h0 hs hr ceta1 Le Nwet P00 fwi

global TempKa TempCa IWV1 IWV2 IWV3 IWV5 WVD1 WVD2

global WVD3 WVD5 pz Vt1

```
Ceta_Step = 1; Ceta_Max = Ceta_A; Ceta_Min = Ceta_A;
fwi = fw;
hsat = 35880;
c = 2.998 * 1e + 8;
Lamda = c / (fwi * 1e9);
% Le: Distance between earth station and rain height above sea level
Rain_Gas_Cloud_Scint;
% Rain attenuation calculation
L_RAINdB = Atten_Rain ···
··· (P_Start, P_Step, Inv_P_End, Ceta_Min, Ceta_Step, Ceta_Max);
% Gaseous attenuation calculation
L_GASEOUSdB = Atten_Gaseous ···
··· (P_Start, P_Step, Inv_P_End, Ceta_Min, Ceta_Step, Ceta_Max);
% Cloud attenuation calculation
L_CLOUD_FOGdB = Atten_Cloud ···
··· (P_Start, P_Step, Inv_P_End, Ceta_Min, Ceta_Step, Ceta_Max);
% Antenna efficiency at receiver range: 0.55 to 0.65
Mu_r = 0.55;
Mu_rmax = 0.65;
Dia = dd;
Mu = Mu_rmax;
D_S = Dia; % Antenna diameter at transmitter side
% Scintillation attenuation calculation
L_SCINTdB = Atten_Scintillation ···
··· (P_Start, P_Step, Inv_P_End, Ceta_Min, Ceta_Step, Ceta_Max, D_S, Mu);
% Free space attenuation calculation
```

```
ceta1d = Ceta_A * pi / 180;
dis = (hsat - hs) / (sin(ceta1d));
% Distance between earth station and Satellite
% Free space loss calculation
Lfree = (4 * π * dis * 1e3 / Lamda)^2;
LfreedB = 10 * log10(Lfree);
% Calculation of total loss:
R = size(L_RAINdB);
G = size(L_GASEOUSdB);
C = size(L_CLOUD_FOGdB);
S = size(L_SCINTdB);
total_loss = L_RAINdB + L_GASEOUSdB + L_CLOUD_FOGdB + L_SCINTdB;
Lt_exact1 = L_GASEOUSdB ···
··· + sqrt((L_RAINdB + L_CLOUD_FOGdB).^2 + (L_SCINTdB).^2);
Lt_exact = Lt_exact1 + LfreedB;
xw = 360 - x;
% Calculation of total power:
c = 2.998 * 1e + 8;
Lamda = c / (fwi * 1e9);
Gmax = Mu * (pi * Dia / Lamda)^2;
Gmax_dB = db(Gmax, 'power');
Gt1 = Gmax_dB;
Gr1 = gg;
Gt = Gt1 * ones(size(Lt_exact));
Gr = Gr1 * ones(size(Lt_exact));
% Total power after adding all attenuation:
```

```
Rate_tran = rr; % Transmission rate
K_boltz = - 228.6;
Nr = 1.5; % Range from 0.7 to 2
Tr = (10^(Nr / 10) - 1) * 290;
Ta = 290;
T_dB = 10 * log10(Tr + Ta);
ip = 0; jp = 0;
Pt = 0;
Pt_Adjust = 0;
for ptt = Pw_min:Pw_step:Pw_max,
ip = ip + 1;
Pt(ip) = ptt;
SNR_dB(:, ip) = Pt(ip) + Gt + Gr - Lt_exact - T_dB - K_boltz - Rate_tran;
end
ip1 = 0;
% Transmit power ranges:
ptt = [Pw_min:Pw_step:Pw_max];
% Get the values of rainfall rate for different ep:
rainfall = rainfall_prob(P_Start, P_Step, Inv_P_End);
SNR_dB_Power_Adjust = SNR_dB;
Ptt = 0;
SNR_MIN = min(min(SNR_dB_Power_Adjust));
Pw_min_Adjust = Pt(1); Pw_max_Adjust = Pw_max;
SNR_dB_Power_Adjust11 = abs(Pttt(1) + Gt(1) + Gr(1)  ...
... - Lt_exact(1) - T_dB - K_boltz - Rate_tran);
PTT = [Pw_min_Adjust:Pw_step:Pw_max_Adjust];
```

```
for ptt1 = Pw_min_Adjust:Pw_step:Pw_max_Adjust,
ip1 = ip1 + 1;
Pt_Power_Adjust(ip1) = ptt1;
SNR_dB_Power_Adjust_K(:, ip1) = Pt_Power_Adjust(ip1) + Gt + Gr - Lt_exact ...
... - T_dB - K_boltz - Rate_tran;
P_SNR = [SNR_dB_Power_Adjust_K(:, ip1)];
P_P = Pt_Power_Adjust;
end
P_SNR = SNR_dB_Power_Adjust_K;
P_P = Pt_Power_Adjust;
P_adjust = [Pw_min_Adjust:Pw_step:Pw_max_Adjust];
P_Raino = rainfall;
ir = 0;
xw = 360 - x;
% Calling system adjustment function
SNR_Adj = Adjustment(SNR_dB_Power_Adjust_K);
% Convert to Watt
DB_CON1 = 10.^(Pt / 10);
% Convert to mWatt
DBM_CON1 = (10^3) * DB_CON1;
% Convert to dBm
Pt_DBM = 10 * log10(DBM_CON1);
% Convert to dBm for adjust power
% Convert to Watt
DB_CON2 = 10^(PTT / 10);
% Convert to mWatt
```

```
DBM_CON2 = (10^3) * DB_CON2;
% Convert to dBm
Pt_Power_Adjust_DBM = 10 * log10(DBM_CON2);
rain_Max = max(rainfall);
rain_Min = min(rainfall);
Pt_Min = min(Pt);
Pt_Max = max(Pt);
SNR_dB_min = min(min(SNR_dB));
SNR_dB_max = max(max(SNR_dB));
Atten_Max = max(Lt_exact);
Atten_Min = min(Lt_exact);
figure
mesh(Pt, Lt_exact, SNR_dB)
uuu12 = sprintf('SNR vs Attenuation & Power ...
... for propagation angle = %g & Freq = %g GHz', Ceta_A, fwi);
title(uuu12)
uuu = sprintf('Total Attenuations(dB)');
xlabel('Transmitted Power(d B)'),
ylabel(uuu),
zlabel('SNR(d B)')
axis([Pt_Min Pt_Max Atten_Min Atten_Max SNR_dB_min SNR_dB_max])
Pw_Min_A = min(Pt_Power_Adjust); Pw_Max_A = max(Pt_Power_Adjust);
SNR_dB_A_min_K = min(min(Fuzzifier_SNR_Adj));
SNR_dB_A_max_K = max(max(Fuzzifier_SNR_Adj));
figure
mesh(Pt_Power_Adjust, Lt_exact, Fuzzifier_SNR_Adj)
```

```
% axis([XMIN XMAX YMIN YMAX ZMIN ZMAX])
uuu1 = sprintf('Adjusted SNR vs Attenuations & Power  ...
... for propagation angle = %g & Freq = %g GHz', Ceta_A, fwi);
title(uuu1)
uuu = sprintf('Total Attenuations(d B)');
xlabel('Adjusted Transmit Power(d B)'),
ylabel(uuu),
zlabel('Adjusted SNR(d B)')
axis([Pw_Min_A Pw_Max_A Atten_Min Atten_Max SNR_dB_A_min_K SNR_dB_A_max_K])
```